NOTCHED BEHAVIOUR OF STITCHED AND UNSTITCHED RFI CFRP LAMINATES

by

JASON BRIAN MITCHELL

H.N.D. Engineering (Materials), Sheffield Hallam University, UK, 1996

B.Eng. (Hon.) Materials Engineering, Sheffield Hallam University, UK, 1998

A THESIS SUBMITTED IN PARTIAL FULFILLMENT OF

THE REQUIREMENTS FOR THE DEGREE OF

MASTER OF APPLIED SCIENCE

in

THE FACULTY OF GRADUATE STUDIES

The Department of Metals and Materials Engineering

We accept this thesis as conforming

to the required standard

THE UNIVERSITY OF BRITISH COLUMBIA

October 2002

In presenting this thesis in partial fulfilment of the requirements for an advanced degree at the University of British Columbia, I agree that the Library shall make it freely available for reference and study. I further agree that permission for extensive copying of this thesis for scholarly purposes may be granted by the head of my department or by his or her representatives. It is understood that copying or publication of this thesis for financial gain shall not be allowed without my written permission.

Department of METALS AND MATERIALS ENGINEERING

The University of British Columbia
Vancouver, Canada

Date 11TH OCTOBER 2002

DE-6 (2/88)

Abstract

This work describes an experimental investigation of the effect of through-thickness stitching on the in-plane crack growth of Resin Film Infused (RFI) carbon fibre/epoxy laminates. Through-thickness reinforcement is a relatively recent approach to compensate for poor out-of-plane mechanical properties in laminated materials and also as a new method of joining laminated aerospace structures.

The effect of Kevlar® stitching on the fracture response of RFI laminates was successfully evaluated using an overheight compact tension (OCT) specimen. It had previously been proven that this small notched geometry allows for stable self-similar damage growth (including fibre failure) in composite laminates, under controlled loading conditions. This work further analyses the usefulness of the OCT geometry.

A detailed physical description of damage initiation and propagation in the *process zone*, (the area of discontinuous damage ahead of the notch tip) was obtained from measurements of surface displacement fields, as well as sectioning and deplying of the failed laminate. The experimental results yield valuable information that may be used to calibrate a finite element model.

The fracture response of these materials was largely unaffected by stitching, except results indicate that poor control of stitch tightness during manufacturing affects the type of damage evolved. When notched perpendicular to, but loaded parallel to the stitching, 'tight' stitching does not inhibit the natural tendency of these RFI materials to delaminate, resulting in crack blunting. However, 'loose' stitching results in a more brittle response – damage grows in a self-similar manner across the specimen width, and consists of heavy fibre breakage in plies oriented to the direction of load. Tested specimens with loose stitching also exhibit significantly less delamination.

Finally, the development and size of the fracture process zone was examined by comparing the experimental data and specimen compliances generated from a simple finite element model.

Table of Contents

List of Tables

List of Figures

Acknowledgements

I would first like the thank Professor Anoush Poursartip for this guidance throughout my thesis, and for giving me this wonderful opportunity of studying abroad. I would like to thank Mr. Roger Bennett as a friend and for his invaluable help with the experimental work, and Mr. Anthony Floyd for the numerical input to this thesis.

I wish to thank to Dr. William Avery at the Boeing Company for supplying the material used in this work.

Thank you to the various members (past and present) of the UBC Composites Group, and the Department of Metals and Materials Engineering, whose friendship and help have made this journey all the easier.

I would also like to express my thanks to my friends both in Canada and the UK, for being there during my thesis as well as two disappointing football tournaments, and one playoff final.

And finally to my family, I thank you; being apart has not been easy, but your faith in me is as always unending.

Chapter One

Introduction and Literature Review

1. Introduction & Literature Review

During the early nineties, it was recognised that the damage tolerance of composite materials must be improved if they are to be increasingly used for aircraft structures [1]. Even though they have the potential to reduce cost and weight, and increase the lifetime and performance of aerospace vehicles, the rate of adoption of these materials has been lower than expected. This is partially because composite structural components must behave on a par with comparable metallic structures for the purpose of safety, although criteria used to assess metallic damage tolerance is not always suitable for composites. Some composite materials are being used for primary structures (such as the Boeing 777, Figure 1-1), as their in-plane properties compare well with metals [2], however, low out-of-plane properties can lead to damage, for example, delamination.

Over the last decade, the technology to design and build large damage-tolerant structures has been widely investigated and reported; of note are through-thickness reinforced structures made by Resin Transfer Moulding (RTM) and Resin Film Infusion (RFI) of stitched carbon fibre preforms. It is thought that through-thickness reinforcement may be a cost-effective way to join composite laminates, providing improved in-plane and through-thickness strength, removing the need for traditional mechanical fasteners.

This study is aimed at gaining a fundamental understanding of how damage initiates and propagates in stitched and unstitched RFI composites, as part of an effort to investigate their suitability for use in aerospace structures.. One important goal is to gain a physical understanding of the damage mechanisms occurring in these materials using small notched specimens, with the aim to predict failure in larger specimens.

Damage in Composites

Carbon fibre reinforced composites (CFRP) consist of layers referred to as 'laminae', as shown in Figure 1-2. Each lamina consists of carbon fibres embedded in a polymeric, e.g. epoxy resin, matrix. The laminae are stacked one on top of another with the fibres oriented at different directions to form a laminate. By changing the fibre orientation the laminate is able to carry load in specific directions.

An accumulation of damage, on a micromechanical level, often occurs before final failure of CFRP composites. This damage is usually a complex combination of matrix cracking, fibre/matrix interface debonding, fibre pull-out, fibre-bridging, and fibre breakage within the lamina, and delamination between the laminae (Figure 1-3). The amount, type and sequence of these damage mechanisms are dependent on the type of loading and are intimately related to the properties of the constituents. All of these mechanisms may increase the laminate fracture resistance by aiding the dissipation of stress concentrations at crack tips, and by absorbing energy in their own right. It is therefore important to study the accumulation of damage and its effect on the degradation of the composite to understand failure in these materials.

The Notch Sensitivity of Composite Laminates

The notch sensitivity of composite laminates has been an area of extensive research for the past 30 years. Notch sensitivity is defined as the extent to which the propensity of a material to fracture is increased by the presence of a surface inhomogeneity such as a notch, crack, scratch or a sudden change in section. Low notch sensitivity is often associated with ductile materials, and high notch sensitivity with brittle materials.

In ductile metals, usually considered to be tough materials, a notch can increase the apparent yield strength (and in some cases the ultimate tensile strength) of the material. This is because a triaxial

state of stress develops at the notch tip that will constrain any plastic deformation and slow the spread of plasticity [3]. By comparison, in carbon fibre reinforced composites with quasi-isotropic stacking sequences a hole or notch can reduce the UTS by half [4].

If a material is notch-insensitive, then the strength of the material will only be affected because the notch is reducing the net section area of the material. On the other hand, a material may be considered notch-sensitive if the notched fracture strength shows a greater reduction, for instance, a square root dependence on the notch length as predicted by linear elastic fracture mechanics (LEFM), Figure 1-6.

The Fracture Process Zone

In composite materials, the notch sensitivity can be affected by various sub-critical damage mechanisms that take place in the fracture process zone (FPZ), an area of discontinuous damage ahead of the notch tip. These damage mechanisms include matrix cracking, fibre debonding, fibre pull-out, fibre breakage and delamination.

The use of a FPZ concept was pioneered for cementitous materials [5]. Recently, the same concept has been applied in detail to notched composites with the view that it is the analogue of the plastic zone in metallic materials [6]. Metals develop a plastic zone in front of a notch or crack tip that may strain harden or soften under an applied load. Crack growth in metals is can be termed 'self-similar', as growth is in the same plane as the notch or crack. Energy is absorbed in creating new surfaces, by shear yielding or plastic flow, hence the term 'plastic zone' (see Figure 1-4). Short fibre composites behave in a similar manner to metals in that crack propagation is reasonably 'self similar', although damage zones are often larger due to the crack being inhibited by the fibres (Figure 1-5). The main reason why comparisons have been made between cementitous materials and composite materials is that they both show a non-linearity of the process zone due to microcracking and fibre bridging [7].

It is thought that the process zone in composites may modify the notch tip stress concentration and impede ensuing catastrophic failure of a structure [6].

Modelling Notched Fracture Behaviour

The use of LEFM has been particularly successful when analysing notched behaviour in metals. However, there are obvious differences when comparing crack propagation in metals to crack propagation in composites. Therefore when directly applying fracture mechanics to analyse through-thickness cracks in composite laminates results have been varied [8].

For instance, early work [9] to investigate the notch sensitivity of advanced composite materials employed LEFM to attempt to explain why, when notched, their tensile fracture strength tends to decrease as the hole size increases. This is commonly referred to as the "hole size effect". The assumption was made that intense energy regions existed at the sides of holes in centrally notched coupons. These regions were modelled as cracks with a length, a, emanating from sides of the holes perpendicular to the load. This approach gave a reasonable correlation to the data, however, the crack length a, was not constant for all hole sizes [10].

A strict LEFM approach predicts failure based on the stress intensity at the notch tip, however it does not account for the fact that in reality stresses do not become infinite at a crack tip. For example, in reality, in a notched metallic specimen the plastic zone acts to keep the crack tip stresses finite [11]. As long as the plastic zone is small compared to the other specimen dimensions, LEFM works well. In a laminated carbon fibre/epoxy composite specimen, sub critical damage mechanisms occur and a 'process' zone develops. However, the simple application of LEFM does not appear to work for CRFP laminates.

Kortschot and Beaumont [12] highlight the problem, using calculated notch-tip stress distributions in notched strength models. They applied the same tensile stress to two double-edge-notched

(DEN) specimens, of the same geometry but different lay-ups, $[90/0]_{2s}$ and $[90_2/0_2]_s$. Predictions using two-dimensional elasticity theory would indicate that the notch-tip stress distributions should be the same for a given applied stress. However, radiographs clearly indicated that this was not the case. More 0° ply splitting in the $[90_2/0_2]_s$ laminate, tended to isolate the load-bearing 0 degree fibres from the stress concentrating effect of the notch. This led to a 50% strength increase over the $[90/0]_{2s}$ specimen. Figure 1-7 shows their interpretation of splitting and delamination.

Much research has been carried out to investigate a common model for the notched strength of laminated composites [8, 10, 13-19]. Many (but not all) recognise that there is a need to account for the process zone, and try to do so by using a characteristic parameter or by trying to physically describe the local failure mechanisms.

Whitney and Nuismer [10] proposed two criteria that use a characteristic parameter for predicting the strength of laminates with through-thickness discontinuities. Their point stress criterion assumes that failure occurs when the stress at a characteristic distance ahead of the hole reaches the tensile strength of the un-notched virgin material. Their average stress criterion is similar but assumes failure when the average stress over a characteristic distance in front of the notch reaches the un-notched strength of the material. They account for the hole-size effect by proposing that the stress concentration around a larger hole is not as localised as that for a small hole (see Figure 1-8). Their model was fine tuned by Pipes et. al. through a strength superposition method [14]. One of the problems with these types of models is that the characteristic lengths are often different for different size notches in the same type of laminate, which might be because sub-critical damage at the notch tip is not accounted for [17].

Mar and Lin [13] also attempted to use a fitted parameter to investigate the hole size effect, calculating their parameter from the elastic constants of the fibre and matrix. Work by Lagace [15]

suggested that the Mar–Lin method provides a better correlation for tensile fracture stresses in carbon/fibre epoxy laminates than the point stress criterion.

The notch size effect was investigated by Kortschot and Beaumont [8, 12, 20, 21] with an emphasis on understanding how the notch-tip stress field was affected by sub-critical damage mechanisms. They were able to yield a relationship between the sub-critical damage and the notch-tip stress distribution, by directly modelling the delamination and splitting zones (see Figure 1-7), observed using radiography in double-edged notched (DEN) specimens. These stress distributions are considered important as they control the rupture of the 0° plies. A failure criterion was subsequently developed to predict notched strength. Their approach was to define a terminal damage state (TDS) as the extent of cracking immediately before failure, and incorporate this into a finite element model (FEM) to ascertain the in-plane stress distribution at the notch tip [12]. Not surprisingly, they found that the notch tip stress concentration was reduced as the delamination height and split length in the TDS increased; this in-turn increased the fracture strength. This was found not to be dependent on specimen width, lay-up or notch length.

Another avenue of thought was introduced by Hillerborg et. al [16] in the mid-nineteen seventies. Referred to nowadays as the damage zone model (DZM) [17] it attempts to model the collective damage (delamination, matrix cracking, fibre breakage etc.) as a fictitious crack akin to a "Dugdale model" [11, 16-18] (see Figure 1-9). Figure 1-10 shows how damage growth is represented by crack opening, and as a reduction of the cohesive stress.

When the stress at the tip of the fictitious crack reaches that of the un-notched material the crack will grow further into the laminate. The stress at point A is assumed, not to instantly fall to zero, but decrease linearly with an increase in crack width as shown. This linear relationship is assumed, as it is difficult to calibrate the stress-crack opening curve.

It is not often feasible for economic reasons to run full-scale tests of large structures. Therefore smaller geometrically similar specimens are sometimes used to help gain an understanding of how large structures may fail. Bažant et. al. [22] have investigated the suitability of a previously developed size effect law for graphite/epoxy laminates. Known as a size effect law, it has been verified for concrete, rocks and toughened ceramics, which are all materials where LEFM is not directly applicable. Their work showed that the nominal strength of composite laminates exhibits significant size effect in composite laminates that are geometrically similar but of different sizes. The size effect law incorporates a characteristic dimension, in this case the specimen width, and is used to scale the nominal strength of the various size specimens.

The Strain Softening Approach

Strain or work hardening is a familiar concept in the metals industry, where an increasing resistance to plastic deformation occurs as deformation proceeds by either slip or twinning. The metal becomes harder and stronger until it reaches a stage where deformation is no longer possible and an increase in stress will only cause fracture. Conversely, if a material exhibits a response that shows a post-peak region defined by a decreasing stress with increasing strain, this is then referred to as a strain softening response. However, the strain softening concept has been criticised and questions concerning its validity as a *material* response have arisen. Kongshavn and Poursartip [6] note that the post-peak region of the strain softening curve is unstable as the work done for an increment of strain, $\partial\varepsilon$, is obviously negative as $\partial\sigma$ is less than zero. Composite materials cease to be a homogeneous continuum after a certain amount of damage is grown (voids and holes are present), and stress and strain are parameters that apply to bodies that are homogeneous continuum. Concerns of violating basic principles can be avoided if a stress-displacement, rather than a stress-strain curve is considered and we state that there is a characteristic dimension at which the material

acts homogeneously. Strain softening should be considered a laminate property, and is particular to a given material system and loading.

None-the-less, of the many approaches that may be used to predict the notched behaviour of S/RFI materials, the strain softening approach seems to have great potential, as it takes into account the FPZ. The response itself can be described, using Continuum Damage Mechanics (CDM), as the deterioration of mechanical properties due to accumulation of damage. This is accounted for by an effective stress based on an equivalent undamaged area.

A typical strain softening curve can be seen in Figure 1-11. An initial linear elastic behaviour becomes non-linear at damage onset, point B. At point C the FPZ is subjected to high local displacements and the damaged material has to discard load to surrounding undamaged or less damaged material.

In the early nineties Matzenmiller et. al [23] produced an anisotropic damage model based on CDM, known as the MLT model. They defined the shape of the strain softening curve by introducing a damage variable that was based on a Weibull function, as shown in Figure 1-12.

The importance of a physical understanding of damage evolution was stressed in experimental work carried out by Kongshavn and Poursartip [6] on quasi-isotropic carbon fibre/epoxy laminates and woven carbon fibre/epoxy sandwich panels. Their work was used to calibrate a finite element model (FEM) that incorporates a strain softening response. They were interested in studying stable damage growth that included fibre failure, and so developed an over-height compact tension (OCT) specimen. In the past it has been necessary to use large specimens to investigate fibre failure, however, their geometry allowed for the development of a reasonably sized process zone suitable for post-test damage analysis in a small specimen.

Improving Damage Resistance in CFRPs

Recent research to improve the damage resistance of CFRP composites has focused on several approaches. These are, matrix toughening [24-29], through-thickness reinforcement [1, 2, 28, 30-61], interface control [62] and the use of delamination arrestors [63].

Matrix toughening involves the replacement of the often hard, brittle matrix with a tougher resin system. Toughened epoxy resins and thermoplastics such as polyimides, polyamides (nylon), polyetheretherketone (PEEK) and polypropylene sulphide have allowed a significant improvement in interlaminar fracture toughness[1], up to an order of magnitude over traditional epoxy systems.

Through-thickness reinforcement, such as stitching, produces a 3-D structure that acts to reduce delamination, pinning the laminae firmly together without greatly altering the laminate structure and without extensive modification of the fabrication process. However, it is possible that inhibiting delamination altogether may increase the notch sensitivity of composite laminates.

Improved interfacial properties and bonding of fibre composites with the matrix material may be achieved by coating the fibres with a thermoplastic. A micro-ductile layer is formed at the fibre/matrix interface that can function as a stress relief medium, reducing compressive stresses caused by matrix shrinking during processing. These coatings may also act as crack inhibitors or arrestors assisting large debonding and fibre pull-out, hence increasing the composite toughness.

Delamination arrest can be achieved using tough low modulus adhesive strips embedded in the interior of the laminate. Ductile adhesive layers between laminae allow for plastic deformation. It is

[1] The interlaminar fracture toughness (IFT) quantitatively characterises the resistance to delamination in terms of critical strain energy release rate, G_c, which in turn represents the total energy absorbed per unit of delamination crack advance area. [79, 80]

thought that suppression of delamination crack propagation is achieved as interlaminar stresses are reduced and edge delamination is arrested.

Reinforcement using Through-thickness Stitching

The aerospace community has undertaken a great deal of research in recent years to investigate ways to reduce material processing costs and improve damage resistance in 2-D composites. Stitching with steel, carbon, glass and Kevlar® in the through-thickness direction has been of great interest. Although a great deal of work has been conducted on stitched composites, many studies contradict each other with respect to the advantages and disadvantages of through-thickness reinforcement on in-plane properties. Mouritz and Cox [33] point out that some researchers report degradation of strength, stiffness and fatigue properties, while others find little or no difference at all when comparing stitched to unstitched counterparts.

The Uses and Advantages of Stitching

Since a secondary process is used to insert the through-thickness yarn after lay-up, stitched CFRP laminates do not have integral 3-D fibre structures like weaving, knitting and braiding. For this reason they have improved interlaminar fracture properties, as well as good in-plane strength and stiffness [30]. Some of the uses and advantages are:

1. Stitching may be cost-effective as a method of joining fabric cloths by stitching along the preform edges; this improves the ease of handling prior to liquid infusion or moulding.

2. It can be used to join composite structures, providing improved in-plane and through-thickness strength, in particular the joining of I-beams to flat composite panels. This is an advantage as the various structural parts can be joined together prior to the resin infusion stage, removing the need to drill and bolt the various parts together with

traditional mechanical fasteners. By removing the need for post processing, manufacturers can prevent any resulting damage that may occur.

3. It provides improvements to interlaminar fracture toughness and low velocity impact damage tolerance [30].

Disadvantages of Stitching: Damage during Fabrication

Much like stitching of household fabrics, a needle must be used to perforate the material to be stitched. In the case of CFRP, this is usually a prepreg[2] laminate or fabric preform that is stitched with a high tensile strength yarn. One of the main disadvantages with the stitching process is that localised fibre damage often occurs as the needle passes through the prepreg or preform. Fibre breakage is unavoidable with approximately 0.5% of fibres being damaged during the process [30, 36]. Stitching a prepreg material may impart more damage than stitching a preform due to the high viscosity of the resin in the prepreg. Alternatively, stitching a preform is thought to result in less fibre damage due to absence of the resin, since the stitching needle can easily be pulled through the lamina [30, 32, 34, 36, 50]. However, processing of preforms requires one extra production step to impregnate the resin before curing. Yarns of differing diameter may be used although the size of yarn will affect the amount of fibre breakage. Fibre spreading around the stitching may also be a problem as composite materials are very orientation dependent, and spreading will force the fibres to be directed away from the angle that they were placed.

Fabrication of Stitched CFRP Composites by Resin Film Infusion Process

Resin film infusion (RFI) is a liquid moulding technique that is essentially a variation of resin transfer moulding (RTM), and has been designed with reduction of processing costs in mind. The

[2] "Prepreg" - short for pre-impregnated. For example, carbon-fibre pre-impregnated with resin, often cured to the B-stage (slightly advanced cure to provide tack and stability), ready for molding or lay-up.

tooling costs and weight of the mould are considerably reduced, as quite often only a single sided tool is required [64-66]. Figure 1-13 shows the basic lay-up for the RFI process. A resin film is laid up on the lower tool and the structural stitched preform is laid on top. A caul plate or tool is then assembled and the whole set-up is vacuum bagged. A vacuum and/or autoclave pressure is applied along with a heat/cure cycle, to allow the resin viscosity to lower and diffuse in to the preform [66]. RFI can be adapted for unidirectional or woven fabrics in the production of, curved or flat, monolithic or sandwich type structures [65]. Figure 1-14 shows a large stitched preform being lowered onto a tool containing resin film.

Mechanical Properties of Stitched Composites

There has been a large amount of mechanical property data published on stitched composites. Some of this research has tried to assess the suitability of stitched composites for various applications such as fuselages, wing panels, I-beams and automotive components [33].

Work carried out by many researchers has mainly used double cantilever beam (DCB), end-notch flexure (ENF) and end-notch cantilever (ENC) tests to investigate the delamination resistance in stitched materials. Many of these studies examine the effects of various stitching parameters such as stitching density, thread type and thread diameter on the mechanical properties of the laminate.

Points from the Literature

From the cross-section of literature reviewed it is apparent that there is a wide variation of results gained by different researchers and for different material systems. Many of these studies do not seem to take thickness effects in account, and often directly compare the unstitched as a baseline for the stitched material. All of the research carried out seems to agree that processing/stitching parameters are important. These parameters include type of composite (resin type, fibre type, and lay-up configuration), stitching conditions (thread type, thread diameter, stitch pattern, stitch density, stitch

tension) and loading conditions. It seems that testing in-plane tension has not been addressed in any great detail.

To demonstrate this wide variation of results, a short outline of some of the main points that can be drawn from current literature on stitched composites is presented below:

- Research to determine the in-plane tensile properties of stitched composites has been mainly concerned with un-notched specimens such as the dog-bone and small tabbed tensile tests [42, 47, 55, 67, 68]. Their results show that stitching has the effect of improving or degrading the tensile strength by less than 15-20%, with the density of stitching having little effect [33]. It is possible that the tensile strength may be adversely affected by the in-plane kinking of fibres or the damage caused to fibres during stitching.

- Open-hole tensile strength has not been well reported. One study referred to by Mouritz [33] reveals that stitching degrades the open-hole tensile strength by up to 56% depending on the areal density of stitching (with the worst case being 1 stitch/10 mm^2). Notched strength does not seem to have been researched, and this seems remarkable when considering the importance of notched strength to the aerospace industry.

- Compression-after-impact (CAI) strength is the most extensively studied mechanical property of stitched composites [30], and also seems to be one of the most controversial. Stitching has been reported to both reduce the CAI strength of CFRP [2], improve [1, 39, 41, 52, 68] and also reported to have not affected it at all [30]. A decrease in compression strength has been attributed to in-plane fibre misalignment caused by stitching [2]. It has also been suggested that kinking of the outer ply fibres due to the stitch surface loop causing spreading and breakage of the surface fibres during fabrication, may reduce the CAI strength[60, 69]. To examine this idea a discontinuously stitched composite was produced

[60] by machining off the surface loop from a stitched composite. This increased the compression-after-impact strength, based on the cross sectional area of the 0° fibres, by 14% over a continuously stitched specimen of the same material. Therefore it was proposed that there is no negative effect of using a discontinuous stitching over continuous stitching.

- Laminated structures often exhibit poor interlaminar properties and are susceptible to delamination should they be subjected to interlaminar stresses. Stitching can increase the Mode I and Mode II fracture toughness of a laminate, characterised by critical strain energy release rates, G_{Ic} and G_{IIc}, by 15-30 times [28, 37, 40, 41, 43, 46, 47, 51, 53, 68, 70-72] and 5-15 times [38, 51, 53, 59] respectively. Interlaminar Shear strength (ILSS) either slightly increased [31] or decreased [73], depending on the material system. In the case of Mode I interlaminar fracture toughness, several studies seem to agree that as little as 1 vol. % of through thickness fibres can create a five to twelve-fold increase in laminated materials [28, 37, 40, 41, 43, 46, 47, 68, 70, 71].

- Delamination area after low velocity impact loading has been shown to both increase [52] and decrease [73] as stitching density increases. The stitching pattern has been shown to be not as critical as the stitching density [73]. Presumably there must be an optimum stitching density that was not reported in this study, as 'over-stitching' would result in degradation of the composite by compromising structural integrity.

- A slight reduction in fatigue life was reported when a stitched glass-reinforced polymer laminate was compared to an un-stitched standard in zero-to-tension cyclic loading [55]. However, in compressive cyclic loading the stitched GRP faired quite well. The reduction in fatigue life was again attributed to damage to the glass fibres during the stitching process and fatigue failure of the stitch/GRP interfaces. In a separate study [31] on fatigue of

Kevlar®/epoxy prepreg stitched with Kevlar® it was found that stitching can improve the damage tolerance and increase fatigue life of the composites.

- Flexural properties were reduced slightly for stitched GRP [56, 73]. This was once again attributed to the stitching process damaging fibres, and stress concentrations in the form of stitch knots that promote damage at low flexural stresses [73]. In the case of stitched sandwich panels [34], flexural properties were found to increase. Although stitching did not affect the load at which core failure occurred, an overall increase in applied maximum load was obtained and the energy absorption in flexure also increased as a result of through thickness stitching.

Statement of Work

It is obvious that there are many conflicting opinions when it comes to the benefits of through-thickness reinforcement of CFRP material. Therefore the objectives of this work are to:

- Investigate what effect the introduction of stitching may have on the in-plane crack growth behaviour of R/FI materials, using the OCT specimen developed by Kongshavn and Poursartip [6].
- Further validate the OCT specimen as a suitable geometry for investigation of notched laminate behaviour.
- Gain a physical description of damage evolution in these materials, allowing for more accurate physically based inputs to a continuum damage mechanics strain softening model.

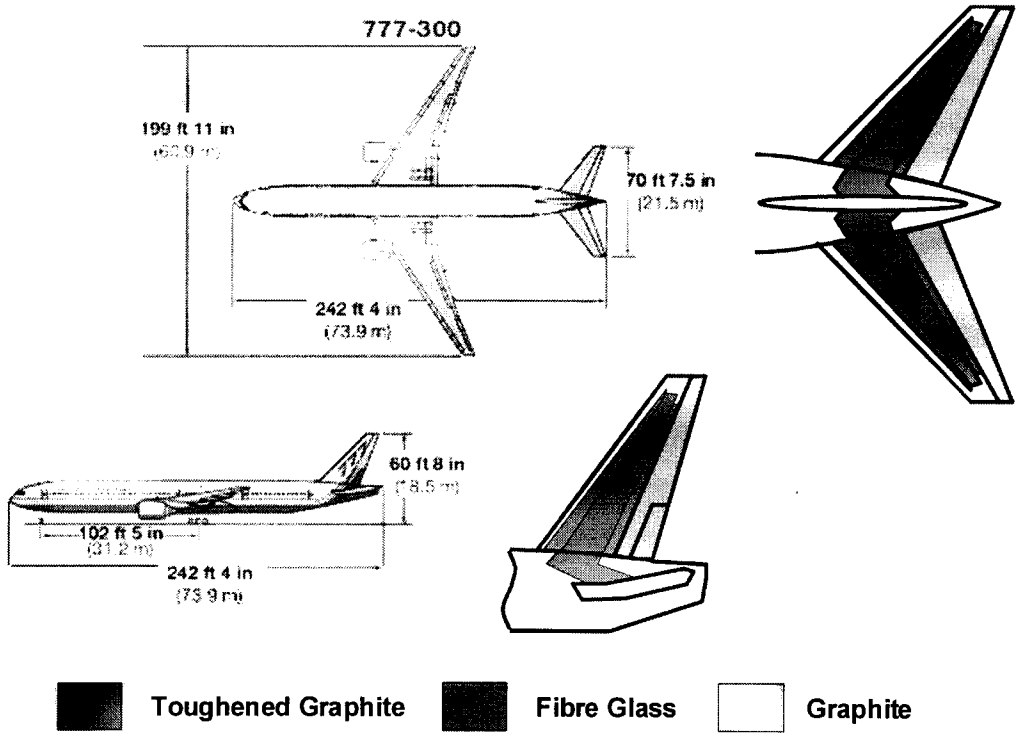

Figure 1-1: Schematic indicating composite structural parts of Boeing 777 tail.

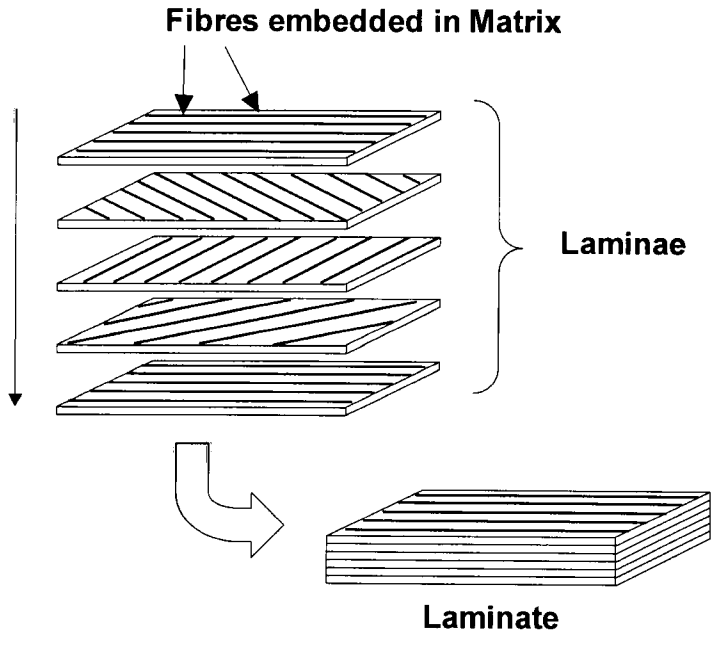

Figure 1-2: Schematic of a fibre reinforced laminate.

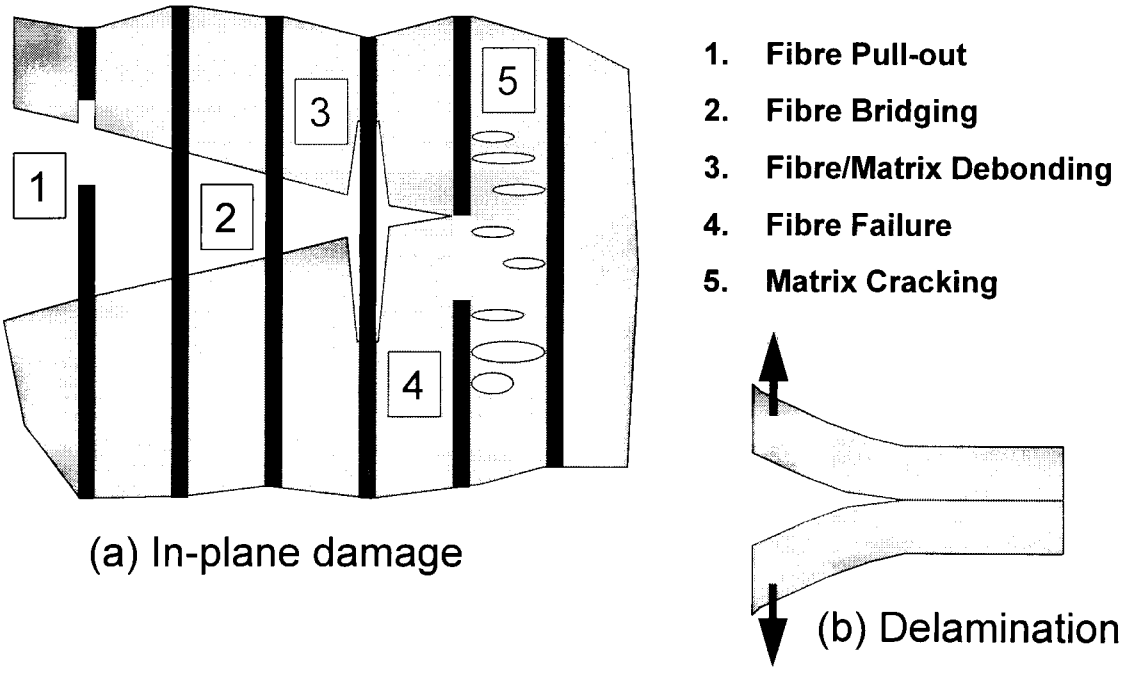

Figure 1-3 Damage mechanisms in CFRP materials

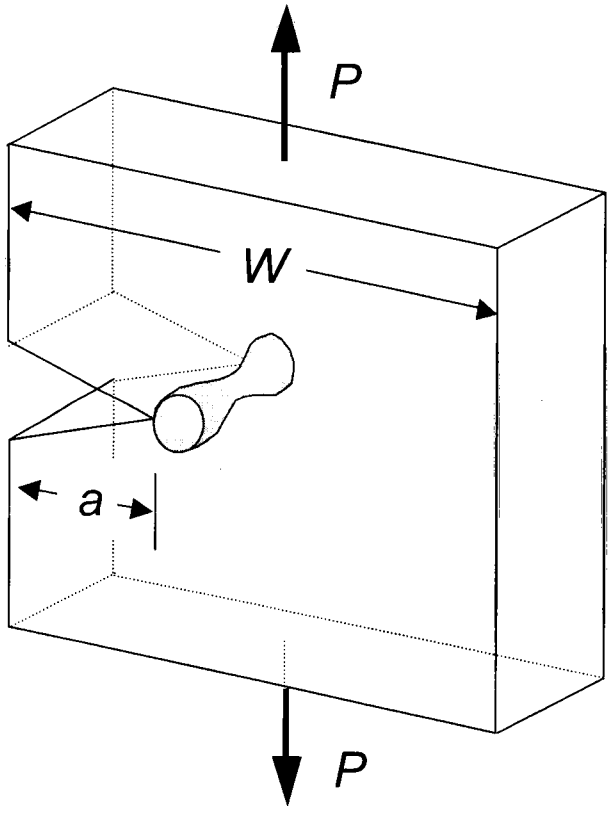

Figure 1-4: Plastic zone in metallic materials, where a, is the crack length.

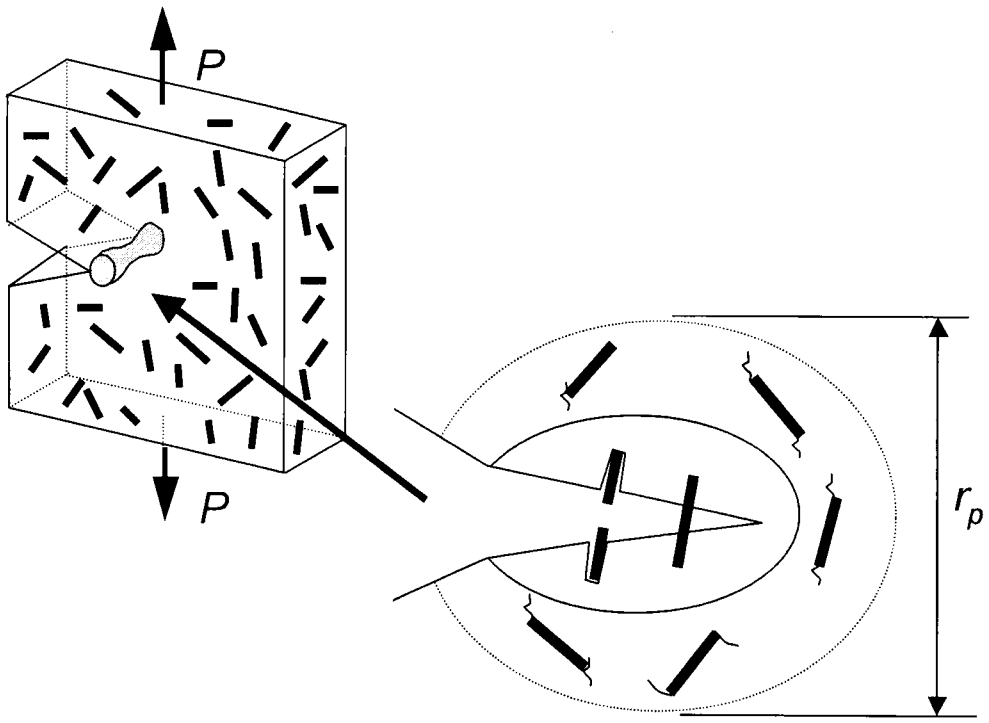

Figure 1-5 Process Zone in short fibre composites, where r_p is the size of the process zone

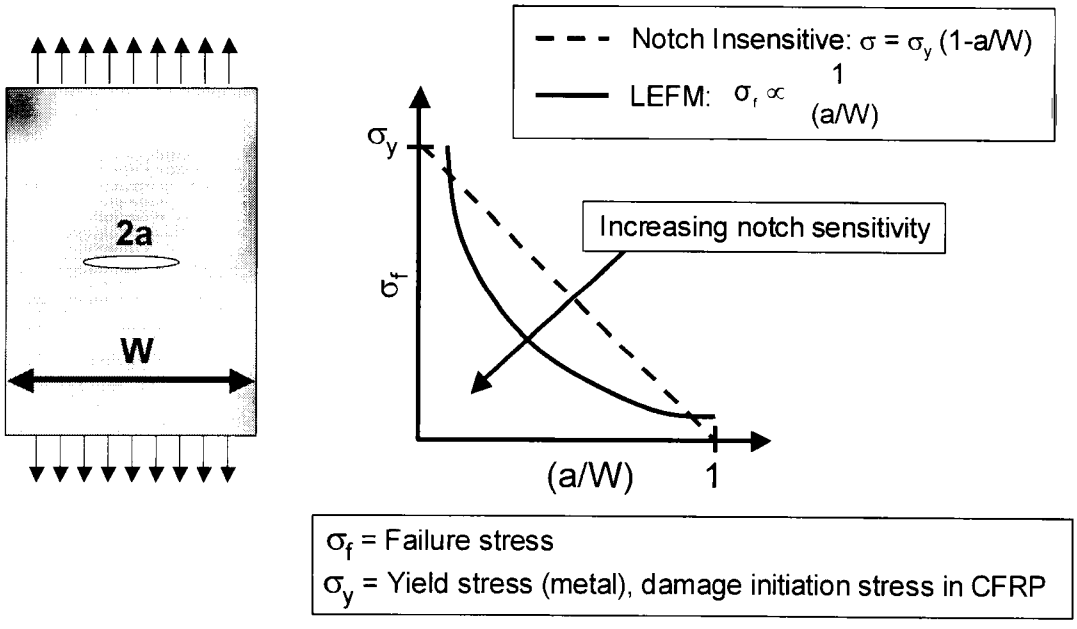

Figure 1-6: Schematic of failure strength vs. notch length (a/W) indicating increasing notch sensitivity.

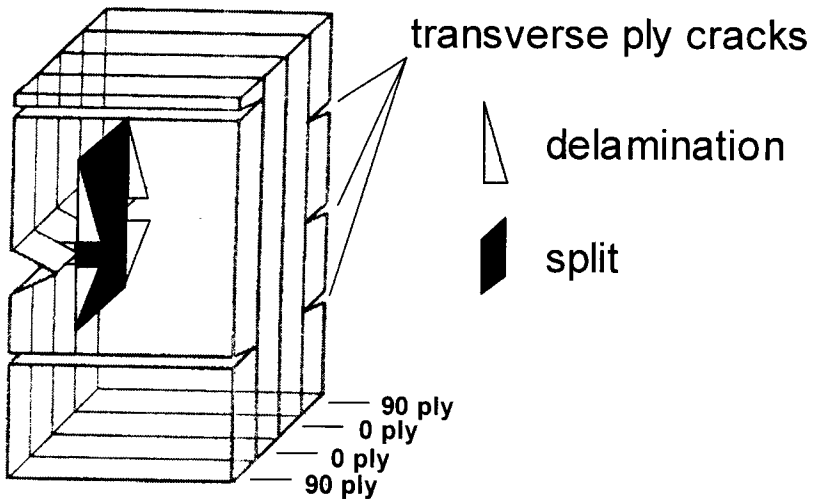

Figure 1-7: Diagram showing 0° ply splits and 0/90 delaminations in a $(0/90)_s$ laminate, adapted from [8].

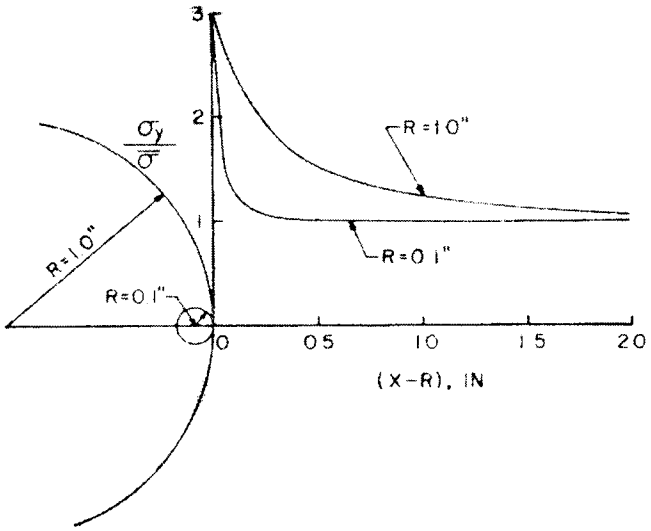

Figure 1-8: Stress distribution for a hole in an infinite isotropic plate [10]

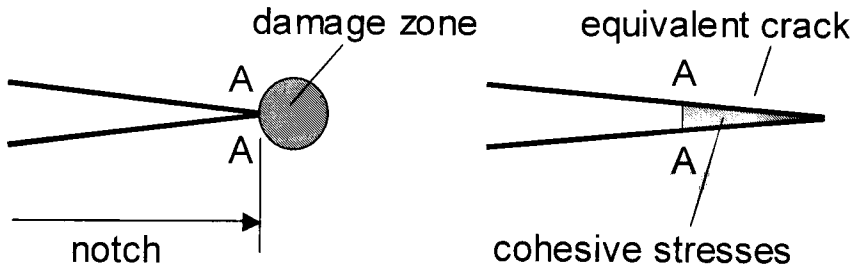

Figure 1-9: Damage zone and equivalent crack used in the damage zone model, adapted from [17].

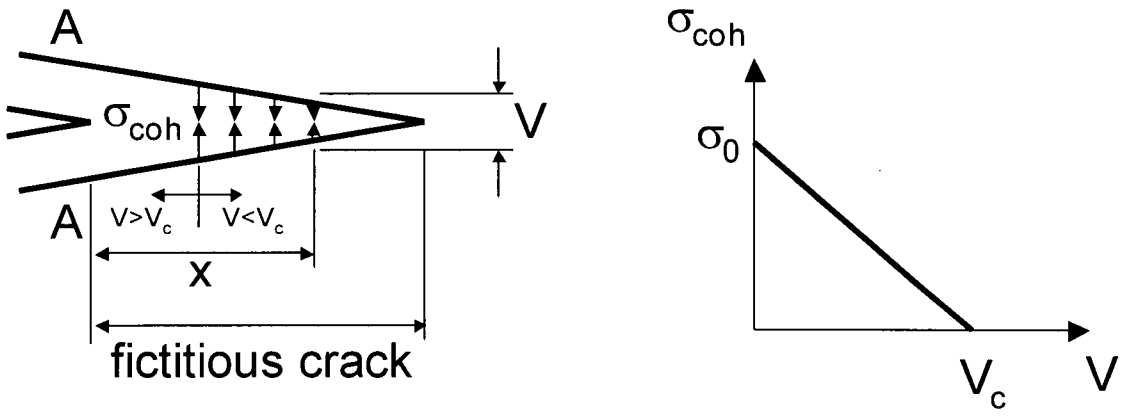

Figure 1-10: Schematic representation of Hillerborg's fictitious crack model and the stress distribution in the fracture process zone. The notch will grow when the maximum stress at the tip of the fictitious crack reaches the un-notched tensile strength. Adapted from [17].

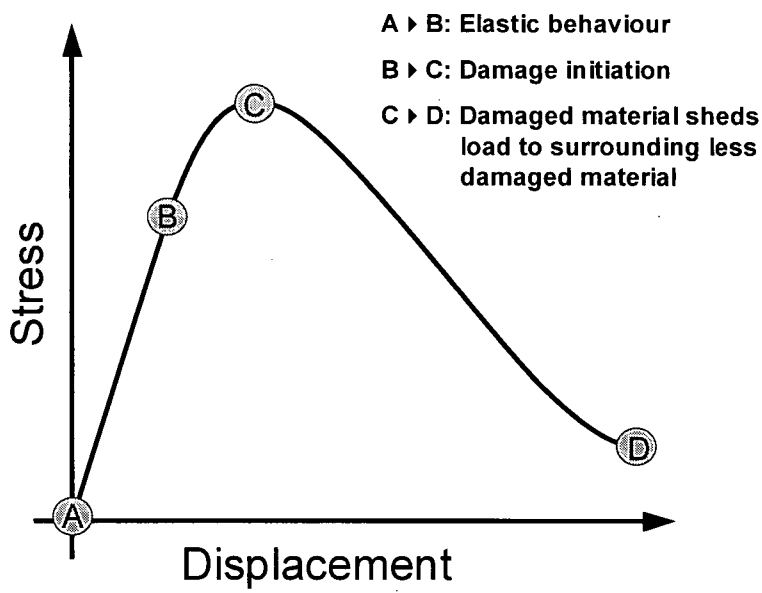

Figure 1-11 Typical strain softening curve, displacement used instead of strain

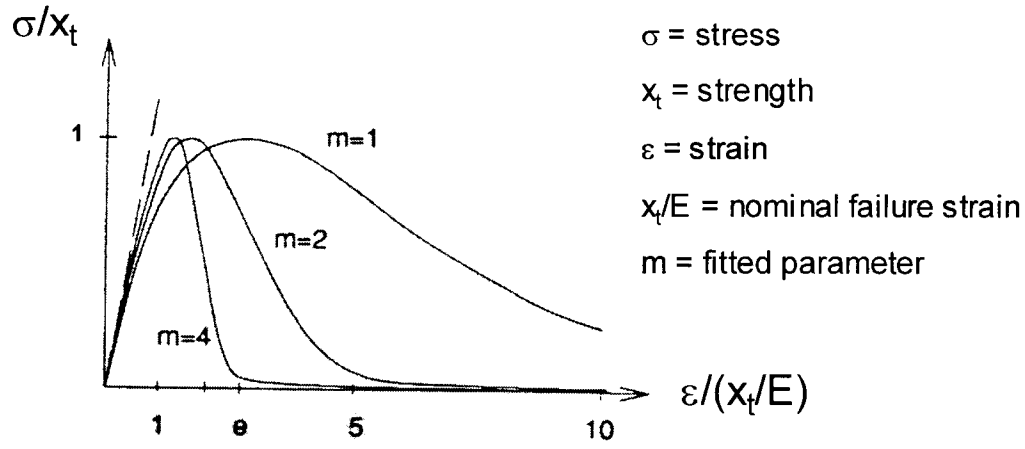

Figure 1-12: Strain softening curve for uniaxial loading [23], based on Weibull distribution of fibre failure. The fitted parameter, m, predicts different degrees of strain softening.

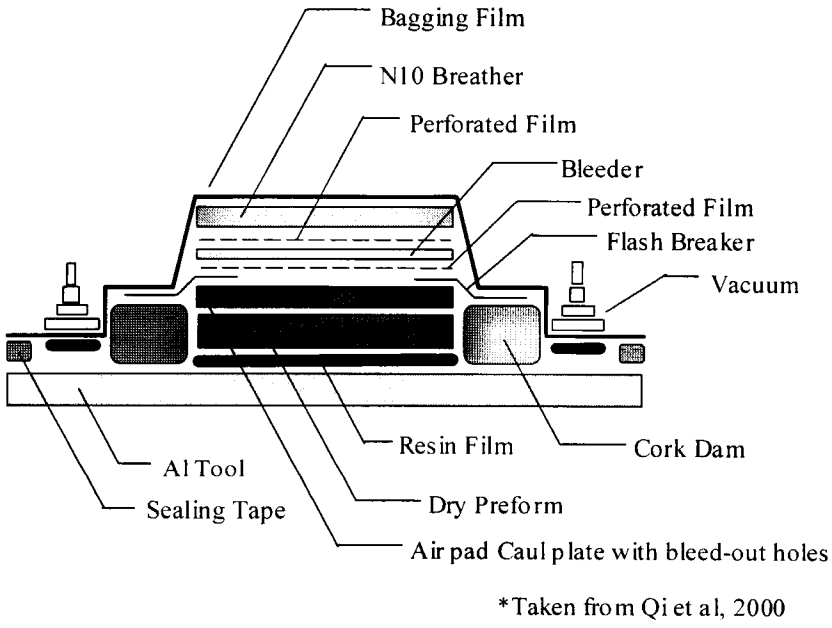

Figure 1-13: Basic R/FI Lay-up with a single sided tool

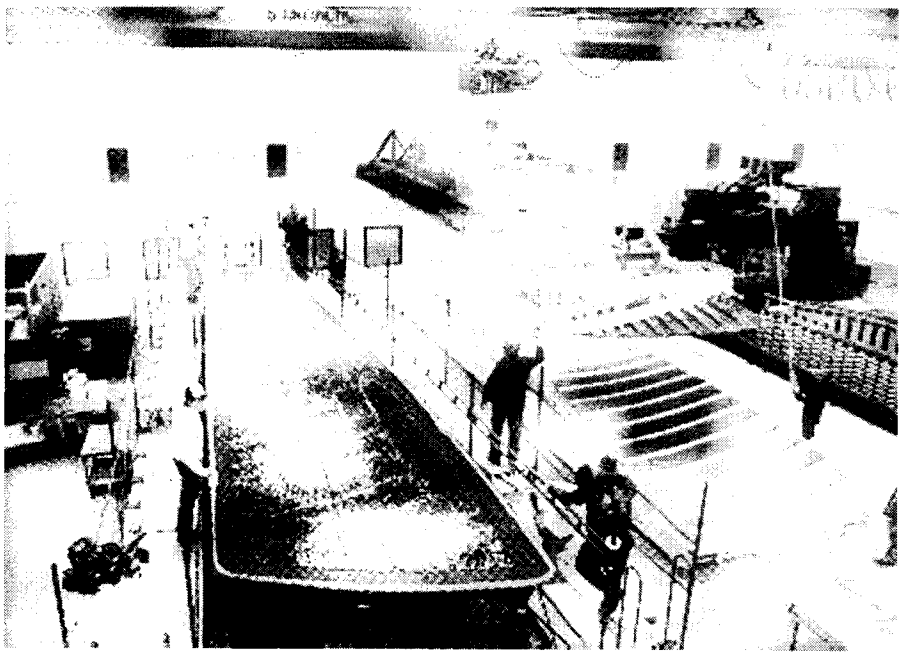

Figure 1-14: Stitched Preform being lowered onto tool containing resin film [66].

Chapter Two

Experimental Method

2. Experimental Method

An overheight compact tension specimen (OCT) initially developed by Kongshavn and Poursartip [6] was modified to study the notched behaviour of stitched and unstitched carbon fibre reinforced composites. This chapter provides details of the experimental method used in this study.

The Overheight Compact Tension (OCT) Specimen

As discussed previously, many studies on stitched materials have been undertaken. However, little or no in-plane crack growth work has been carried out, probably because it is difficult to get a crack to grow sufficiently to allow for any kind of post-test analysis in small specimens.

The compact tension (CT) specimen has been widely used to investigate the notched fracture behaviour of metallic materials. This is often because, as the name suggests, it allows for small specimen size, and therefore material waste is kept to a minimum. This is the reason that this specimen geometry was investigated by Kongshavn and Poursartip [6], who were interested in studying stable damage growth which included fibre fracture. Their research required a process zone (the area of discontinuous damage ahead of the notch tip) of reasonable size for post-test analysis. After initial testing, the standard CT specimen was modified to overcome problems associated with damage to the loading arms, by increasing the specimen height to twice the specimen width (the standard CT specimen height is approximately equal to the specimen width). Theirs was an empirical approach to finding a successful working geometry, and as the geometry worked for the material system that they were testing no further development was attempted.

Stable Damage Growth

The Griffith criterion for crack growth (e.g. Broek [11]) considers an infinite cracked plate of unit thickness with a central crack (of length $2a$). The plate is stressed to a stress σ and fixed at its ends.

As the external load cannot do any work, the energy for crack extension must be delivered by the release of elastic energy. Thus following condition for crack growth must be met:

$$\frac{dU}{da} = \frac{dW}{da}$$

where U is the elastic energy and W is the energy required for crack growth. From this, Griffith calculated dU / da (per unit plate thickness) using stress field calculations for an elliptical flaw:

$$\frac{dU}{da} = \frac{2\pi\sigma^2 a}{E}$$

where E is the Young's modulus. Quite often dU / da is replaced by G, referred to as variously as the 'strain energy release rate', 'the elastic energy release rate' or 'the crack driving force':

$$G = \frac{dU}{da} = \frac{2\pi\sigma^2 a}{E}$$

Conversely, the energy consumed during crack propagation is:

$$R = \frac{dW}{da}$$

R is referred to as the crack resistance. It is often assumed that the energy required to produce a crack is the same for each increment of da, thus reporting R to be a constant[3]. Consequently, for crack propagation to occur G (the crack driving force) should be at least equal to R (the crack resistance), which is a constant and thus G must exceed a critical value referred to as G_{Ic}.

All of the tests performed in this and previous studies were conducted under displacement control. During crack extension, load drops are observed that may cause G to drop below R. If this is the

[3] The reader is referred to standard LEFM textbooks [e.g. Broek [11]] for discussion of cases where R is not constant; and other more complicated fracture problems.

case then the crack will be arrested and the specimen geometry is exhibiting stable crack growth.

Further OCT Geometry Development for R/FI Material

For the stitched R/FI material system used in this study, further development of the OCT geometry was required. Preliminary OCT experiments performed with the same geometry as Kongshavn and Poursartip showed signs of specimen twisting and crushing at the loading pin-holes. Loads measured in this material were typically two to three times higher than those seen previously. In this work, specimen twisting was controlled using steel stiffeners lined with Teflon® at the back end of the specimen. Also, to overcome crushing the loading pin diameter was doubled to allow for a more even distribution of load. Figure 2-1 shows the schematic of the modified OCT geometry, as developed and used in this study.

OCT Experimental Set-up & Test Procedure

Measurement of Load and Crack Mouth Opening Displacement

All of the OCT tests were conducted using an Instron universal testing machine with an 88.96 kN (20,000lb) load cell. The specimens were quasi-statically loaded at a rate of 0.508 mm/min through the loading pins under displacement control. Under displacement control a fixed displacement is applied producing a resultant load[4]. Figure 2-2 shows the experimental set-up (note the steel 'stiffener' or 'guide' on the right). Figure 2-3 is a photograph of the loading jig in the Instron testing frame. A safety shield was erected in front of the test fixture with a hole machined in the centre to ensure a clear field of view for the camera (see below).

The crack mouth opening displacement (CMOD) was measured using an Instron 2620-825 strain gauge extensometer (±5 mm range) that was attached across the notch opening. Small slots were cut

[4] If we were using load control, a fixed load would be applied , which would result in a displacement that would be dictated by the compliance of the system.

into the end of the specimen either side of the notch opening to accommodate the blades of the CMOD gauge. The gauge was held in place with elastic bands attached to the blade hooks and secured to the loading pin bolts (Figure 2-3).

Load and CMOD (displacement) data was captured using a personal computer equipped with an A-MIO-16E DAQ card and Labview data acquisition software. The captured data was then plotted as load versus displacement using Microsoft Excel.

Measurement of Displacement in Front of the Notch Tip

By inscribing lines on the specimen at intervals of 2.5mm above and below the notch tip with a metal scribe, it was possible to measure the displacement in front of the notch tip. Inscribing lines in this way will damage some surface fibres but this does not effect test results or damage growth patterns. Photographs were taken before loading and at regular intervals during the tests using a NIKON F-601 camera. This was mounted on a tripod in front of the test fixture and was equipped with a NIKON AF 105 mm macro lens. A KODAK Professional T400CN, black and white film (developed using a colour process) was used exclusively throughout testing. After processing, the 152×203 mm (6×8 inch) photographs were scanned using an HP Scanner at a resolution of 300 dpi. An in-house image analysis program was then used to measure the displacements of the lines ahead of the notch tip. For example, photograph number 1 taken prior to testing was compared with other photographs taken throughout the experiment.

Material under Investigation

This study concentrates on two resin film infused (R/FI) carbon fibre (mixture of standard and intermediate modulus fibres) – epoxy resin (3501-6) laminates manufactured by The Boeing Company, Seattle, Washington, USA. One system contained through thickness reinforcement, the other did not and was used as a baseline. Both systems had a lay-up of $[+45/-45/0_2/90/0_2/-$

45/+45] for one sub-laminate (or stack). For the purpose of this thesis, the material systems will be described as 'Unstitched' and 'Stitched'. The elastic properties of this material were obtained from standard quasi-static tests and are listed in Table 2-1.

Two different thicknesses of unstitched material were examined, with 4 and 6 sub-laminates (herein referred to as 4-stack and 6-stack). The stitched material is essentially the same as the unstitched material, however through thickness reinforcement has been incorporated prior to infiltration in the form of Kevlar® stitching. Three different thicknesses of stitched material were examined with 4, 5 and 6 sub-laminates (herein referred to as 4-stack, 5-stack and 6-stack).

All specimens were cut to size (approx. 207mm × 104mm) from a larger panel with a diamond disc saw. They were then notched with a band saw giving a relatively blunt notch tip. Holes for the loading pins were cut with either a carbide tipped hole saw or a diamond hole drill. All specimen dimensions are given in Table 2-2.

A Note on Baseline Materials

There seems to be some disagreement between researchers when discussing the effect of stitching on the thickness of the processed specimen [2, 33]. Obviously any change in thickness or compaction will have an effect on the elastic modulus, E, and the overall fibre volume fraction, V_f. Reeder [2] states that introducing stitching will increase the thickness of the laminate, however, Mouritz [33] proposes that the thickness will be reduced and subsequently the fibre volume increased depending on the tautness of the stitching. Mouritz also suggests that many researchers do not adequately consider this when comparing their stitched to their 'baseline' unstitched specimens. Furthermore, Mouritz approaches the idea of comparing a stitched laminate with an equivalent unstitched laminate (same material system and lay-up) "with some measure of scepticism". This is because stitching causes fibre misalignment and fibre volume fraction differences that "translate

directly into errors in reported stresses or stiffnesses" [33]. However, one could counter that if the purpose of an investigation is to characterise the damage mechanisms in a stitched laminate it is certainly wise to compare to damage evolution in an unstitched laminate of the same material and lay-up.

Test Orientation Definitions

Tests were carried out at two orientations for both the stitched (S/RFI) and unstitched (RFI) material for all available thicknesses, these were: the longitudinal principal direction (0°) and the transverse principal direction (90°). In the primary principal direction the laminates are loaded parallel to the 0° plies, and in the transverse principal direction the laminates are loaded at right angle to the 0° plies (see Figure 2-4). For ease of reference this thesis will refer to tests in the primary principal direction as the 0° OCT tests, and tests in the transverse principal direction as the 90° OCT tests. Figure 2-5 shows the direction of stitching in both the 0° and the 90° OCT tests.

Microstructural Investigation

On receipt of the RFI material from the Boeing Company, a slight visual difference was noticed in the stitching of the 5-stack S/RFI material. Therefore, before OCT testing was conducted on the S/RFI material a short study was carried out to inspect any microstructural differences between the 4-, and 6-stack S/RFI material (similar stitching) and 5-stack S/RFI material.

2.1.1 Visual Inspection of Stitching in the S/RFI panels

On first visual inspection of all three thicknesses the most apparent feature are the larger surface loops present in the 5-stack material (see Figure 2-6). The stitching in the 5-stack appears 'loose' and the surface loops compacted and flattened out. Stitching in the 4- and 6-stack material is much more

uniform, with smaller surface loops. The difference suggests that some manufacturing parameter was changed during the production of the 5-stack panels, from that of the 4- and 6-stack panels.

Through Thickness Inspection

By cross sectioning and polishing samples of the 4- and 5-stack S/RFI material, one can observe the individual stitches and their path through the laminate. Figure 2-7(a) is a micrograph of a very straight, taut stitch in the 4-stack S/RFI material; this is also the case in the 6-stack S/RFI material. Notice also the porosity near the stitch, this may have been caused by poor resin infiltration during processing. Figure 2-7(b) is a micrograph of a very 'wavy', 'loose' stitch in the 5-stack S/RFI material. The cause of this waviness is likely to be a manufacturing parameter such as bobbin tension during stitching, or compaction of the laminate during the vacuum assisted RFI process. The 5-stack S/RFI specimen exhibited fraying of the stitch during polishing. This was not the case when polishing the 4-stack S/RFI specimen, possibly indicating poor wetting of the thread during processing of the 5-stack material. Notice also the resin pooling at the kinks in the stitch. One other feature that is noticeable from the cross sectioning of the laminates is fibre breakage caused by the manufacturing process; Figure 2-8 shows this damage in the 6-stack S/RFI material.

Stitch Cross Section and Fibre Misalignment

Removing the surface layer of the 4-stack and 5-stack S/RFI material revealed some interesting detail concerning the fibre misalignment – an important consideration as composite material properties are very much dependent on the direction of their load bearing fibres. Simple geometry was used to calculate the misalignment caused by stitching.

The micrographs in Figure 2-9 show a portion of a 0° ply in the 4-stack S/RFI material. They indicate a resin rich band in apparently around the stitching, and reveal the stitching to be quite uniform and circular in nature. It has been reported (see Introduction & Literature Review) that the

stitching process causes in-plane fibre misalignment, Figure 2-10 illustrates this very well, and also shows evidence of resin pooling that occurs as a result. This spreading and pooling may be detrimental to the highly directional properties of the composite. Fibre misalignment around the stitch in the 4-stack material was calculated to be between approximately 12-14°.

Unlike the 4-stack materials stitching, the 5-stack stitches are not uniform in diameter as shown in Figure 2-11. Some are drawn out and elongated, increasing the distance that the fibres are spread out over and in some cases increasing the size of the resin rich area around the stitch. In addition, poor wetting of the stitches in the 5-stack material (see section Through Thickness Inspection) may have occurred. For instance, if the resin has filled the larger areas around the stitches, sufficient process time may not have been allowed for full infiltration of the stitches. A much wider range of fibre misalignment angles around stitches were calculated in the 5-stack material, 7.5-14°. This further indicates that further control may have been lost over the directional properties of these composites.

These misalignment angles are consistent with the findings of Mouritz and Cox [33], however misalignment will mainly depend on the thread diameter. Such influence was reported by Pelstring and Madan [1] who concluded that increasing the diameter of the thread gives a progressive deterioration of in-plane tensile strength.

In summary:

1. The visual examination of microstructure showed that the 4- and 6-stack S/RFI material have taut stitching, whereas the 5-stack S/RFI material has 'loose' stitching.
2. The stitching in the 4- and 6-stack material is fairly uniform and circular in nature.
    - Fibre misalignment in the 4-stack material was calculated to be between 12-14°
    - Fibre misalignment in the 5-stack material was calculated to be between 7.5 - 14°,

further indicating control has been lost over directional properties of the composite.

Table 2-1: *Elastic Properties of RFI Material used in this study. Where y-direction coincides with primary principal direction [74].*

E_x	30 GPa
E_y	75 GPa
G_{xy}	17.1 GPa
ν_{xy}	0.161

Table 2-2: *Specimen Dimensions, where t is the specimen thickness, d is the loading pin-hole diameter, c is the distance between pin centres, H is the specimen height, f_H is the spacing between inscribed lines, a is the initial notch length, and W is the distance from the centre of the pin-hole to the back end of the specimen.*

Date	Test	Material	Boeing Panel ID #	Specimen Dimensions (mm)								
				H	Width	t	d	c	a	W	a/W	f_H
1-Jun-00	SS67-s0	4-stack S/RFI	BA-T-5	208	106	5.90	19.1	38.6	32.30	81	0.40	2.5
1-Jun-00	SS68-s0	4-stack S/RFI	BA-T-5	207	106	5.90	19.1	38.6	32.40	80	0.40	2.5
8-Jun-00	SS69-s0	5-stack S/RFI	extra-1	205	105	7.30	19.1	38.7	32.20	80	0.40	2.5
9-Jun-00	SS70-s0	5-stack S/RFI	extra-1	205	105	7.00	19.1	38.6	32.20	80	0.40	2.5
8-Jun-00	SS71-s0	4-stack S/RFI	BA-T-1	206	105	6.10	19.1	38.7	32.40	80	0.41	2.5
9-Jun-00	SS72-s0	4-stack S/RFI	BA-T-1	207	105	6.10	19.1	38.6	32.50	80	0.41	2.5
8-Nov-00	SS73-s0	6-stack S/RFI	BA-T-6	208	108	8.80	19.1	39.0	35.68	83	0.43	2.5
9-Nov-00	SS74-s0	6-stack S/RFI	BA-T-6	208	85	8.80	19.1	38.7	34.93	60	0.58	2.5
16-Nov-00	SS75-s0	6-stack S/RFI	BA-T-6	208	97	8.80	19.1	38.3	34.60	71	0.49	2.5
9-Feb-01	SS76-s90	4-stack S/RFI	BA-T-5	207	106	6.10	19.1	38.8	32.10	80.6	0.40	2.5
9-Feb-01	SS77-s90	5-stack S/RFI	extra-1	207	106	7.30	19.1	38.5	32.10	80.6	0.40	2.5
9-Feb-01	SS78-s90	6-stack S/RFI	BA-T-6	208	106	8.80	19.1	38.6	32.00	80.6	0.40	2.5
9-Feb-01	SS79-s0	6-stack S/RFI	BA-T-6	205	105	8.80	19.1	38.7	32.10	79.6	0.40	2.5
23-Feb-01	SS80-u0	6-stack RFI	BA-T-4	206	106	8.38	19.1	38.7	32.24	80.6	0.40	2.5
23-Feb-01	SS81-u90	6-stack RFI	BA-T-4	207	107	8.38	19.1	38.7	32.64	81.6	0.40	2.5
23-Feb-01	SS82-u0	4-stack RFI	u-extra	206	108	5.59	19.1	38.7	33.04	82.6	0.40	2.5
23-Feb-01	SS83-u90	4-stack RFI	u-extra	206	108	5.59	19.1	38.7	33.04	82.6	0.40	2.5

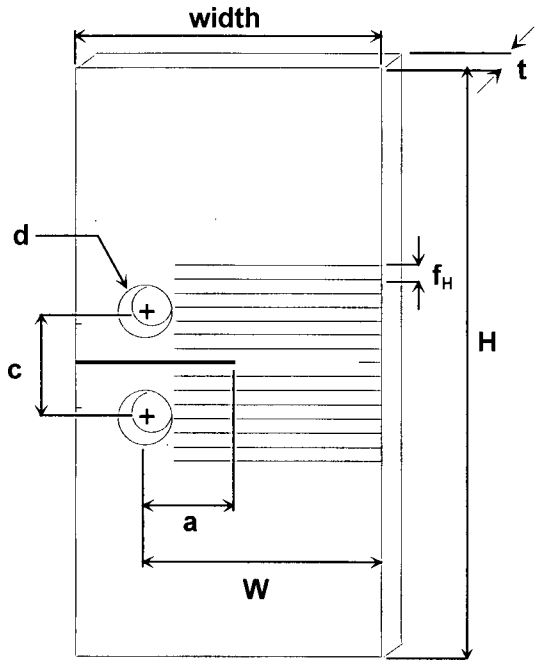

Figure 2-1: Schematic of the OCT specimen geometry (where t is the specimen thickness, d is the loading pin-hole diameter, c is the distance between pin centres, H is the specimen height, f_H is the spacing between inscribed lines, a is the initial notch length, and W is the distance from the centre of the pin-hole to the back end of the specimen.)

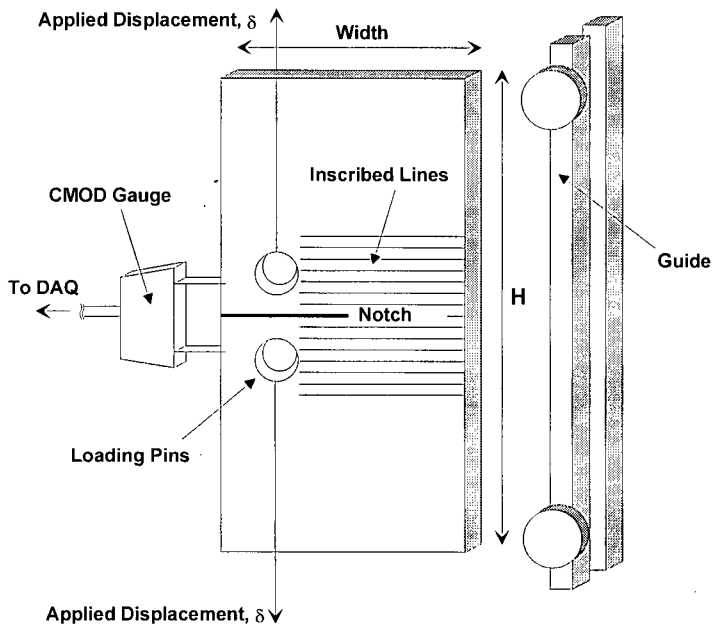

Figure 2-2: Schematic of Experimental set-up, showing position of the stiffener guide and CMOD gauge.

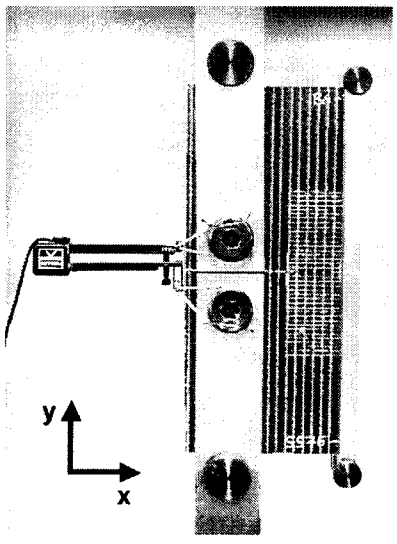

Figure 2-3: Shows an RFI specimen in the loading jig, note the stiffener on the right hand side

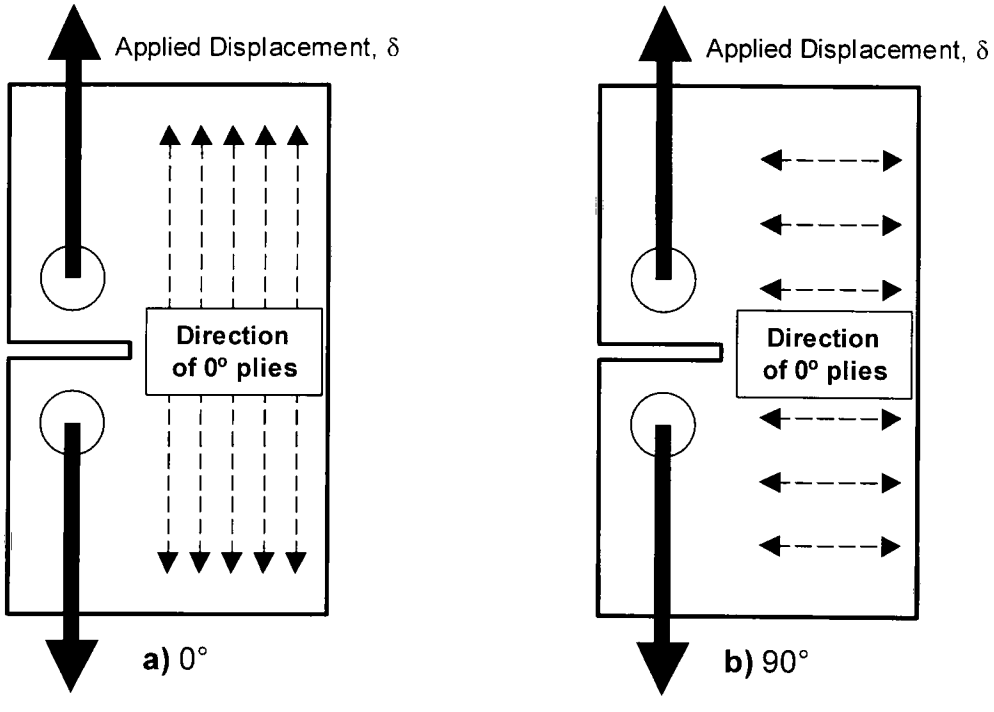

Lay-up [+45/-45/0_2/90/0_2/-45/+45] for one sub-laminate

Figure 2-4: Schematic showing direction 0° plies in the two test orientations: (a) shows the primary principal direction (0°) where 0° plies lay parallel to the loading direction and (b) shows the transverse principal direction (90°) where the 0° plies lay at right angles to the loading direction.

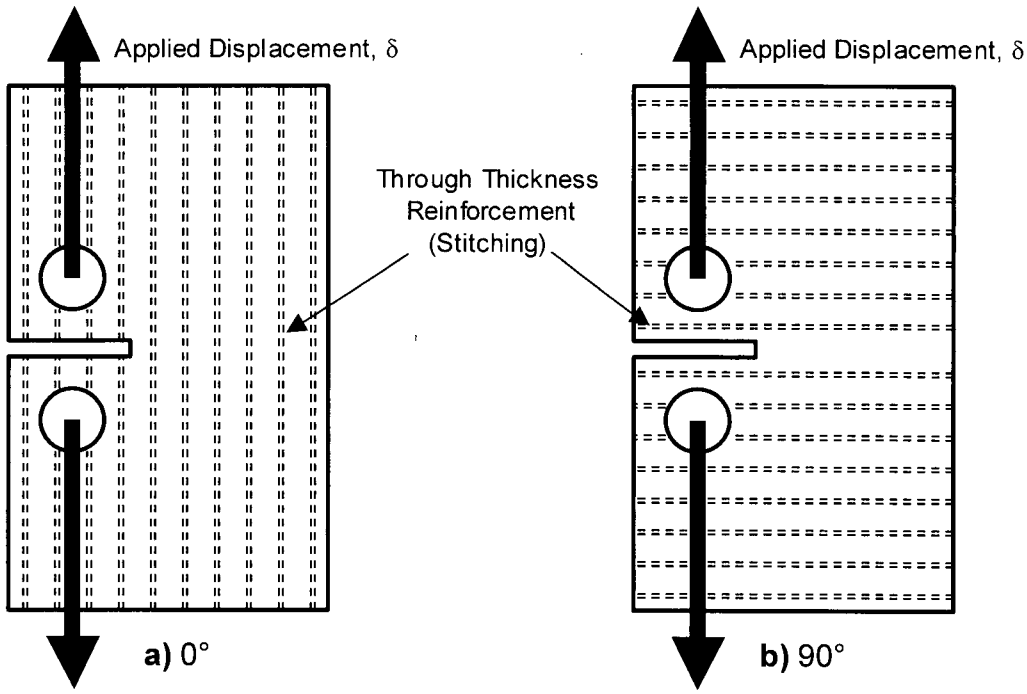

Lay-up [+45/-45/0_2/90/0_2/-45/+45] for one sub-laminate

Figure 2-5: Schematic showing direction of through thickness reinforcement (Kevlar® stitching) and direction of applied displacement (load) with respect to the direction of 0° plies in each sub-laminate. Figure (a) shows the primary principal direction (0°) and (b) shows the transverse principal direction (90°).

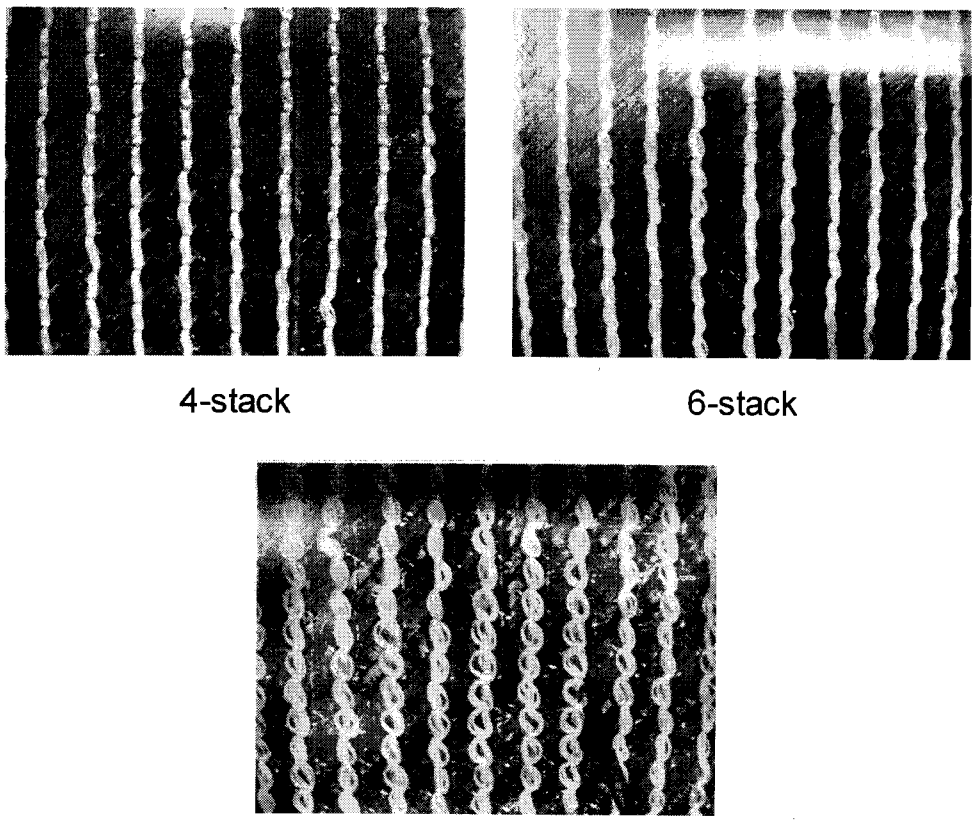

Figure 2-6: Surface Loops in 4-, 5- and 6-stack stitched/RFI material.

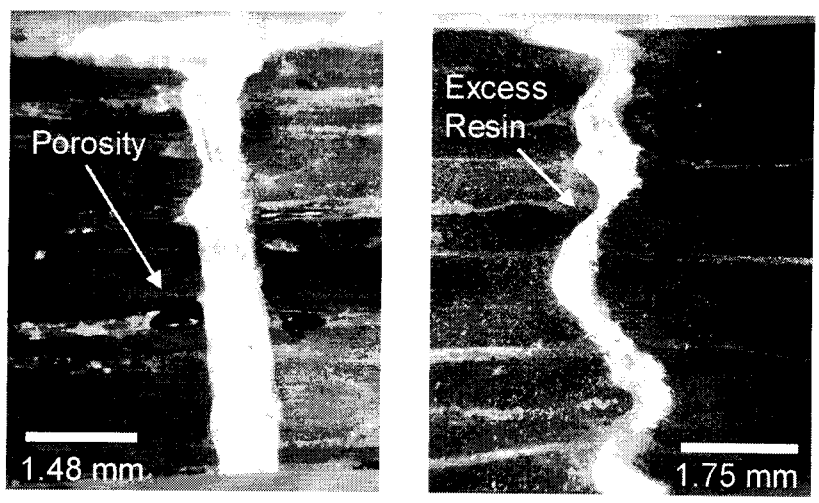

Figure 2-7: Micrographs of (a) Straight 'tight' stitching in 4-stack stitched RFI sample and (b) Wavy 'loose' stitching in 5-stack stitched RFI sample.

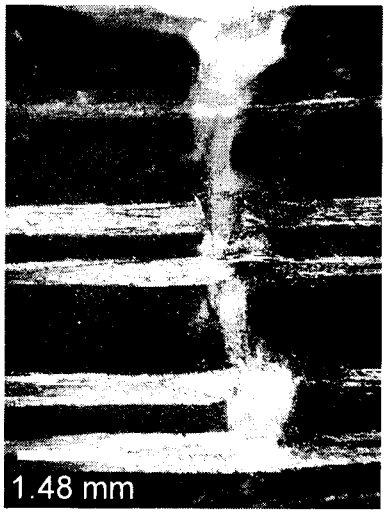

Figure 2-8: An example of fibre damage caused by the stitching process (6-stack S/RFI). It is interesting that that as the stitch reaches the surface of the material it spreads out to form a surface loop. The loops presumably cause a greater fibre misalignment than further within the material.

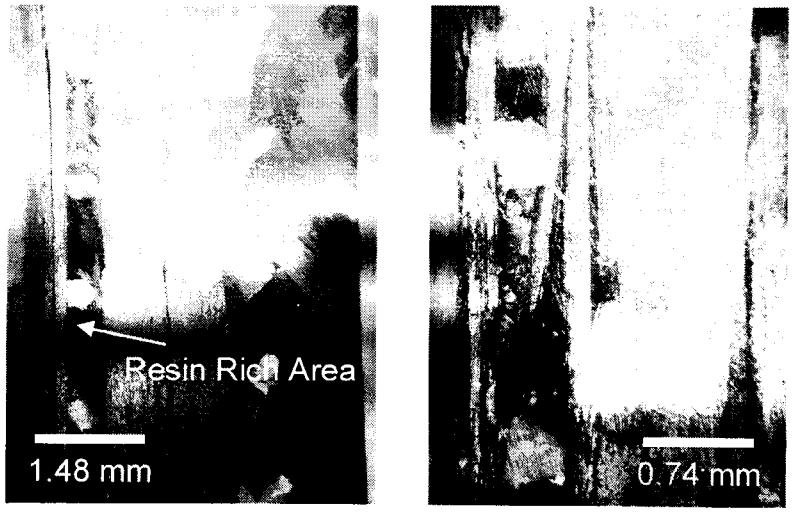

Figure 2-9: Micrographs of stitched 4-stack RFI material (a) shows a resin rich area between the tows apparently caused by stitching and (b) shows a higher magnification view of (a) clearly indicating the damage caused by stitching and 'circular' stitches.

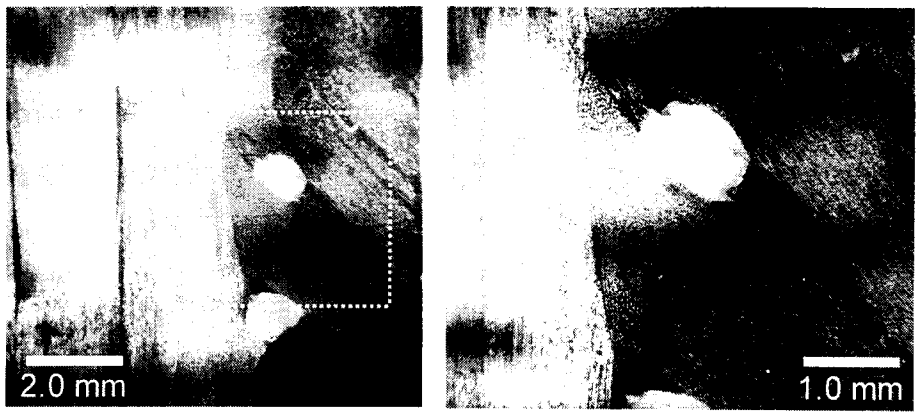

(a) (b)

Figure 2-10: Micrographs of carbon fibre spreading of stitched 4-stack RFI material because of the stitching process. Notice the resin rich area around the stitch.

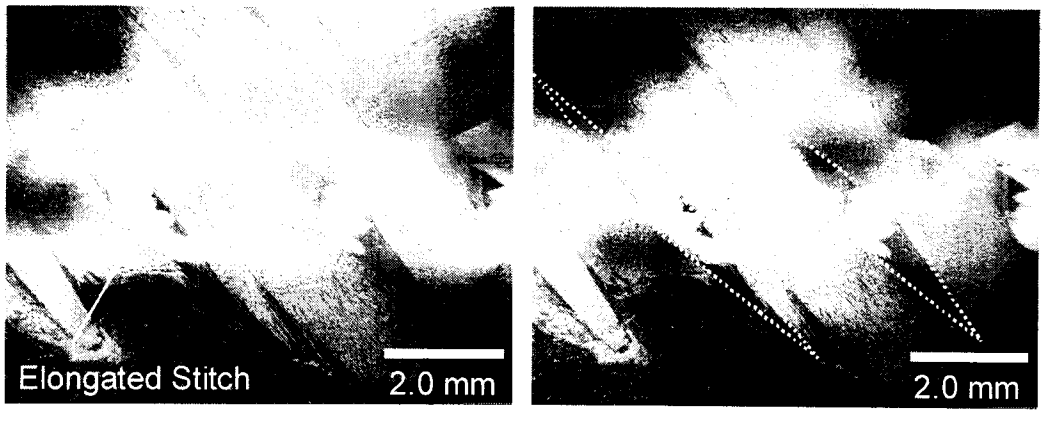

(a) (b)

Figure 2-11: Micrographs of carbon fibre spreading of stitched 5-stack RFI material. Notice the elongation of the stitch causing a longer resin rich area.

Chapter Three

Examining Damage Growth

3. Examining Damage Growth

This chapter is aimed at presenting the damage evolved in the OCT specimens during testing. Damage growth in the various thicknesses and specimen orientations is explored, as well as the effectiveness of the OCT specimen to grow damage in both the S/RFI and RFI material.

Visual Indication of damage growth in OCT specimens

During each OCT test, careful note was made of damage evolution on the surface of each specimen. Figure 3-1 shows the two types of surface damage growth that were encountered.

Both the stitched and unstitched 4- and 6-stack specimens showed surface damage growth parallel to the loading axis, when loaded in the primary principal direction (0° specimens). In the stitched specimens, damage appeared to grow upwards between stitch rows. In the 5-stack 0° specimens surface damage growth was perpendicular to the load jumping from stitch row to stitch row as it crossed the specimen.

In essence, the surface damage in the 4- and 6-stack 0° specimens grows upwards and damage in the 5-stack 0° specimens grows across the specimen. As the surface damage growth is consistent in both the stitched and unstitched 4- and 6-stack 0° specimens it does not appear that it is significantly affected by stitching.

When loaded in the transverse principal direction (90° specimens), damage growth was consistent for all specimen thicknesses. Damage growth was observed perpendicular to the load, parallel to the notch, as observed with the 5-stack 0° specimens.

The Effect of Stitching on Surface Delamination

As one might expect, surface delamination is greatly reduced when through-thickness stitching is incorporated into RFI materials. The photographs in Figure 3-2 show the resulting surface delamination in two 4-stack 0° OCT tests, one unstitched and one stitched, both of which suffered back face compression failure. The unstitched specimen are very highly delaminated, whereas the stitched specimen was less so. It must be noted that the crack mouth opening displacement and maximum load attained were greater in the unstitched specimen by 6% and 13% respectively, hence this may have some bearing on the extent of the delamination, however delamination is still more prominent in the unstitched specimen.

Examining the Fracture Process Zone

After each OCT test, two techniques were used to characterise the damage behaviour around the notch tip. To examine the amount of fibre failure and also the crack path in each ply, a 'deplying' technique was used [75]. This involved oxidising (burning off) the epoxy resin from the area of interest and removing each ply individually (Figure 3-3). To examine through-thickness matrix cracking, delamination and process zone height, cross-sections were removed perpendicular to the notch in the fracture process zone (Figure 3-4). As both of these tests are destructive, a selection of specimens was chosen for both deplying and sectioning.

Deplying

Five specimens were de-plied (see Table 3-1); both RFI and S/RFI materials were investigated as well as 0° and 90° test orientations. Only the damaged areas of the OCT test specimens were de-plied. Each sample was placed in a furnace at 420°C for approximately 4-6 hours. The RFI specimens required a shorter oxidation time than the S/RFI specimens. Possible reasons for this are: the resin rich areas around the stitches had not been fully oxidized after 4 hours, or that degradation

of the Kevlar® stitching was more prevalent after 6 hours and thus made deplying easier thereafter.

Once the samples were cooled, each ply was carefully removed with a surgical blade and tweezers, laid out and sealed to preserve the lay-up sequence. Once complete, the plies were scanned in order to provide a permanent copy, and a trace was then made of the damage and broken fibres on transparency film. This was scanned and imported into image manipulation software. This is a very labour intensive process, requiring care not to impart more damage to each ply during removal.

Deply Results

Results for each specimen are presented in this section, with a summary of damage given in Table 3-2.

Stitched 4-stack 0° (SS71-s0)

Figure 3-5 shows the results for damage observed in test SS71-s0, a S/RFI 4-stack 0° specimen.

1. Fibre damage was generally observed in the -45° plies, where damage has grown perpendicular to the fibre tow placement.
2. Damage has not grown in a self-similar manner across the specimen. Fibre failure extends to approximately 2-10 mm ahead of the notch tip depending on the ply orientation.
3. Damage on the right side of the deplied area is back face compression failure, which occurred during the latter stages of testing.
4. On examination of the 90° plies it is apparent that the stitching was very straight across the sample with little or no deviation of the stitching path, with one resin rich area around a stitch touching another as shown in Figure 3-6(a).

5. Only the surface +45° plies show any damage, certainly caused by the small amount of surface delamination between stitches witnessed during testing.

6. Fibre damage does not seem to be present in the 0° plies, however there is evidence of tow splitting (Figure 3-7).

Unstitched 6-stack 0° (SS80-u0)

Figure 3-8 shows the results for damage observed in test SS80-u0, an RFI 6-stack 0° specimen.

1. Very little fibre damage was obvious in most of the 0° and 90° plies. The average bundle thickness of the tow is smaller in the 0° plies than in the stitched 4-stack 0° plies with wider resin gaps between them. Therefore damage may have in grown in these resin rich areas in these plies. In the 90° plies, the fibre tows are thin and close together.

2. The +45° and –45° plies show damage growing parallel to the fibre tow placement. The -45° plies situated towards the centre of the laminate contain fibre damage perpendicular to the tow placement that extends between 7 – 10 mm. Less fibre damage than is evident in plies toward the surface of the laminate.

Stitched 5-stack 0° (SS69-s0)

Figure 3-9 shows the results for damage observed in test SS69-s0, a S/RFI 5-stack 0° specimen.

1. The most notable difference when examining the 5-stack 0° deplied specimen compared to the 4-stack stitched and 6-stack unstitched 0° specimens described above, is the damage growth path.

2. Damage growth is self-similar, growing across the specimen by means of major fibre breakage in most plies. However, note that damage does not initially grow straight across the

specimen. During the early stages of the test the damage has grown in much the same manner as the stitched and unstitched 4, 6-stack 0° specimens. It initially grows forward at 45° for approximately 12 mm before returning close to the notch mid-plane where it continues across the specimen (Figure 3-10). This phenomenon can be seen in all -45° plies, as they show significant fibre breakage perpendicular to fibre tow placement (Figure 3-11). The +45° plies on the other hand, display little fibre breakage initially as the damage is growing parallel to fibre tow placement.

3. It is interesting to note that even though the damage in the 0° plies seems to have changed direction during the test, returning the notch mid-plane, this is not evident in the +45 plies.

4. Unlike the 4-stack stitched 0° specimen the stitching in the 5-stack material follows a 'wavy' path across the specimen in most plies, illustrated in Figure 3-6(b).

5. Damage in the -45° plies extends approximately 15 – 30 mm in length depending on the ply. Damage length in the 0° plies is greater and extends between 20 – 30 mm across the specimen width.

6. The deply also revealed a -45° ply drop between the second and third stack from the surface of the laminate. The drop occurs in front of the notch tip, and lies half way between the notch tip and the back end of the specimen.

Stitched 4-stack 90° (SS76-s90)

Figure 3-12 shows the results for damage observed in test SS76-s90, a S/RFI 4-stack 90° specimen.

1. All plies contain major fibre damage with the exception of several 0° plies, now oriented parallel to the notch mid-plane. These damaged plies either display splitting of the tow,

usually because the notch has been cut in the centre of the tow, or show slight damage near the notch as the fibre damage has grown to the once resin rich area between tows (see Figure 3-13).

2. Damage across the specimen is self-similar with the 90° (now oriented parallel to the direction of loading), +45° and -45° plies all showing fibre breaking along the notch mid-plane.

3. Further examination of the -45° plies indicates that the damage jumped from one stitch to another across the specimen, causing fibre breakage as it moved from one resin rich area around the stitch to another. It is likely that damage in the -45° and +45° plies was assisted by the resin rich areas between tows in the 0° plies.

4. Damage length in both the -45° plies and 90°plies extends 30 mm across the specimen. Damage in the +45°plies extends 15 – 20 mm across the specimen.

Unstitched 4-stack 90° (SS83-u90)

Figure 3-14 shows the results for damage observed in test SS83-u90, an RFI 4-stack 90° specimen. This sample behaved in much the same way as the 4-stack stitched 90°, with damage in all plies.

1. Self-similar fibre damage across the specimen in the notch mid-plane was substantial with damage lengths of 32, 25 and 20 mm recorded for the 90°, -45° and +45° plies respectively.

2. Once again the 0° plies show splitting of the tow if the notch lies in the tow.

Comparing the behaviour of 5-stack stitched 0°, 4-stack stitched 90° and 4-stack unstitched 90°

The deply analysis results indicate that the 5-stack stitched 0° and the 90° specimens all show self-

similar fibre damage growth. However, the 5-stack stitched 0° damage path is slightly different from that of the 90° specimens.

1. Whereas fibre damage grows straight across the specimen (mostly in the notch mid-plane) in the 90° specimens, damage in the 5-stack 0° specimen initially grows up and forward at 45° and then arcs back down towards the notch mid-plane.

2. It is probable that any damage growth parallel to the applied load is restricted in the 90° specimens due to the large number of 0° plies that now lie parallel to the notch mid-plane. It is due to the lay-up that the crack growth is self-similar in nature, since this is the path of least resistance.

3. In the case of the 4-stack stitched 90° specimen, the stitching now lies perpendicular to the direction of applied load and damage has certainly grown along the stitching, jumping from one stitch to the next. This is further aided by the resin pooling around the stitches.

4. Therefore, it seems that the stitched 5-stack material is exhibiting damage growth resembling the 4-stack stitched 0° specimens in the early stages of testing, with damage growth then switching to resemble the 90° specimens (see Figure 3-15).

Other Deply Comments

Apart from fibre damage, the deplied specimens also reveal the localised damage that occurs as the needle and yarn penetrate during stitching of the S/RFI materials. They also illustrate the misalignment of fibres at each stitch position. The shape and size of the hole left by the stitch gives an indication of the size of the resin rich area around the stitch.

Sectioning

The areas of interest were cut from the tested OCT specimens at a height well above any surface delamination present. Sectioning was carried out with a slow speed diamond saw at intervals in front of the notch tip. The use of a diamond saw was necessary to minimise further damage to the specimens in the delicate process zones. Polaroid photographs were taken of the sections; these were scanned and stitched together using image manipulation software.

Sectioning Results

Deply results reveal only the amount of fibre damage and damage path within the specimen as the matrix material has been oxidised. From the deply alone it is obvious that damage is growing differently in some specimens compared with others. Sectioning the sample in front of the notch tip reveals other types of damage, such as matrix cracking and delamination and can be used to reinforce information gained in the deply, regarding crack growth path. Five samples in total were sectioned, four stitched specimens and one unstitched specimen (see Table 3-3). Figure 3-16 shows the labelling convention used for the sectioning schematics. The micrographs and associated damage plot have been labelled, front (F) and back (B) to indicate the observation direction. Results for each specimen are presented in this section, with a summary of damage given in Table 3-4.

Stitched 4-stack 0° (SS68-s0)

Figure 3-17 shows the damage observed in test SS68-s0, a S/RFI 4-stack 0° specimen, sectioned at 2 mm ahead of the notch tip.

1. The process zone, at just over 68 mm in height, consists of substantial delamination as well as some fibre and matrix damage at the notch mid-plane.

2. The delamination is most prominent between -45° and 0° plies, however some delamination

can be seen between the 0°and 90° plies but to a lesser extent.

3. Figure 3-18 shows a closer view of the notch mid-plane. Fibre breakage is evident about the notch mid-plane along with heavy delamination.

4. Further sectioning carried out on this specimen indicated that the process zone extended approximately 7.8 mm across the specimen width of 80.4 mm.

Stitched 5-stack 0° (SS70-s0)

Figure 3-19 shows the damage observed in test SS70-s0, a S/RFI 5-stack 0° specimen, sectioned at 5 mm ahead of the notch tip.

1. The process zone is approximately 60 mm in height and consists of large amounts of fibre and matrix damage about the notch mid-plane.

2. Some delamination is present and, in several instances, runs the length of the process zone. Delamination is most prominent between -45° and 0° plies and also between 0°and 90° plies but to a lesser extent.

Figure 3-20 again shows the damage observed in test SS70-s0, sectioned at 2mm ahead of the notch tip. But this time only the notch mid-plane is shown, highlighting the fibre damage across the specimen

Figure 3-21 shows the same specimen again sectioned at 10.5 mm ahead of the notch tip.

1. The process zone height is now only approximately 21 mm, and consists of a great deal of matrix cracking and delamination with less fibre damage than the section at 2mm.

2. Delamination is contained within approximately 8.25 mm either side of the notch mid-plane.

3. Note the waviness of the stitching, and how it interrupts the delamination damage.

4. The distinct fibre damage at the notch mid-plane that was present at 2 mm is absent at this distance in front of the notch tip.

5. Further sectioning carried out on this specimen indicates that the process zone extends approximately 25.9 mm across the specimen width of 80 mm.

Stitched 6-stack 0° (SS73-s0)

Figure 3-22 shows damage observed in test SS73-s0, a S/RFI 6-stack 0° specimen, sectioned at 2 mm ahead of the notch tip.

1. The height of the process zone is similar to the stitched 5-stack 0° specimen, at approximately 61 mm, but consists almost entirely of substantial delamination running the length of the process zone. In fact, this specimen was so highly delaminated that it had to be pieced back together for photographing.

2. Delamination is most prominent between the 0° and -45° plies, with four large delaminations running the length of the process zone. One delamination was also recorded between a 0° and a 90° ply.

3. The fibre damage and matrix cracking at the notch mid-plane in the 5-stack 0° is absent in the 6-stack. Although close inspection of the delaminated pieces showed some fibre cracking in the off-axis plies (+45° and -45°). This fibre damage is consistent with the deply analysis see presented previously.

4. Further sectioning carried out on this specimen indicated that the process zone extended approximately 7.2 mm across the specimen width of 82.6 mm. At 5 mm in front of the

notch tip the damage height was only 7 mm with one delamination between one 0° and one 90° ply and one delamination between one 0° and one -45°ply.

Stitched 5-stack 90° (SS77-s90)

Figure 3-23 shows damage observed in test SS77-s90, a S/RFI 5-stack 90° specimen, sectioned at 9.6 mm ahead of the notch tip.

1. The height of the process zone is approximately 5.5 mm and consists almost exclusively of fibre breakage and matrix cracking along the notch mid-plane.
2. The minimal delamination that is present has mainly been caused by the other types of damage, and merely acts to interconnect this damage. The damage is self-similar in nature.
3. All plies contain fibre damage that does not seem to be more prevalent at any one orientation.
4. Further sectioning carried out on this specimen indicates that the process zone extended approximately 36.1 mm across the specimen width of 80.6 mm. Damage height is constant across the specimen width.

Stitched 6-stack 90° (SS78-s90)

Figure 3-24 shows damage observed in test SS78-s0, a S/RFI 6-stack 90° specimen, sectioned at 1 mm ahead of the notch tip.

1. The height of the process zone is approximately 7.08 mm, and consists exclusively of fibre breakage and matrix cracking along the notch mid-plane.
2. Damage is self-similar in nature.

3. All plies contain fibre damage, and as with the 5-stack stitched 90°, does not seem to be more prevalent at any one orientation.

4. Further sectioning carried out on this specimen indicates that the process zone extends approximately 32.5 mm across the specimen width of 80.6 mm. Damage height is constant across the specimen width.

Unstitched 6-stack 90°(SS81-u90)

Figure 3-25 shows damage observed in test SS81-u90, a RFI 6-stack 90° specimen, sectioned at 2 mm ahead of the notch tip.

1. The height of the process zone is approximately 11.45 mm, when taking into account delamination in the surface plies. However discounting this delamination the process zone height is approximately 5.08 mm, and consists exclusively of fibre breakage and matrix cracking along the notch mid-plane.

2. A small amount of delamination is present at the surface of the specimen.

3. All plies contain fibre damage and this damage does not seem to be more prevalent at any one orientation.

4. Further sectioning carried out on this specimen indicated that the process zone extended approximately 34.4 mm across the specimen width of 81.6 mm. Damage height is constant across the specimen width.

Comparing Damage Along the Notch Mid-plane

Comparing the damage along the notch mid-plane helps indicate the key points from the above physical descriptions of damage.

Figure 3-26 reviews the damage observed along the notch mid-planes in the sectioned stitched 0° OCT specimens. Figure 3-26(a) to (c) show the damage at 2 mm ahead of the notch tip for a 4-, 5-, and 6-stack specimens respectively. The 4- and 6-stack specimens contain more delamination damage and less fibre damage compared to the 5-stack. The 4-stack specimen does however show some fibre damage at the notch mid-plane, but not as much as the 5-stack specimen. The 5-stack specimen is so badly damaged that on sectioning much of the material at the notch mid-plane fell away.

This difference in damage evolution is interesting when recalling the differences in stitching covered in Chapter 3, where the 5-stack material was reported to have mechanically 'looser', 'wavy' stitching whereas the 4- and 6-stack material have much 'tighter', 'straight' stitching. Figure 3-26(d) shows how the damage has grown in the 5-stack 0° specimen at 10.5 mm. The process zone is now much taller, and the damage is not as confined to the notch mid-plane.

Figure 3-27 reviews the damage observed along the notch mid-plane in the sectioned 90° OCT specimens. In all cases the damage is constrained to the notch mid-plane, and all exhibit a great deal of fibre breakage, indicating (not surprisingly) self-similar growth pattern when correlated with the deply results. Surface delamination was more prevalent in the unstitched 90° specimen, than it was for the stitched specimen.

Summary

- The process zone was examined with two techniques; deplying and sectioning
- Deplying indicated damage growth path in each individual ply.
    - All 90° specimens show a truly self-similar crack growth, self-similar behaviour with extension of the notch across the specimen.

- The stitched 5-stack 0° specimen showed a somewhat self-similar behaviour, with initial damage growing forward at 45° (mimicking the 4-stack stitched specimen) after which the damage growth returns to the notch mid-plane and continues to grow across the specimen.
- Both the stitched 4-stack 0° and the unstitched 6-stack 0° showed minimal crack growth with damage growing only a short distance ahead of the notch tip at 45°.

- Sectioning confirmed self-similar crack growth in 90° specimens and revealed that the damage in the 5-stack 0° grows in a more brittle manner than the 4- or 6-stack 0° specimens, which shows a greater amount of delamination. Sectioning also confirmed that delamination mainly occurred between the 0° and -45°plies for this test geometry within this lay-up configuration (Figure 3-28), with some delamination occurring between 0° and 90°plies.

Table 3-1: Deply Specimens

Test #	Material Type	Orientation	No. Stacks	Deply Zone Dimensions	
				Height (mm)	Width(mm)
SS71-s0	S/RFI	0°	4	64	61
SS69-s0	S/RFI	0°	5	37	61
SS80-u0	RFI	0°	6	75	59
SS76-s90	S/RFI	90°	4	34	61
SS83-u90	RFI	90°	4	38	61

Table 3-2: Length of damage found in the Deply specimens and approximate length of damage recorded from line analysis.

Test #	Material Type	Orientation	No. stacks	Total Length of Damage from Deply Analysis	
				Ply Orientation	Damage Length (mm)
SS71-s0	S/RFI	0°	4	-45°	2–10
SS80-u0	RFI	0°	6	-45°	7–10
SS69-s0	S/RFI	0°	5	0°	20–30
				-45°	15–30
SS76-s90	S/RFI	90°	4	90°	30
				-45°	30
SS83-u90	RFI	90°	4	90°	32
				-45°	20–25
				+45°	20

Table 3-3: Sectioning Specimens

Test Number	Material	Orientation	No. Stacks	Process Zone		Specimen width /mm
				Width /mm	Max. Height /mm	
SS68-s0	S/RFI	0°	4	3	68	80.4
SS70-s0	S/RFI	0°	5	19	60	80
SS73-s0	S/RFI	0°	6	5	61	82.6
SS77-s90	S/RFI	90°	5	26.5	5.5	80.6
SS78-s90	S/RFI	90°	6	33	7.08	80.6
SS81-u90	RFI	90°	6	27	5.08*	81.6

*This excludes surface delamination

Table 3-4: Length of damage found in the Sectioning specimens and approximate length of damage recorded from line analysis (see Chapter 4).

Test #	Material Type	Orientation	No. Stacks	Total Length of Damage from Sectioning Analysis (mm)
SS68-s0	S/RFI	0°	4	7.8
SS70-s0	S/RFI	0°	5	25.9
SS73-s0	S/RFI	0°	6	7.2
SS77-s90	S/RFI	90°	5	36.1
SS78-s90	S/RFI	90°	6	32.5
SS81-u90	RFI	90°	6	34.4

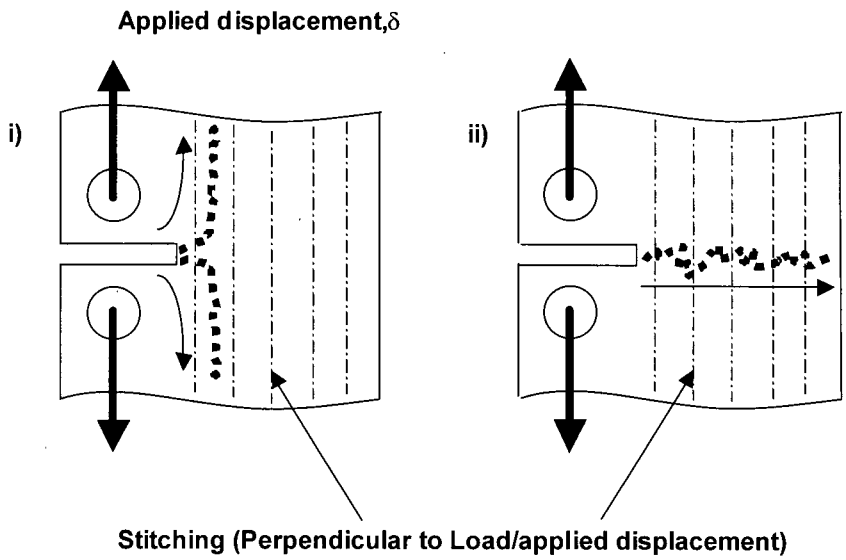

Figure 3-1: Surface damage growth schematic for i) 4- and 6-stack 0° OCT specimens, ii) 5-stack 0° and 4-, 5- and 6-stack 90° OCT specimens.

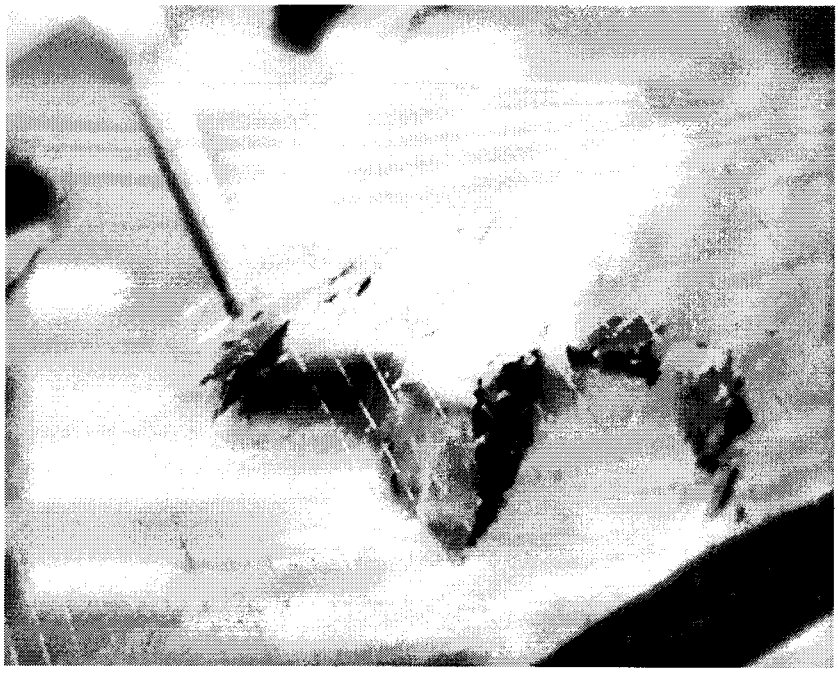

(a)

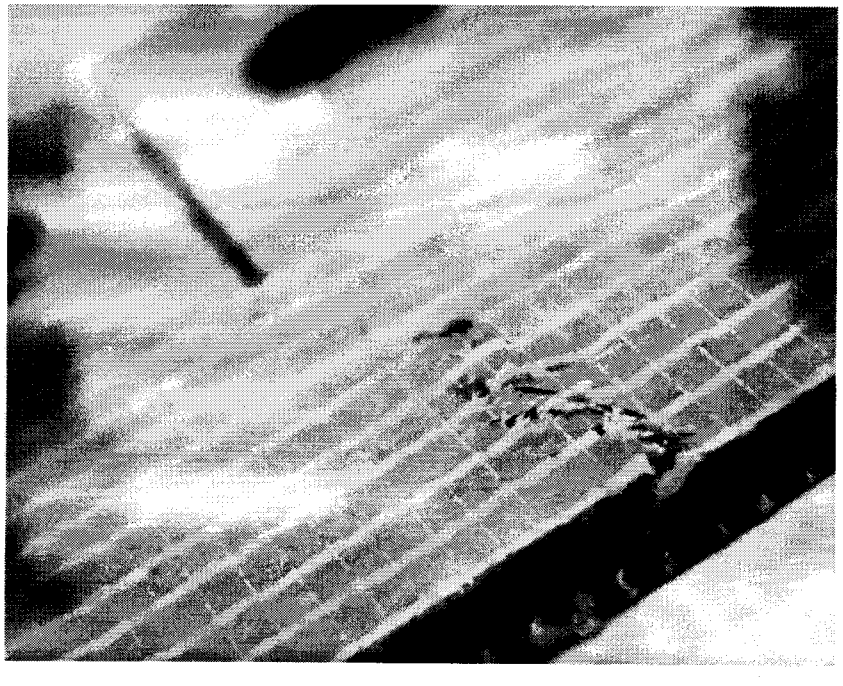

(b)

Figure 3-2: Delamination damage in S/RFI Composites, tested by over-height compact tension method a) 4-stack un-stitched 0° specimen (SS82-u0) and b) 4-stack stitched 0° specimen (SS72-s0)

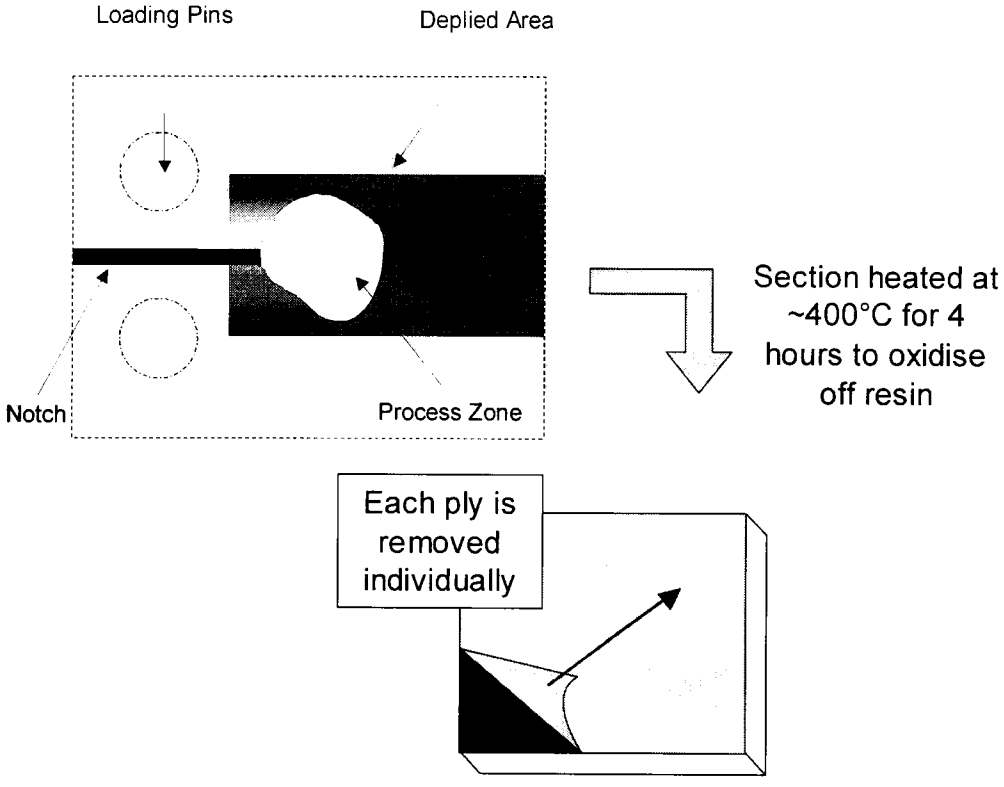

Figure 3-3: Schematic of deplying technique, where an area of interest is cut from the tested OCT specimen

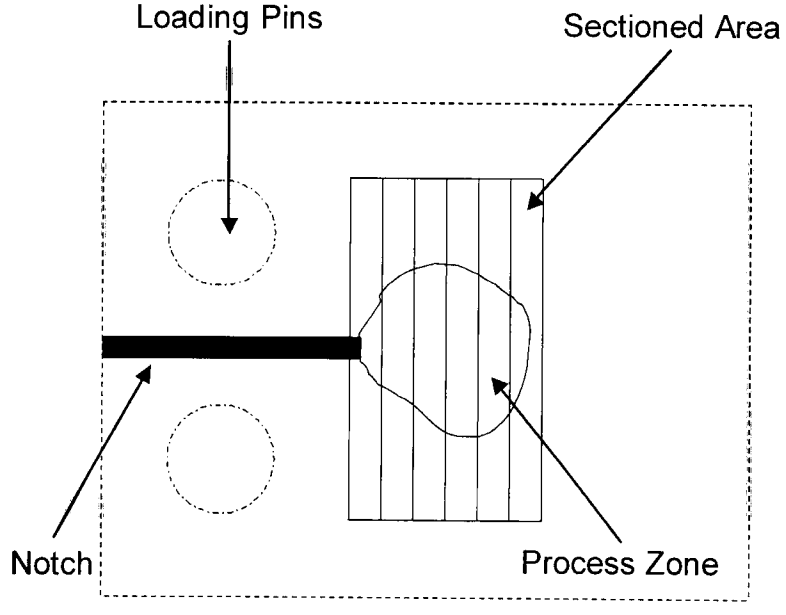

Figure 3-4: Schematic of sectioning technique, showing a typical area sectioned in the process zone ahead of the notch tip

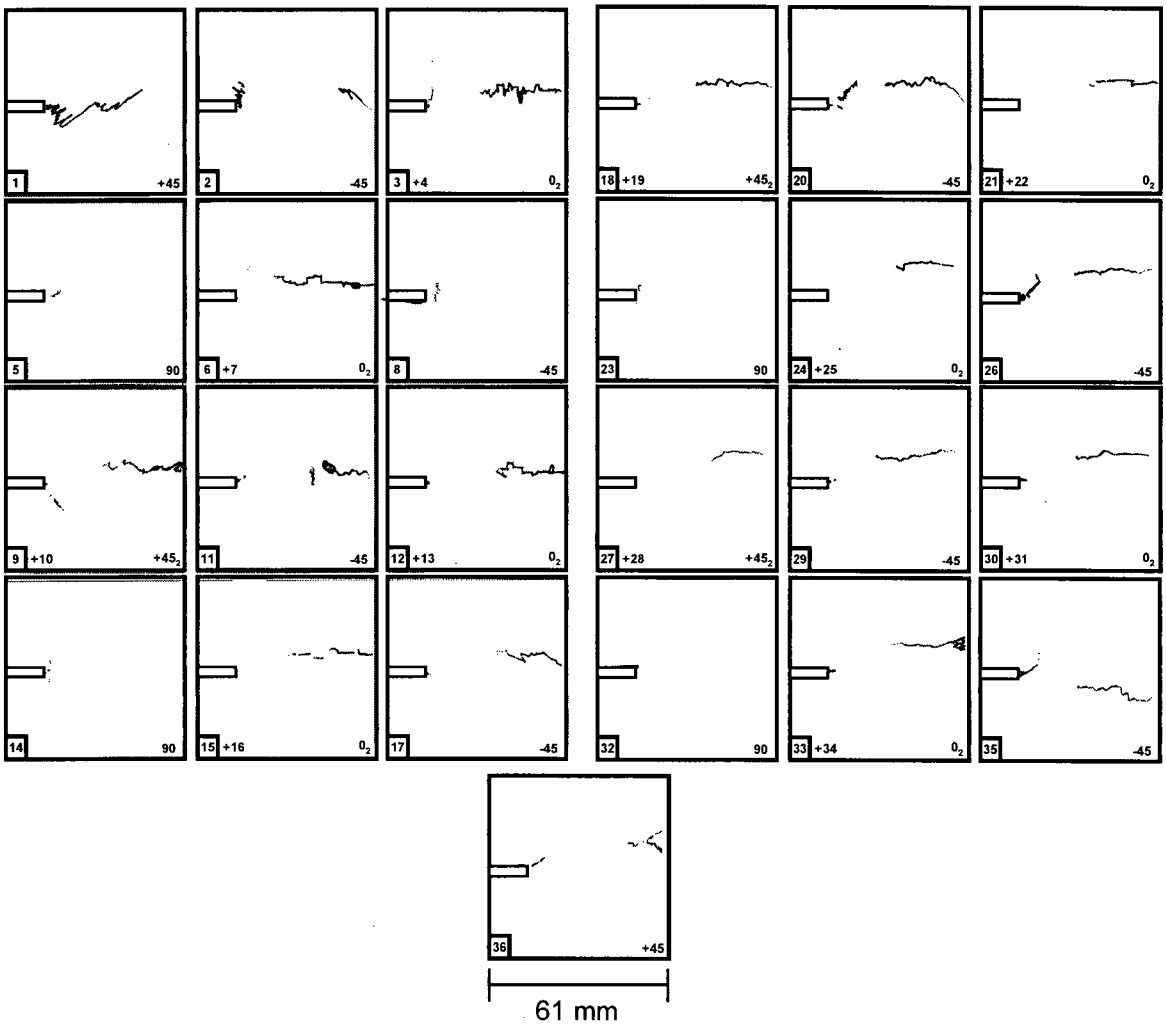

Figure 3-5: Deply documentation of test SS71-s0; S/RFI 4-stack 0° test – each ply is numbered (the plus sign indicates that two plies at the same orientation were removed together). Each ply orientation is marked at the bottom right-hand side of each ply.

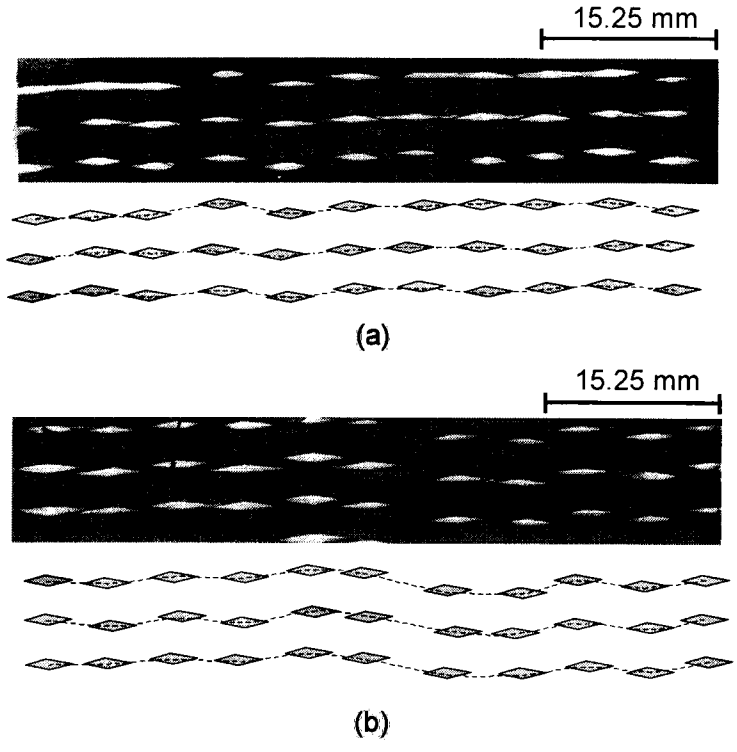

Figure 3-6: Photographs and schematics showing (after deply), (a) typically straight stitching in 4-stack stitched specimens and (b) waviness of 5-stack stitched specimens

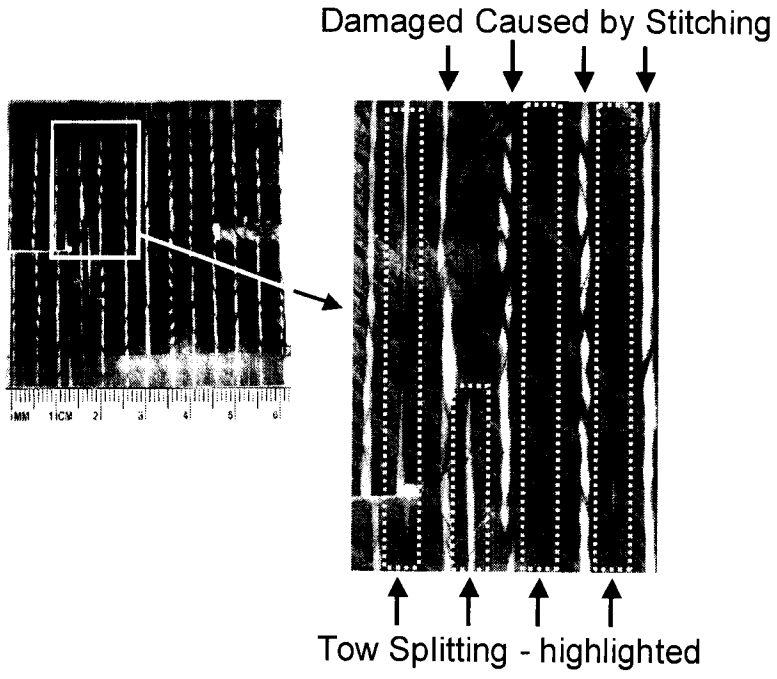

Figure 3-7: Photograph showing splitting damage in 0° ply in a 4-stack S/RFI deplied specimen

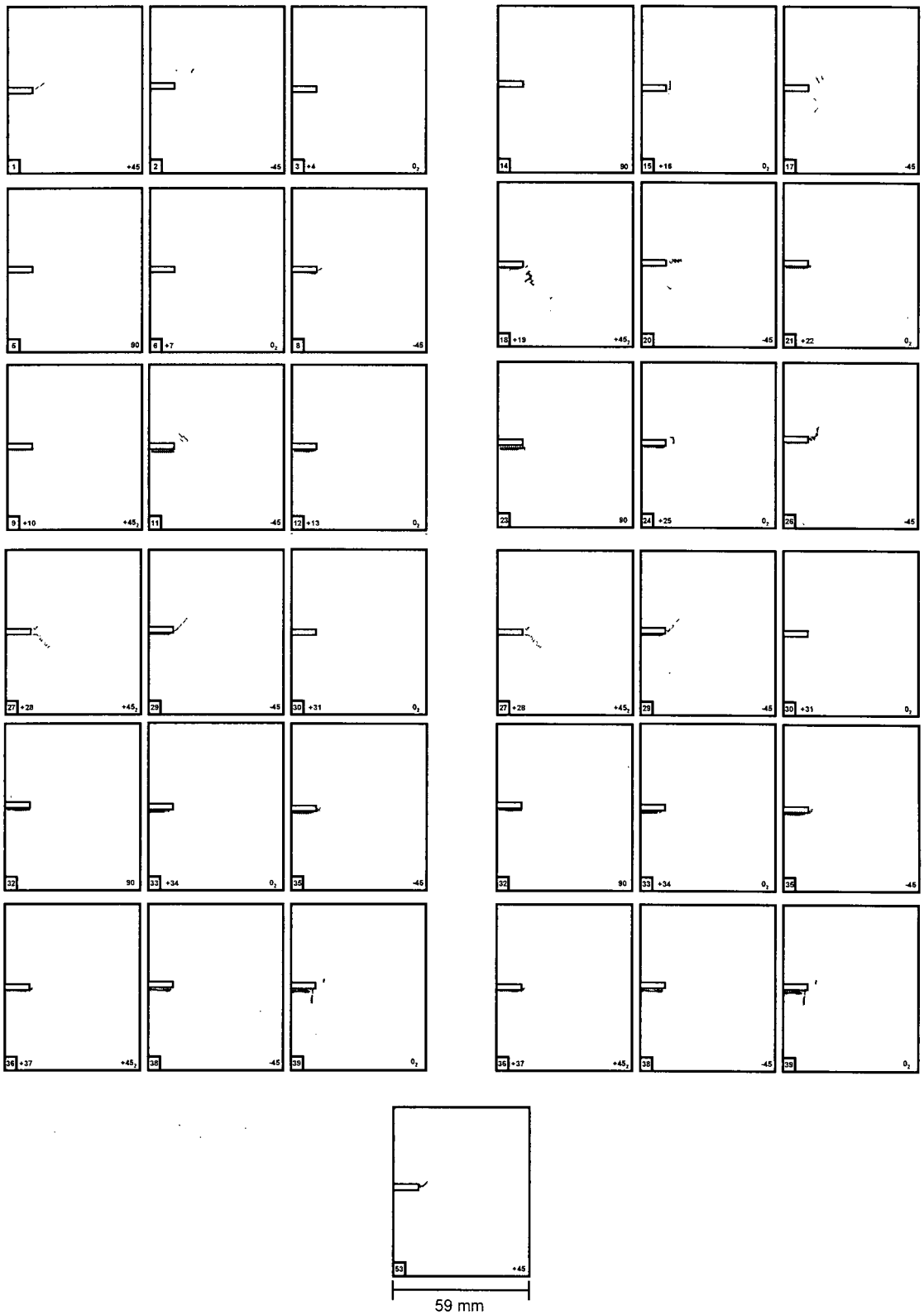

Figure 3-8: Deply documentation of test SS80-u0; 6-stack RFI 0° test – each ply is numbered (the plus sign indicates that two plies at the same orientation were removed together). Each ply orientation is marked at the bottom right-hand side of each ply.

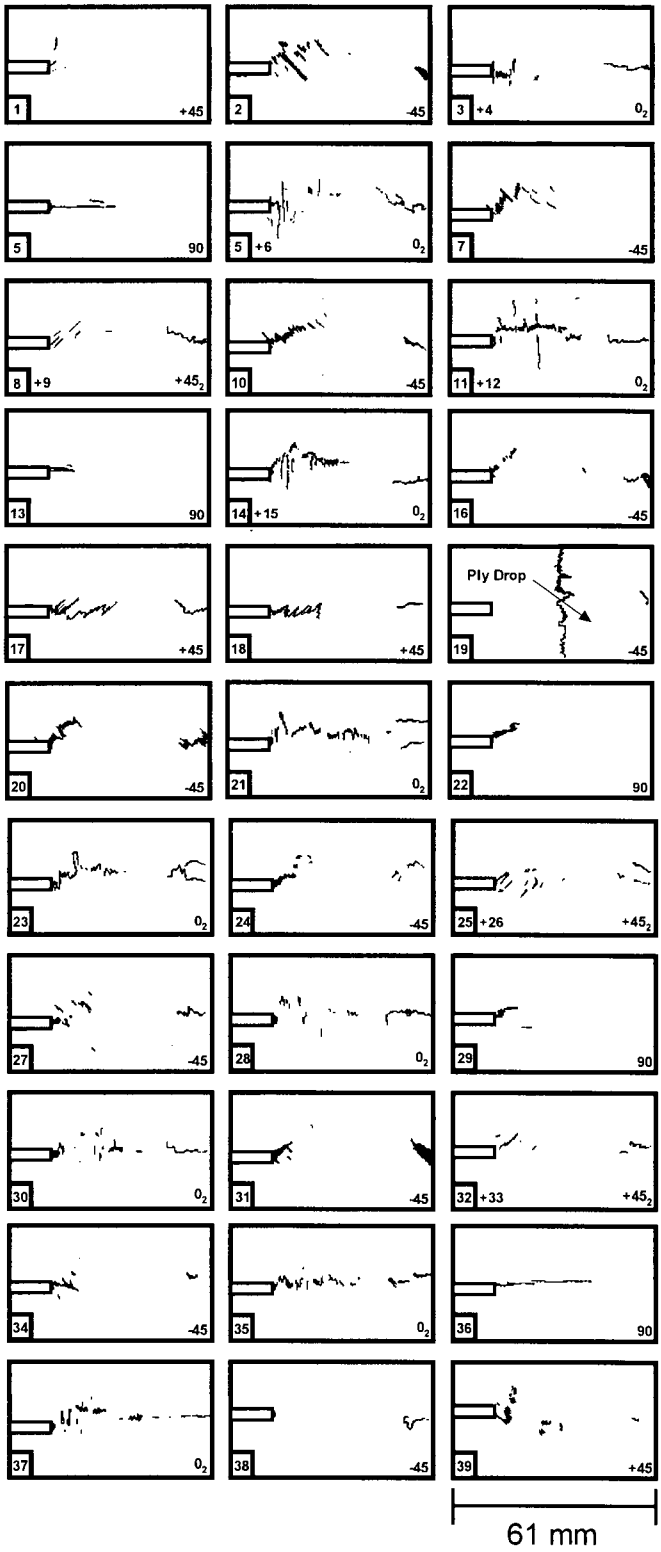

Figure 3-9: Deply documentation of test SS69-s0; 5-stack S/RFI 0° – each ply is numbered (plus sign indicates that two plies at the same orientation were removed at once). Each ply orientation is marked at the bottom right-hand side of each ply.

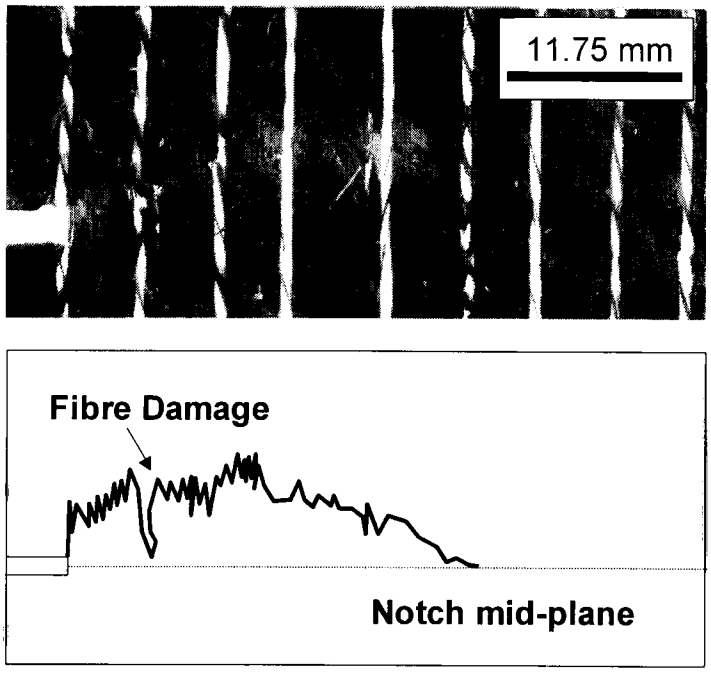

Figure 3-10: Photograph and Schematic of damage growth in 0° plies in the 5-stack 0° specimen. Note growth is perpendicular to tow direction.

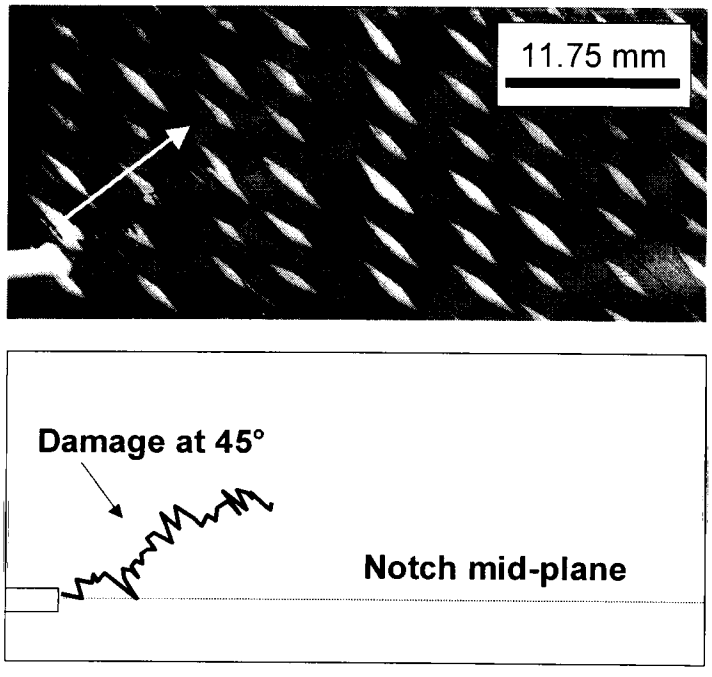

Figure 3-11: Photograph and Schematic of damage growth in -45° plies in the 5-stack 0° specimen. Note growth is perpendicular to tow direction.

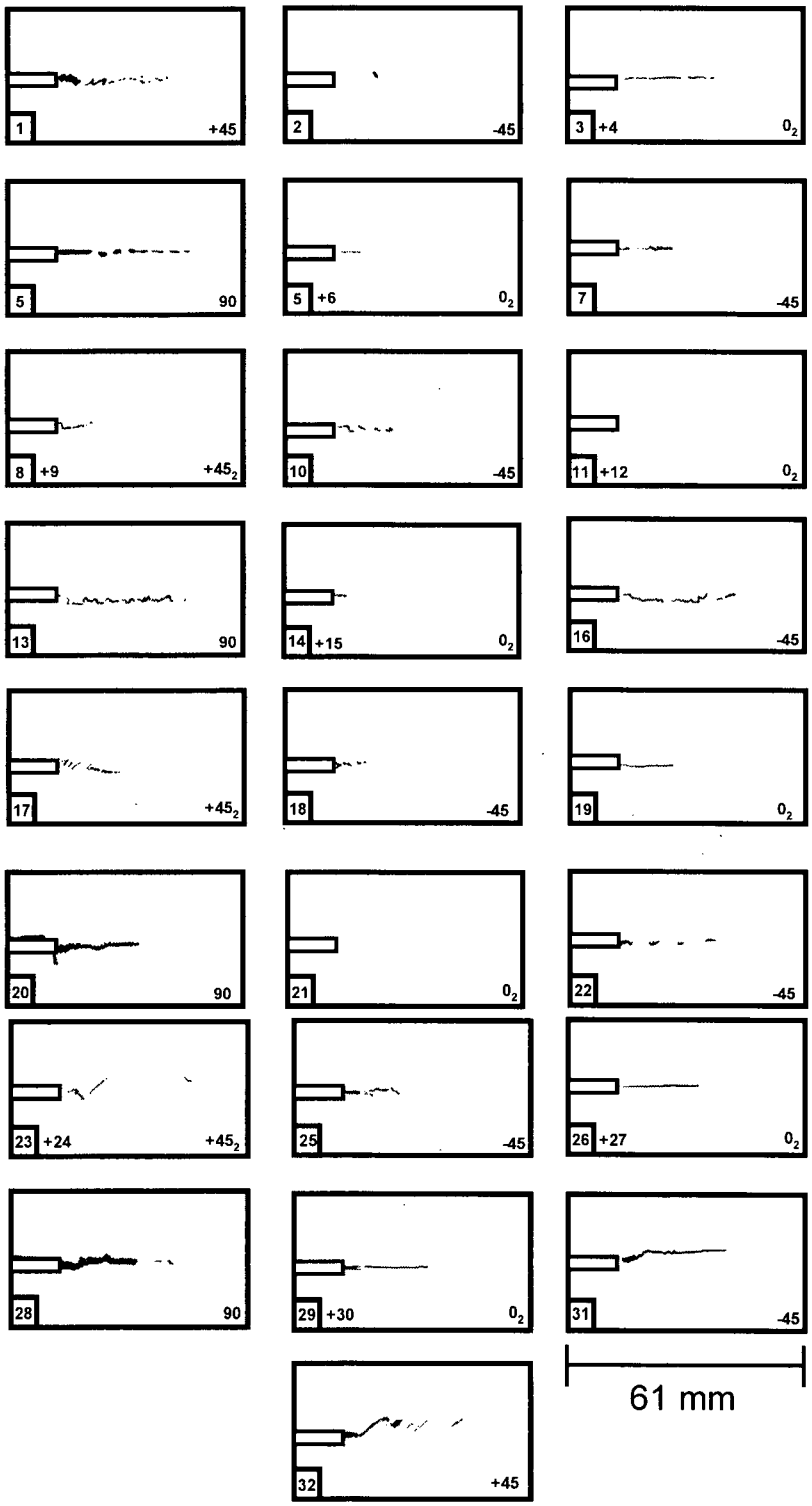

Figure 3-12: Deply documentation of test SS76-s90; 4-stack S/RFI 90°– each ply is numbered (plus sign indicates that two plies at the same orientation were removed at once). Each ply orientation is marked at the bottom right-hand side of each ply.

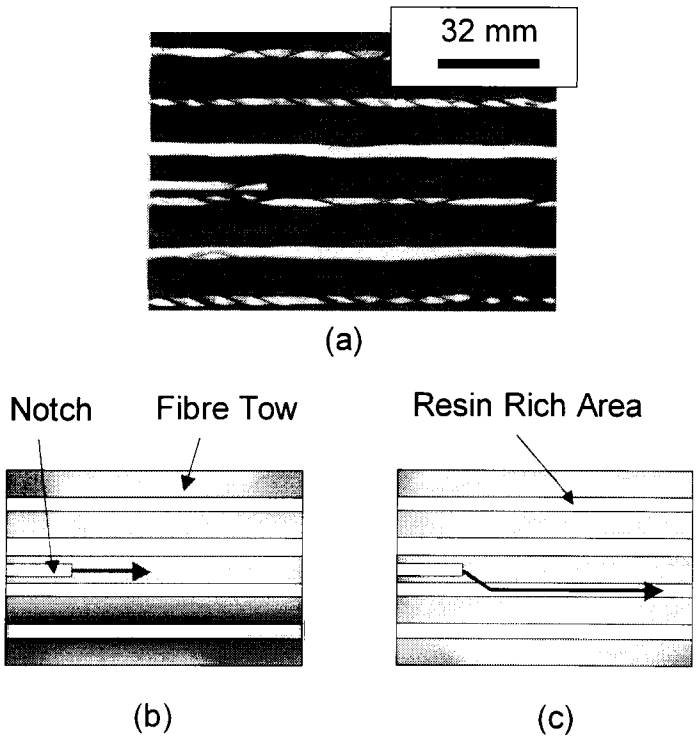

Figure 3-13: (a) Photograph of a 0° ply in a 4-stack stitched 90° specimen, note the large resin rich areas between the fibre tows, (b) schematic of 0° ply indicating splitting in tow, (c) schematic of 0° ply indicating possible damage path along the resin rich area between tows.

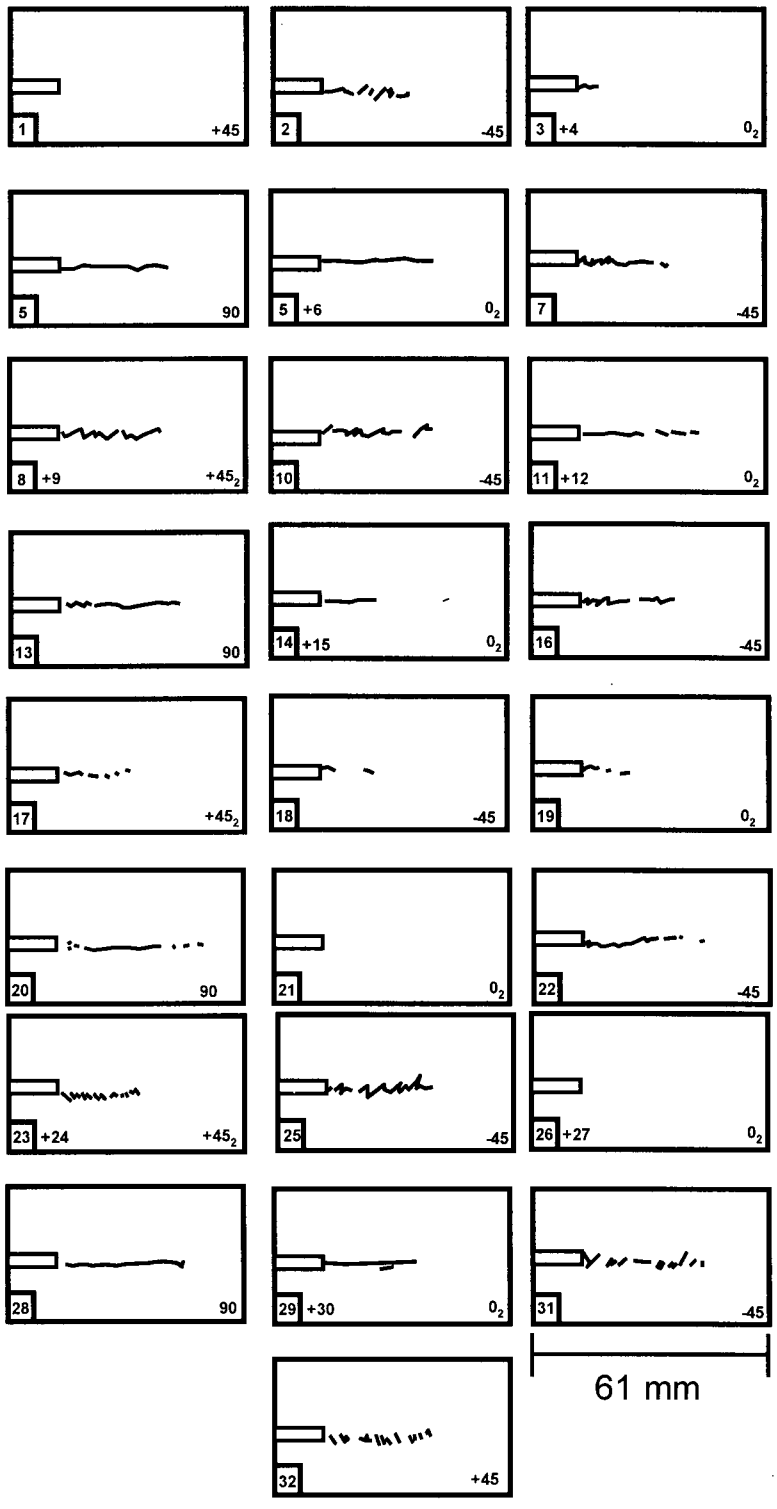

Figure 3-14: Deply documentation of test SS83-u90; 4-stack RFI 90°– each ply is numbered (plus sign indicates that two plies at the same orientation were removed at once). Each ply orientation is marked at the bottom right-hand side of each ply.

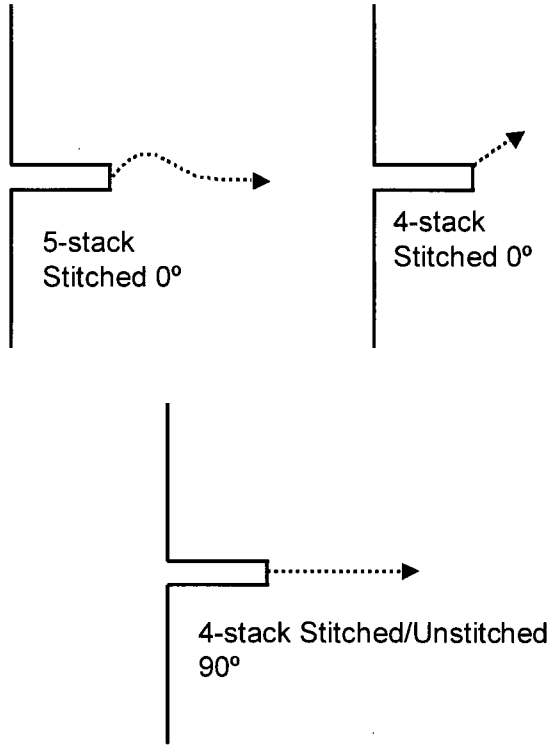

Figure 3-15: Schematic of damage growth paths in various specimen thicknesses and orientations after deply analysis.

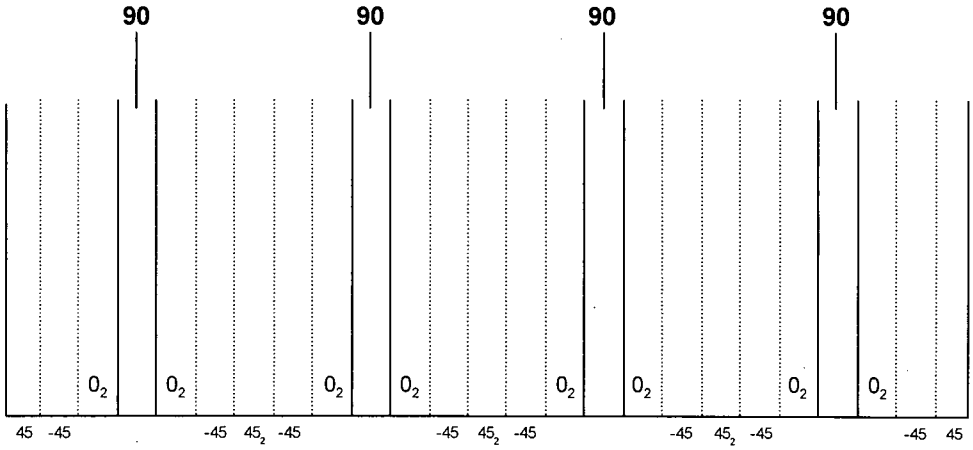

Single Stack Lay-up: $[+45/-45/0_2/90/0_2/-45/+45]_s$

Figure 3-16: Labelling convention for sectioning diagrams (4-stack illustrated).

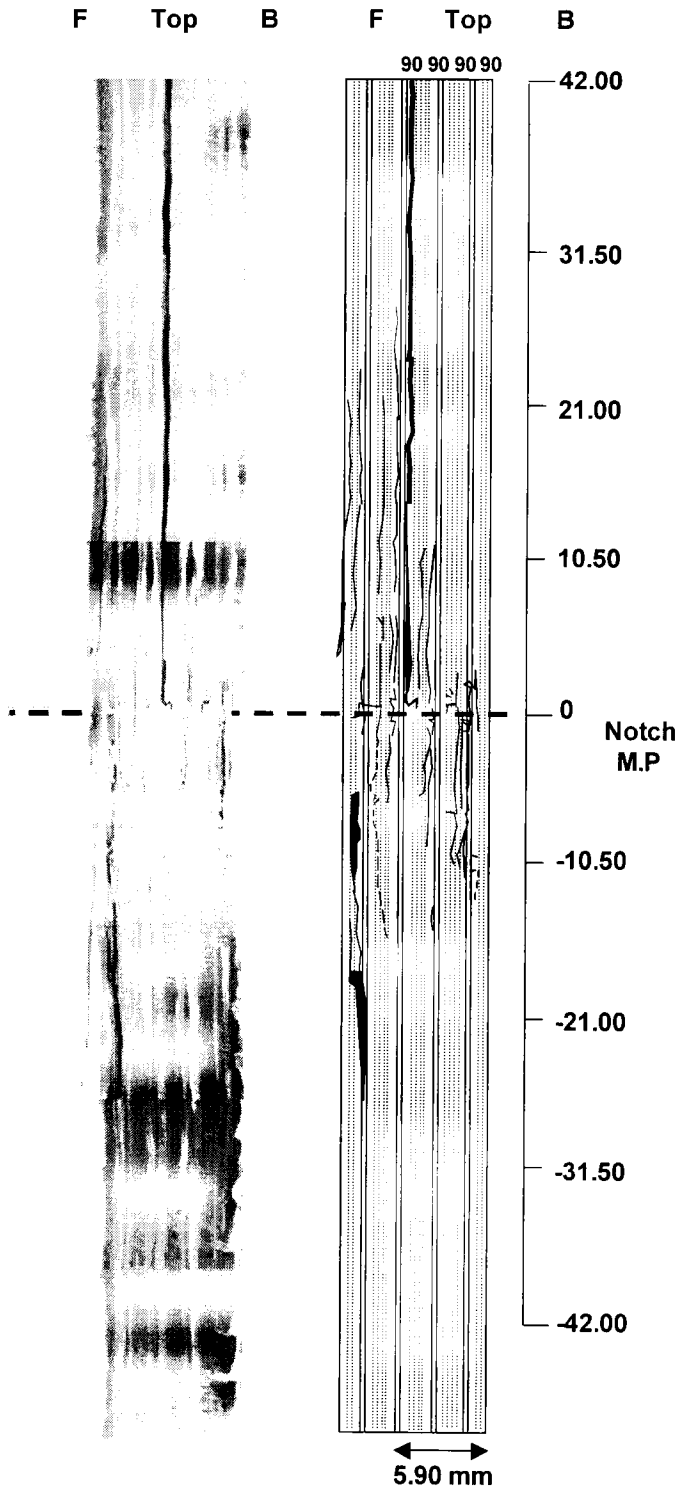

Figure 3-17: Cross-sectioning technique performed on a stitched 4-stack 0° specimen (SS68-s0-C) at 2.00 mm in front of the notch tip, (all dimensions are in mm).

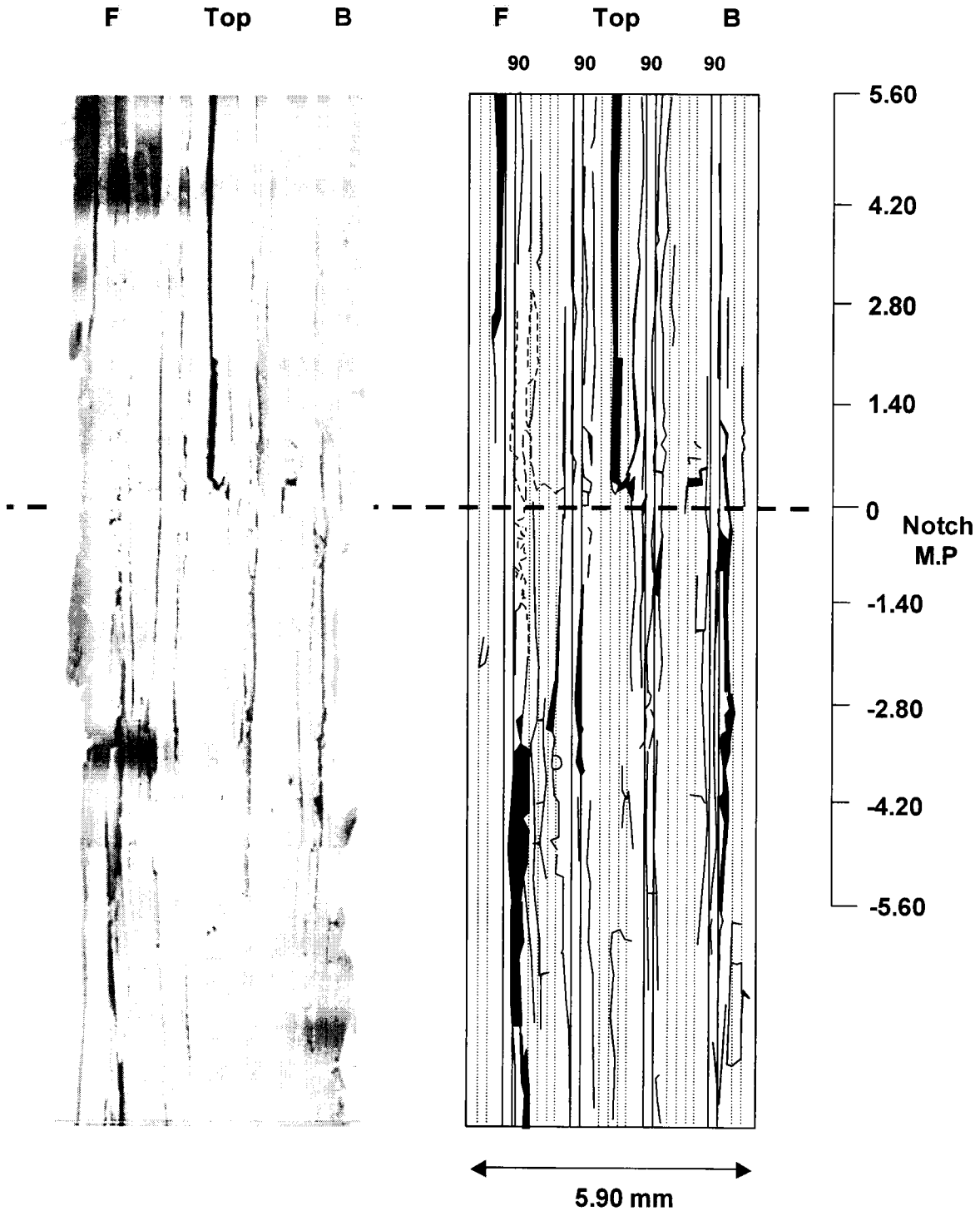

Figure 3-18: Cross-sectioning technique performed on a stitched 4-stack 0° specimen (SS68-s0-C) at 2.00 mm in front of the notch tip, (all dimensions are in mm).

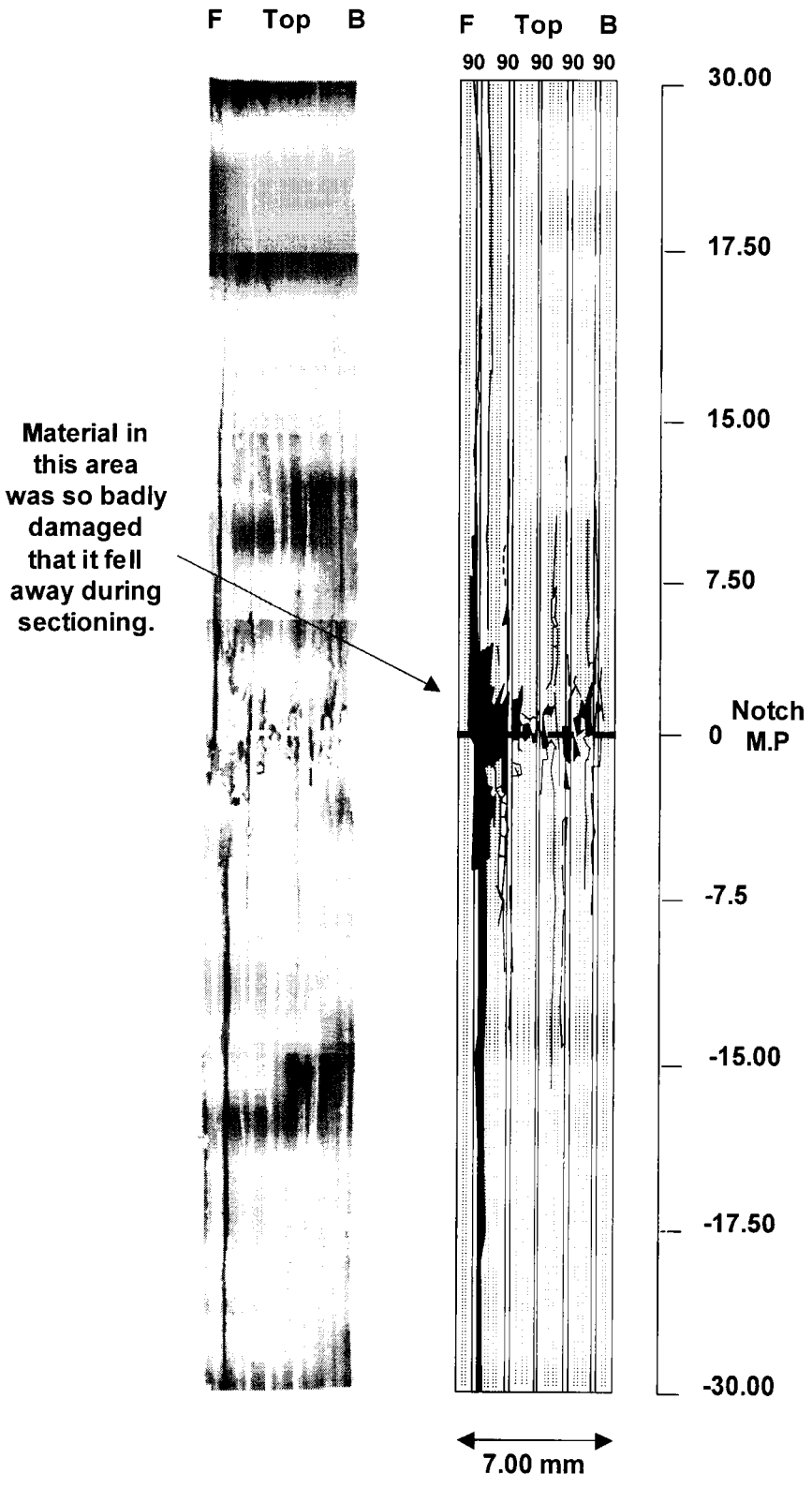

Figure 3-19: Cross-sectioning technique performed on a stitched 5-stack 0° specimen (SS70-s0-B) at 2.00 mm in front of the notch tip, (all dimensions are in mm).

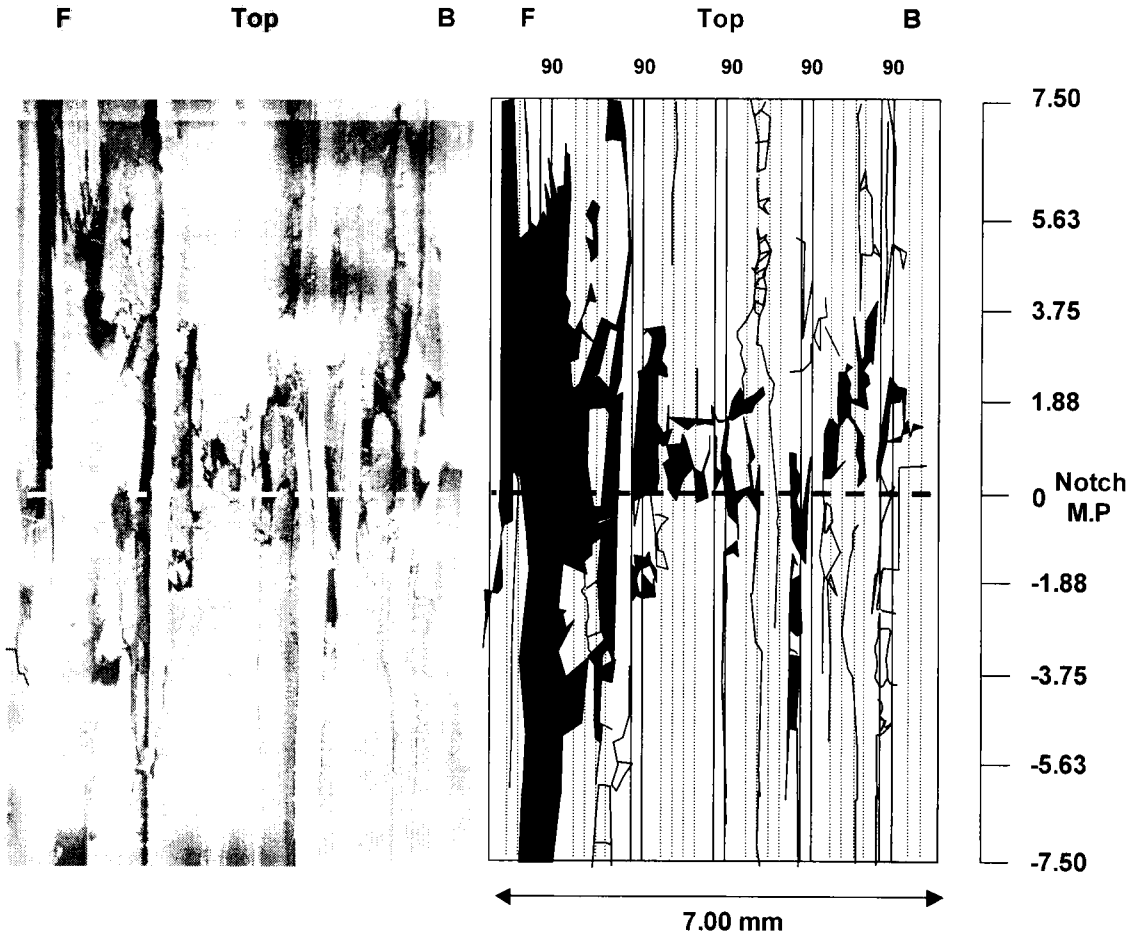

Figure 3-20: Cross-sectioning technique performed on a stitched 5-stack 0° specimen (SS70-s0-B) at 2.00 mm in front of the notch tip, Closer view than Figure 3-19. (all dimensions are in mm).

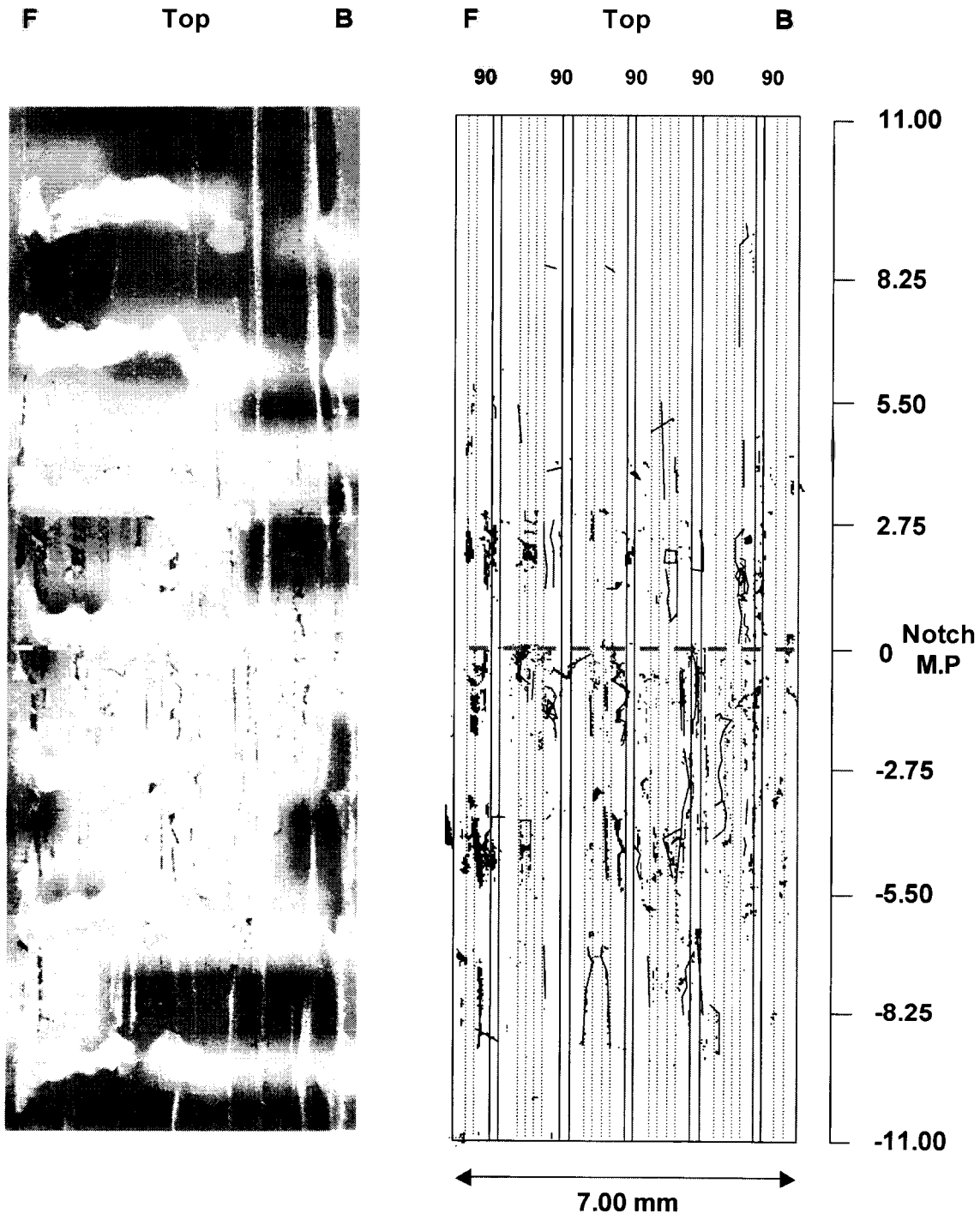

Figure 3-21: Cross-sectioning technique performed on a stitched 5-stack 0° specimen (SS70-s0-E) at 10.57 mm in front of the notch tip, (all dimensions are in mm).

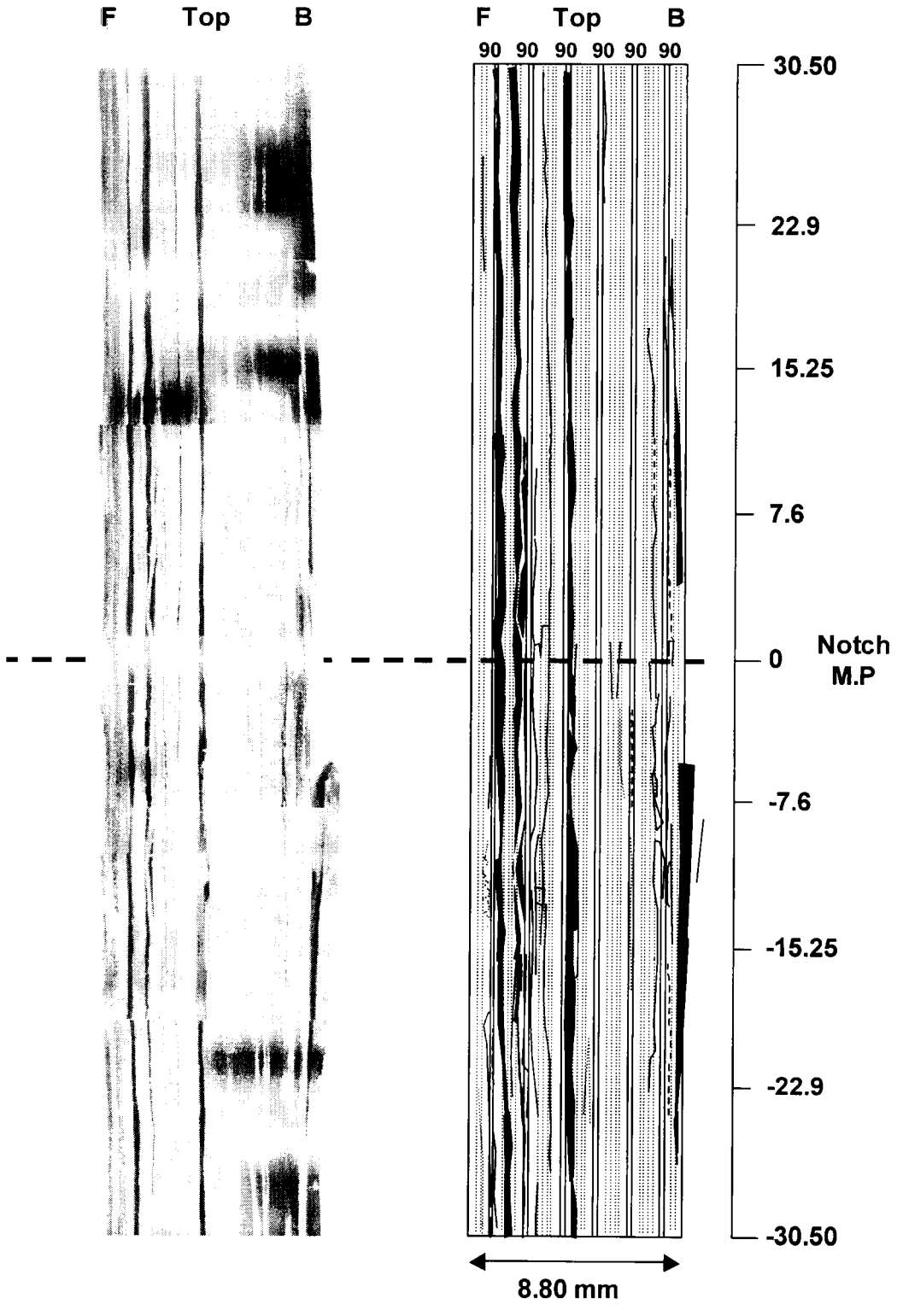

Figure 3-22: Cross sectioning for a stitched 6-stack 0° specimen (SS73-s0-A) at 2 mm in front of the notch tip, (all dimensions are in mm).

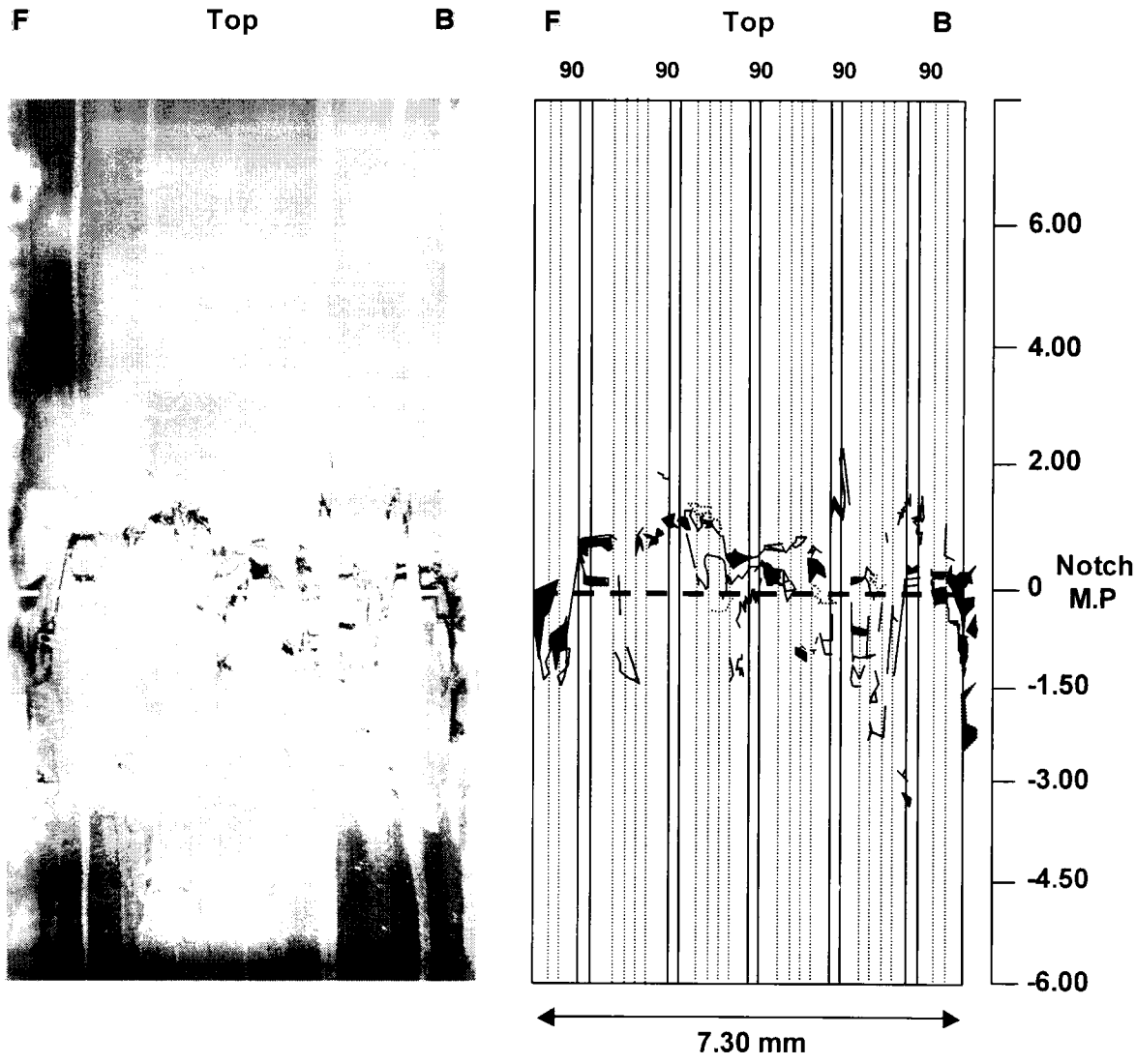

Figure 3-23: Cross sectioning for a stitched 5-stack 90° specimen (SS77-s90-A), sectioned at 9.6 mm ahead of the notch tip, (all dimensions are in mm).

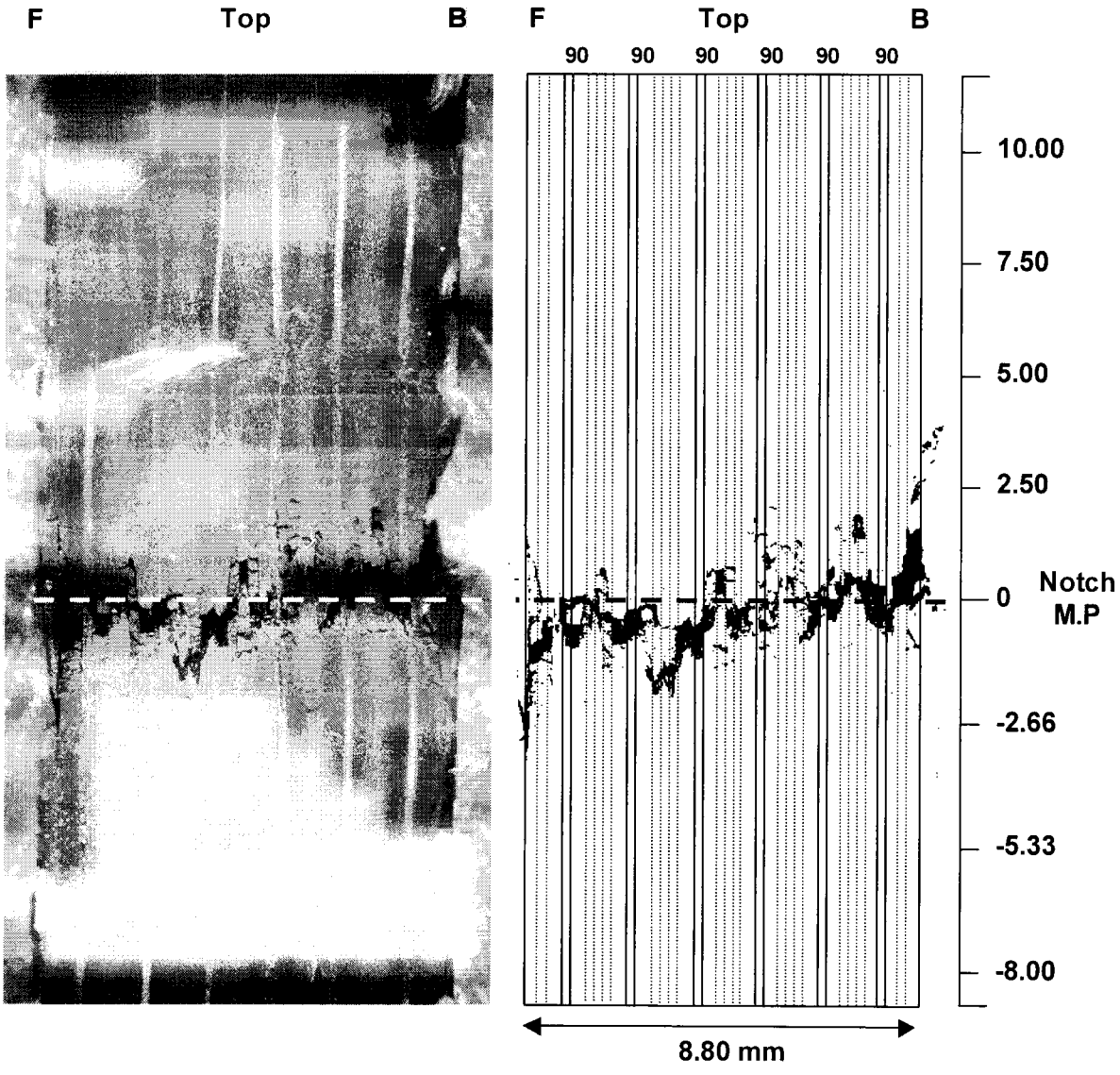

Figure 3-24: Cross sectioning for a stitched 6-stack 90° specimen (SS78-s90-A) at 1 mm ahead of the notch tip, (all dimensions are in mm).

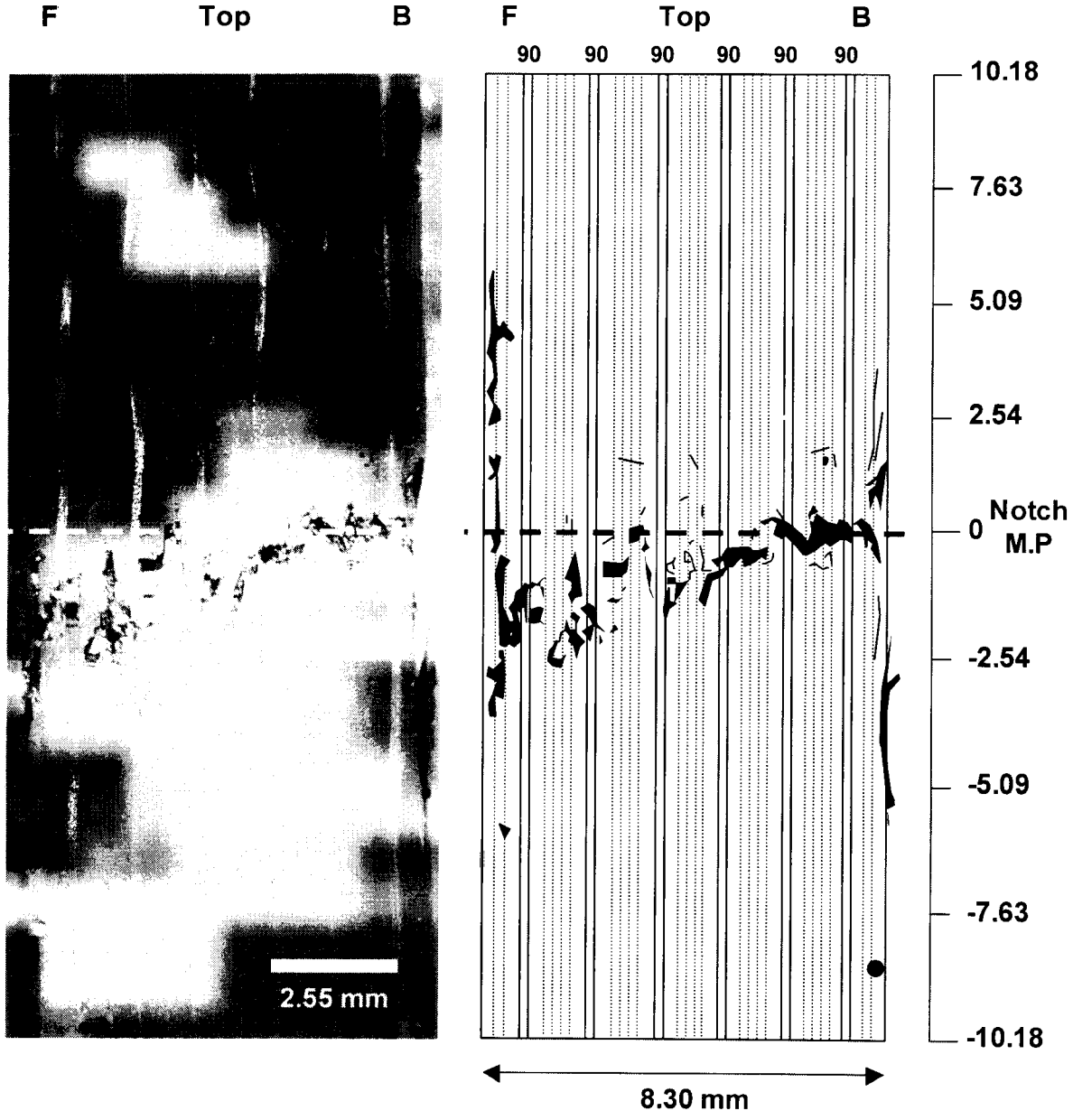

Figure 3-25: Cross sectioning for an unstitched 6-stack 90° (SS81-u90) specimen, sectioned at 2mm ahead of the notch tip. A schematic overlay of the damage is also shown (all dimensions are in mm).

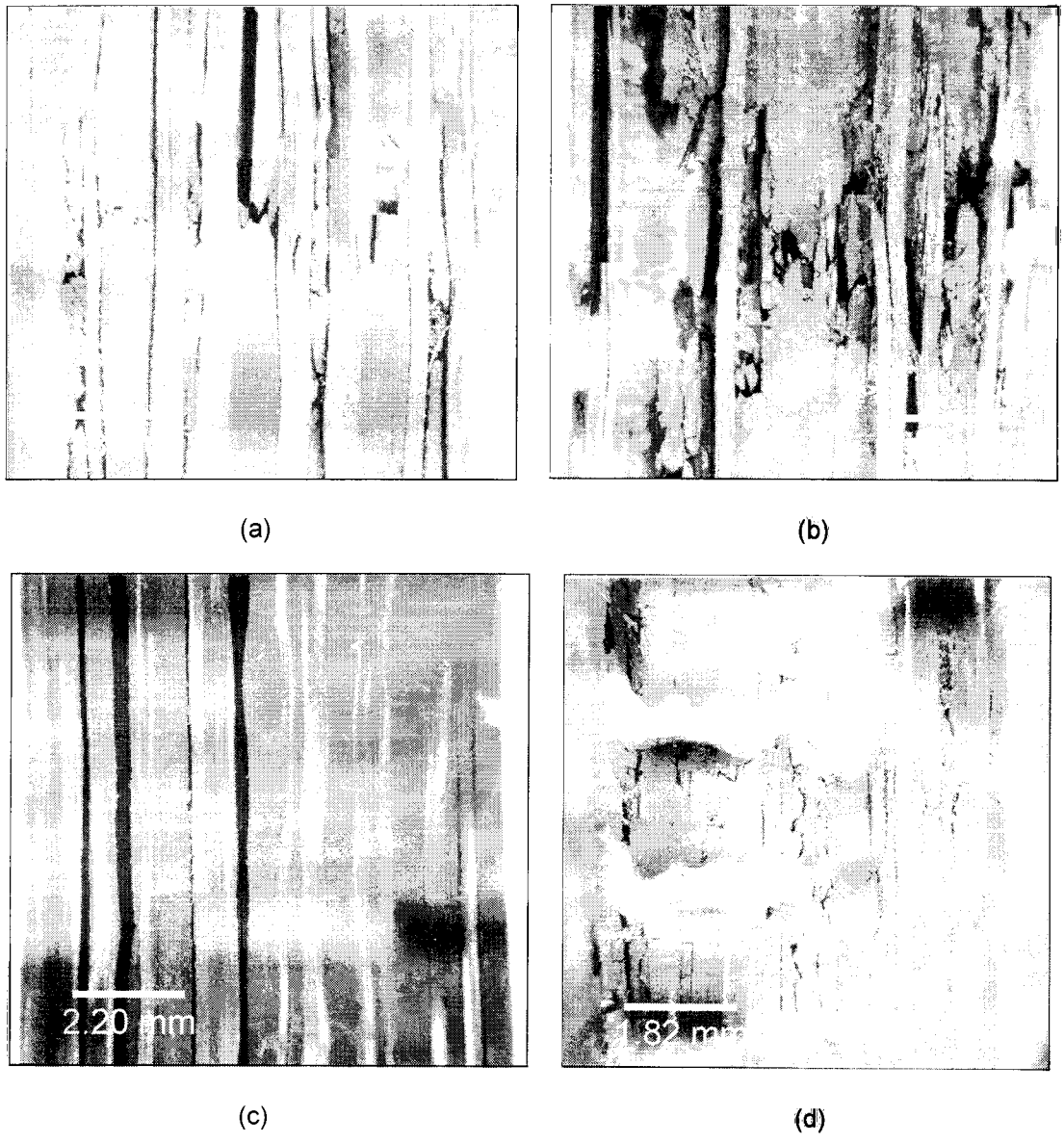

Figure 3-26: Micrographs of notch mid-planes in (a) 4-stack (SS68-s0) stitched 0°– 2 mm, (b) 5-stack (SS70-s0) stitched 0°– 2 mm, (c) 6-stack (SS73-s0) stitched 0°– 2 mm, (d) 5-stack (SS70-s0) stitched 0°- 10.5 mm

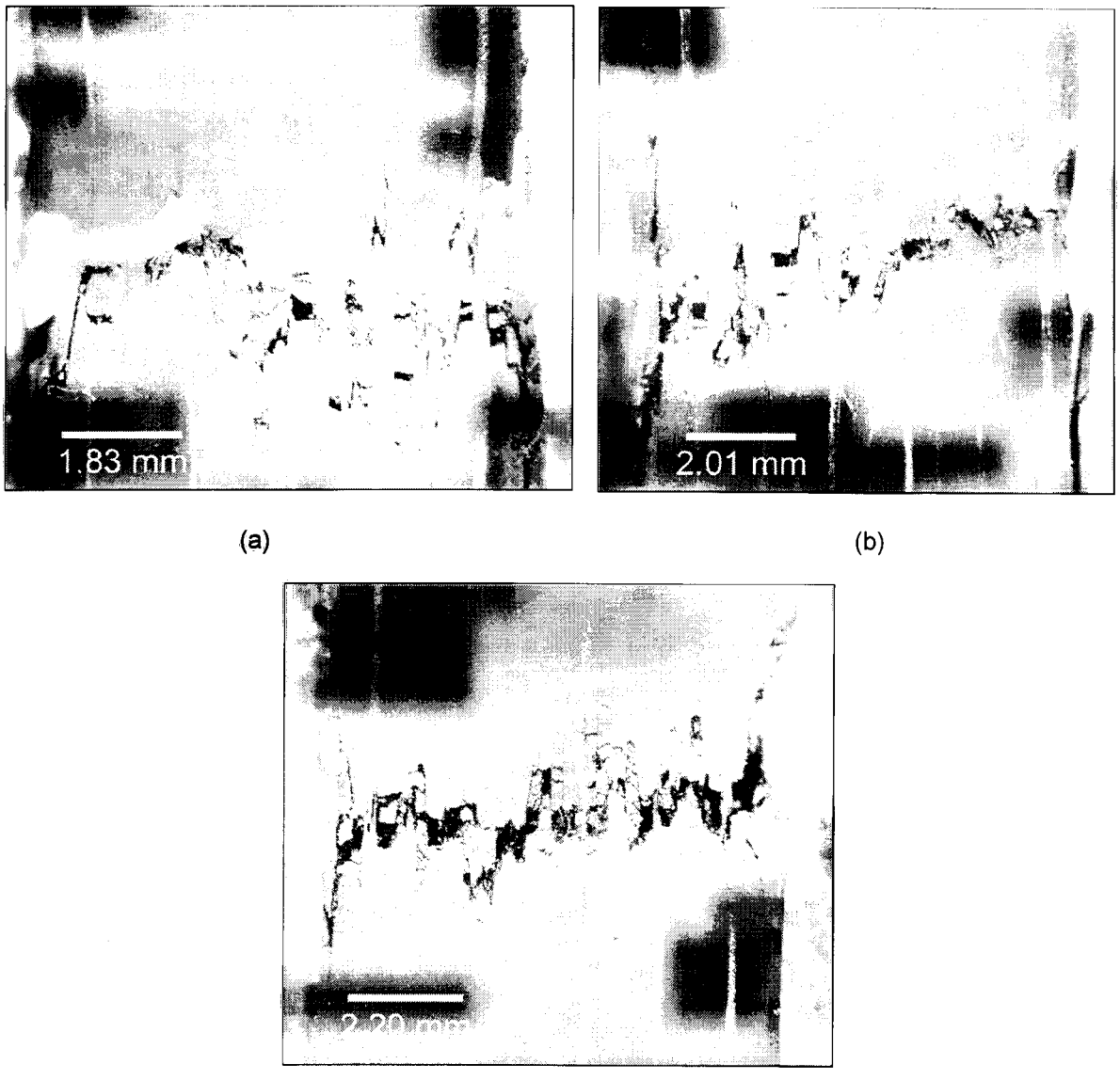

Figure 3-27: Micrographs of notch mid-planes in (a) 5-stack (SS77-s90) stitched 90°– 9.6 mm, (b) 6-stack (SS81-u90) unstitched 90°– 1 mm, and (c) 6-stack (SS78-s90) stitched 90°– 2 mm.

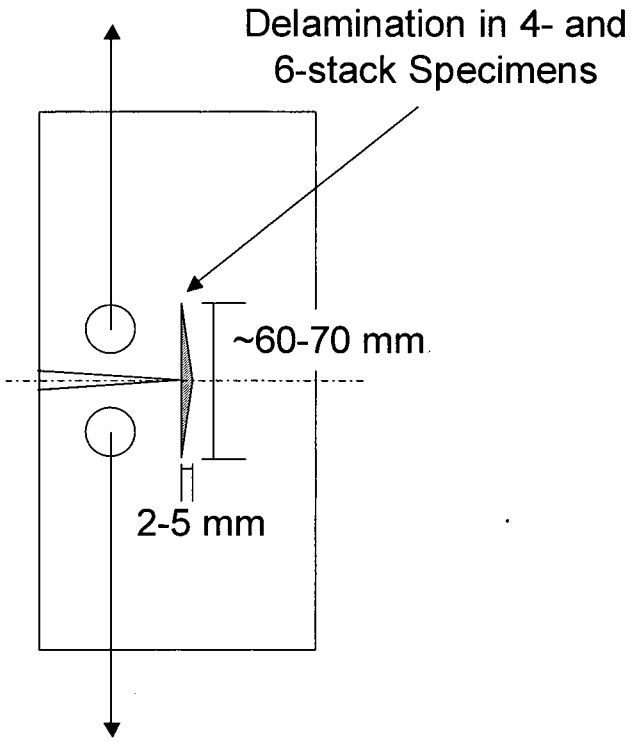

Figure 3-28: Schematic illustrating the type of delamination in the 4- and 6-stack 0°specimens. Delamination extends upwards parallel to the applied load between some 0° and 45°plies, and extends only a short distance forward across the specimen.

Chapter Four

OCT Results & Line Analysis

4. OCT Results & Line Analysis

In this chapter, the results of the OCT tests are presented and a surface line analysis technique that aids in determining damage progression is introduced. Load-CMOD (crack mouth opening displacement) plots for all OCT tests conducted on both stitched and unstitched materials are examined in detail.

Comparing the Load – Crack Mouth Opening Displacement (CMOD) Curves

A total of seventeen OCT tests were conducted. A summary of these experiments highlighting specimen type, dimensions, peak loads, etc., is given in Table 4-1. Tests were carried out at two orientations, the primary principal direction (0°) and the transverse principal direction (90°) (see Figure 2-4) for both stitched and unstitched materials for all available thicknesses. Four OCT tests were performed on the unstitched material and thirteen on the stitched. Fewer unstitched experiments were performed as results compared favourably with data from previous research [76]. There were two main responses observed when examining the load-CMOD curves, as shown schematically in Figure 4-1.

Figure 4-2 to Figure 4-6 are the actual shapes of the curves for the various orientations, thicknesses and materials obtained during testing. Figure 4-7 shows a comparison of the damage onset loads and maximum loads attained during OCT testing and Figure 4-8 shows the same data normalised for specimen thickness. From this comparison, it is apparent that stitching has not in general affected maximum loads over the unstitched material. In some cases where it has reduced them, this could be attributed to fibre damage and misalignment due to stitching.

Comparison of Stitched 0° Specimens and Stitched 90° Specimens

Figure 4-2 shows the difference in behaviour of the 4-stack stitched material when loaded in the two principal orthogonal directions, Figure 4-3 and Figure 4-4 show the results of the 5 and 6-stack stitched materials respectively.

The 0° direction is stiffer than the 90° direction for all thicknesses and the maximum loads obtained for the 90° tests are approximately 60% lower for the 4- and 5-stack materials and approximately 67% lower in the 6-stack material. The shape of the 4- and 6-stack specimen curves are different depending on the direction the material was tested, however for the 5-stack material this was not the case.

The 4- and 6-stack 0° specimens show linear loading until damage onset, after which, the load continues to rise amid several load drops until final specimen failure by back face compression. The 5-stack 0° specimens also exhibit linear loading until damage onset, after which the load peaks and then steadily decreases with large intermittent load drops. This behaviour is similar to the curves for all 90° specimens, although the 5-stack 0° tests show a greater stiffness and maximum load.

Comparison of Unstitched 0° Specimens and Unstitched 90° Specimens

The 4 and 6-stack unstitched materials behaves differently depending on the loading direction (Figure 4-5 and Figure 4-6).

Results were similar to the stitched material, once again the 0° direction is stiffer than the 90° direction for both thicknesses and the maximum loads obtained for the 90° tests were also approximately 69% and 66% lower for the 4- and 6-stack materials respectively. The shapes of the curves are similar to the their stitched counterparts, however notice the slight difference in shape

between the 4-stack stitched and unstitched 0° tests, the stitched specimen's load appears to plateau whereas the unstitched does not.

Comparison of Stitched and Unstitched Materials

The stitched and unstitched 0° data is compared in Figure 4-9, in general, the load-CMOD response is very similar. The 4-stack stitched and unstitched stiffnesses compare well, although the peak load obtained in the stitched material was approximately 15% lower. The 6-stack unstitched material is slightly stiffer than the stitched which has a peak load approximately 4% lower.

Figure 4-10 compares the stitched and unstitched data for the 90° tests. The curve shape is very similar for both the 4- and 6-stack, stitched and unstitched specimens. The peaks loads are also comparable, with the stitched material offering only a 6% and 2.5% improvement over the 4- and 6-stack unstitched materials respectively.

The Effect of Specimen Thickness

The effect of specimen thickness is shown in Figure 4-11 (for the 0° tests) and Figure 4-12 (for the 90° tests), where each curve has been normalised with the thickness of the specimen. The 0° OCT behaviour normalises well regarding initial specimen stiffnesses, however once again the anomalous 5-stack 0° behaviour is highlighted when compared to the 4- and 6-stack 0° specimens. The 90° specimen behaviour normalises very well with thickness.

Surface Line Analysis

This technique allows the measurement of material displacement in front of the notch tip, which is an indicator of the progression of damage across the specimen width during testing. Horizontal lines were inscribed on the surface of the specimen at 2.5 mm intervals above and below the notch mid-

plane. Each analysis was performed on a pair of lines at equal distance above and below the notch mid-plane. The chosen lines were closest to, but not directly affected by, surface delamination or visual damage under the surface of the specimen. During each test, photographs were taken at regular intervals or after a significant event (such as a load drop or loud sound). These were then scanned at 300 dots-per-inch using a Hewlett Packard desktop scanner.

The photographs were then imported into a computer software package (see Figure 4-13) capable of point-to-point measurement. Two photographs were imported, one taken before the test and one taken during the test. A point-to-point calibration is made and an origin is set at the same point on both photographs. The line displacements on each photograph are taken at incremental distances ahead of the notch tip, and the results are presented as half the total displacement between the pair of lines. As, will be shown in the following section, the point of zero displacement of each line in front of the notch tip approximately corresponds to the length of internal damage. This method has been proven to provide a good indication of damage progression across the specimen in the presence of self-similar damage growth [6]. Figure 4-14 (a) shows a typical line analysis plot, with the corresponding Load-CMOD in Figure 4-14 (b), photographs taken for the line analysis are indicated.

Interpretation of Line Analysis Plots

The damage characterised in the previous chapters by the deplying and sectioning techniques can be used to help interpret the line analysis plots, which in turn can be used to help interpret the load-CMOD data. Results presented so far have revealed two distinct types of behaviour observed during testing i.e. the specimens either exhibit self-similar or crack blunting behaviour. Line analysis results also reports these two types of behaviour.

Self-similar (Brittle) Behaviour (All 90° Specimens and Stitched 5-stack 0°)

The deply and sectioning results have revealed that all 90° specimens and the 5-stack 0° S/RFI specimens exhibit self-similar damage growth. The load-CMOD curves for these specimens also show a distinct difference in shape when compared to the other 0° OCT specimen data. The line analysis data allows us to expand on this inconsistency, by allowing us to track the progression of the damage during the test.

Figure 4-14 shows a surface line analysis plot and corresponding load-CMOD curve for a 5-stack S/RFI 0° specimen (SS69-s0). Each plotted line represents a point (or photograph) during the test; the point at which these lines intersect the x-axis represents the approximate position of the damage front within the specimen, heavy fibre damage plus any damage associated with the process zone. This plot clearly illustrates a moving damage front, gradually stepping from left to right across the specimen throughout the test.

The deply evaluation of this specimen indicated a damage length of approximately 20–30 mm across the width of the specimen, therefore why does photograph 29 on the plot indicate an internal damage of approximately 38–41 mm? Quite simply, this is because at the end of the test the specimen suffered back-face compression failure just after photograph 28. Subsequently, there is in fact damage present, however it is not directly associated with notch extension. Taking this into account, final crack extension before back-face compression failure was likely to be between photographs 24 and 28, or between 27 and 34 mm, which corresponds well with the deply that reports an average of 26.6 mm of heavy fibre damage in the 0°plies. The results from the line analysis indicate a slightly longer damage zone as it includes not only the fracture process zone but also elastic strain in the specimen, as measurements were not taken at the specimen flanks (edges), but at lines marked on the surface of the specimen.

Kongshavn and Poursartip [6] also complied line analysis data, and demonstrated that major load drops during testing can represent large crack extensions for their material system. Figure 4-14(b) show a large load drop between photographs 22 and 24, however the line analysis plot only indicates crack growth of only 2 mm, therefore for this specimen the large load drop did not represent a large crack extension. Figure 4-15 shows the surface line analysis plot and corresponding load-CMOD curve for another 5-stack S/RFI 0° specimen (SS70-s0). The line analysis suggests self-similar damage growth across the specimen for approximately 26-28 mm, in good agreement with the sectioning results for this specimen (25.9 mm), again taking into account the fact that the line analysis picks up elastic strain as well as the process zone.

The line analysis plots for 4, 5 and 6-stack stitched 90° specimens (SS76-s90, SS77-s90 and SS78-s90) and the 4 and 6-stack unstitched 90° specimens (SS83-u90 and SS81-u90) are comparable to the 5-stack 0° specimens (Figure 4-16 to Figure 4-20). All plots indicate self-similar damage growth and all final damage lengths are in good agreement with deply (SS76-s90, SS77-s90, SS83-u90) and sectioning (SS78-s90, SS81-u90) results, as summarised in Table 4-2 and Table 4-3.

Crack Blunting Behaviour (Stitched 4 and 6 Stack 0°)

This type of behaviour occurs in 4 and 6-stack stitched and unstitched 0° OCT tests. Figure 4-21(a) and Figure 4-22(a) are line analysis plots of 4-stack stitched 0° tests (SS68-s0, SS71-s0). On comparison with the plots of the 90° and 5-stack 0° tests, one first notices that signs of self-similar growth are absent. The 4 and 6-stack 0° plots do not display evidence of a moving damage front from left to right across the specimen. Sectioning of test SS68-s0 revealed a fibre damage length of only 7.8 mm, however the corresponding line analysis suggests damage has grown much further into the specimen. In addition, the deply of test SS71-s0 revealed that damage had progressed only 10

mm across the specimen not 26 mm as the line analysis suggests. This discrepancy can be explained by comparing the shape of the lines to those of the 90° tests, all exhibit a characteristic kink in the outer most lines. For example, the sectioning results of test SS73-s0 (Figure 4-23), a stitched 6-stack 0° specimen indicated that damage was comprised of a great deal of delamination, with a small amount of fibre breakage. The sectioning also indicated that the specimen had not undergone self-similar crack growth, indeed the opposite seemed to have occurred, and the crack was blunted. Therefore there must be a correlation between this and the characteristic kink in the lines in Figure 4-23(a).

Another example is shown in Figure 4-24, the line analysis plot and associated load-CMOD curve for test SS80-u0, an unstitched 6-stack 0°specimen. Photograph 29 on this plot shows the characteristic kink at approximately 11 mm in front of the notch tip, which correlates well with the deply results for this specimen that recorded damage growth up to 10 mm. Comparisons of the damage recorded during deply and sectioning with the line analysis are given in Table 4-2 and Table 4-3.

The schematic in Figure 4-25 describes visually how the kink is formed in the line analysis. Line a–b represents the point at which crack blunting occurs, damage no longer grows across the specimen but grows upwards in the form of delamination.

The reader will also have noticed that an equivalent strain axis has been plotted on the line analysis for the 4 and 6-stack, stitched and unstitched 0° specimens. The equivalent strain is calculated from the displacement of the inscribed lines on the specimen surface (Figure 4-26). In addition, the equivalent strains at the characteristic kinks in the outermost lines of each line analysis are listed in Table 4-4. It is interesting to note that all of the characteristic line kinks occur at equivalent strains below approximately 1.3% and that the strain-to-failure of a typically AS-4 carbon fibre is between

1.3 and 1.65% (depending on the diameter) [77]. This also suggests that the material in front of the kink is below the strain-to-failure of the carbon fibres and hence could explain why fibre damage was not observed during deply or sectioning.

Displacement of Lines Farther Away from the Notch Mid-plane

Figure 4-27 and Figure 4-28 indicate the importance of choosing lines that are not affected by surface damage and are as close to the notch mid-plane as possible. Figure 4-27 shows the effect of carrying out line analysis at 25mm (line 10) and 12.5mm (line 5) from the notch mid-plane for a 6-stack stitched 0° test (SS73-s0). The sectioning results for this specimen conclude that fibre damage is only present up to 7.2 mm; taking measurements at line 10, Figure 4-27(a), clearly predicts the damage zone to be much greater, however, taking measurements at line 5, Figure 4-27(b), the characteristic kink in the line analysis is present at approximately 7mm.

The line analysis carried out for SS68-s0, a 4-stack 0° specimen, gives further confirmation of this effect (Figure 4-28). Whereas, line 6 (15mm) agrees with sectioning, indicating that damage has grown to approximately 7–8mm, line 9 (22.5mm) over-predicts the amount of damage present.

This effect is present as the line analysis plots are basically an integration of the strain in front of the notch tip, and therefore the error is greater the further the line is from the notch mid-plane. Lines closer to the notch mid-plane do not suffer from an accumulation of strain, as do the lines further from the notch mid-plane.

Compliance Behaviour of Specimens that Exhibit Self-Similar Crack Growth

Investigating the compliance[5] behaviour of specimens that exhibit self-similar growth is an

[5] Compliance is defined as the ease in which a body can be deformed elastically, and equals deflection/force (δ/P) or reciprocal specimen stiffness.

interesting method of combining load-CMOD, line analysis and deply data, whilst confirming the occurrence of self-similar crack growth.

In theory, a specimen with a notch length, a, that has been tested and has suffered some crack extension, of length b, should possess a similar compliance to that of a specimen with a pre-cut notch of length equal to $a + b$ (Figure 4-29). Therefore it is possible to compare the compliance data from a range of specimens containing different notch lengths to compliance data obtained during one OCT test that exhibits self-similar growth.

Obtaining compliance data experimentally from OCT specimens with a range of notched lengths is somewhat time consuming, and therefore a finite element program (LS-DYNA version 960) was used to generate compliance data for a range of notch lengths [78]. The program was used to analyse a fine mesh of half the specimen geometry using the elastic properties of the S/RFI material as inputs (see Table 2-1). By progressively removing the boundary conditions along the notch mid-plane (also the line of mesh symmetry) before each numerical run the notch length was gradually increased. The finite element analysis generates pin Force-CMOD data, from which the compliance can simply calculated from the secant modulus of the data point at the ultimate pin force.

On the experimental side, the line analysis plots indicate the amount of damage extension for a given Load and CMOD during an OCT test. Therefore, by taking the secant modulus of the data points associated with the lines from the line analysis plot, one can calculate the compliance of the specimen for a given crack extension. Consequently, one can track the change in compliance throughout the test.

Figure 4-30 shows the load-cmod curve and corresponding line analysis of test SS69-s0, a stitched 5-stack 0° specimen that exhibits self-similar crack growth. An important feature of this particular line analysis are the plotted lines of photographs 3–9 which all report 10 mm of damage in front of the

notch tip. All of these lines 'hinge' at 10 mm, and therefore it is likely that the line analysis is reporting only elastic strain up to photograph 9 and not damage. This can be confirmed as photographs 3–9 were taken during the linear part of the load-CMOD curve. As an indication of the extent of strain present, a region of <1% strain has been indicated on this line analysis.

The experimental specimen compliances from the load-CMOD curve and relative crack extensions from the line analysis can be plotted as shown in Figure 4-31(a). Also plotted are the compliances from the finite element analysis, in this case the crack extension represents the initial notch length defined in the mesh. As expected the compliance rises with crack extension, however the experimental curve is somewhat offset from the FE compliances. This offset can be explained as follows: after testing two S/RFI OCT specimens that have two different notch lengths, a_1 and a_2 where $a_1 > a_2$, the specimens will only exhibit the same compliance if the length of damage in the specimen with the smaller notch length, a_2, is greater than a_1. Therefore, the damage does not affect the compliance the same extent as a true notch or crack, as not all plies in the laminate are damaged to the same extent. Although the 0° plies may show heavy fibre damage across the specimen, other orientations may not.

By plotting the effective change in crack length from the compliance (effective change in notch length) versus the change in crack length from the line analysis, Figure 4-31(b), the length of internal damage measured from the line analysis is shown to be consistently 6–10 mm greater than the effective notch length from the FE compliance. This is reasonable as the FE compliance predictions do not necessarily include any damage and do not take into account the full fracture process zone, i.e. Figure 4-33. The line analysis measurements also include line displacement caused by elastic strain, as indicated in Figure 4-31(b). The extent of this elastic strain can be seen by comparing two photographs of the same OCT specimen taken one year apart, Figure 4-32, notice how the notch

opening has relaxed over time.

Fibre breakage in each ply was investigated through deply analysis. Two types of fibre breakage were defined, heavy and light. Heavy fibre damage was defined as continuous fibre breakage that is no longer capable of carrying load, as opposed to regions of damage in which fibre breakage is not continuous and is found ahead of any heavy fibre damage in the FPZ. The average length of heavy fibre damage in the 0° plies was 26.6 mm, and the average amount of light fibre damage being 4 mm. Figure 4-34 compares these results to the line analysis and equivalent notch length from the FE compliance results. The equivalent notch length is the effective crack extension for the same compliance as the data point at photograph 28 in Figure 4-31(b). The notch length indicated by the FE analysis for the same compliance as photograph 28 is 27 mm, comparable to the heavy fibre damage length in the deply. This specimen suffered back-end compression failure at the end of the OCT test, and therefore the final length of damage should be read at photograph 28 in the line analysis not photograph 29, which shows 34 mm of damage within the specimen. This is reasonable as the average amount of light fibre damage suggests an average process zone size of approximately 4 mm, and also elastic strain in the specimen will increase the length of damage reported by the line analysis. One must also ask what accuracy one would expect from this type of analysis considering the possibility of human error involved when taking the various measurements, therefore results within 2 or 3 mm seem acceptable.

A similar analysis was carried out on a stitched 4-stack 90° specimen (SS76-s90). Figure 4-35 shows the load-CMOD curve and corresponding line analysis of test. The line analysis for this test strongly resembles test SS69-s0, in that damage quickly grows to 9 and 10 mm (photographs 3–8), this is also thought to be elastic strain accumulation. Compliance versus crack extension has been plotted for this specimen in Figure 4-36(a), with the corresponding effective crack length from the compliance

plotted against crack length from the line analysis in Figure 4-36(b). These plots indicate that the fracture process zone does not remain constant throughout the test. The fracture process zone starts to develop as the load-CMOD curve becomes non-linear, after photograph 8. It is likely that the FPZ grows larger until the peak load is attained and then gradually gets smaller as the test progresses. The length of damage recorded by the line analysis is 32 mm, the equivalent notch length from the for the compliance predicted by the FE model is 31.5 mm, see Figure 4-37. Deplying revealed an average heavy fibre damage length of 29 mm, with less than 1 mm of light fibre damage length in the 90°plies. This therefore confirms that the process zone is very small at the end of the test.

Summary

1. Correlating the shape of the Load-CMOD curves with the line analysis, deply and sectioning gives an indication of how damage has grown in each specimen, revealing if stable damage growth has transpired.

2. Two Load-CMOD responses were identified:

    - When tested in the 0° direction, both 4 and 6-stack stitched and unstitched exhibit linear loading until damage onset, after which, the load continues to rise amid several load drops until final specimen failure by back face compression.

    - Both stitched 5-stack 0° and 90° specimens show elastic response until damage onset, after which the load peaks and then steadily decreases with large intermittent load drops, although the 5-stack 0° tests show a greater stiffness and maximum load.

    - Maximum loads obtained during testing for the stitched material were comparable to the unstitched material.

3. There where two main types of line analysis plot observed, self-similar and crack blunting. Both can be correlated to the types of load-cmod curves obtained.
    - Line analysis plots for specimens that exhibit self-similar growth show a moving damage front across the specimen from left to right.
    - Line analysis plots for specimens that exhibit crack blunting show characteristic kinking in the lines of the plot that correspond to the point at which damage is arrested.
    - The line analysis plots compare well to the damage recorded by deply and sectioning techniques, taking into account that the line analysis records the process zone and elastic strain in the specimen.
4. Further validation of the line analysis technique was achieved using compliance data generated from FE analysis. This data was manipulated to find an effective notch length that could be compared to the length of damage found in the deply and line analysis. The line analysis predicts an internal length of damage greater than that of the deply and compliance, indicating evidence that a process zone has developed in this material. One would expect the line analysis to show a greater damage length than the compliance, as damage does not grow as a crack extending completely through thickness. Some plies may be damaged more than others and therefore to achieve a comparable compliance the length of damage in the specimen will be greater.
5. Additional line analysis plots and corresponding load-CMOD curves for tests that were not deplied or sectioned are giving in appendix A.

Table 4-1: Test Summary for overheight compact tension experiment specimen dimensions, maximum load applied and crosshead speeds. S/RFI and RFI denote stitched and unstitched materials respectively.

Date	Test	Material	Boeing Panel ID/ #	Specimen Dimensions (mm)								P_{max}		Crosshead Speed
				H	Width	t	d	c	a	W	a/W	(lbs)	(kN)	mm/min
1-Jun-00	SS67-s0	4-stack S/RFI	BA-T-5	208	106	5.90	19.1	38.6	32.30	81	0.40	7822.27	34.77	0.508
1-Jun-00	SS68-s0	4-stack S/RFI	BA-T-5	207	106	5.90	19.1	38.6	32.40	80	0.40	6494.14	28.87	0.508
8-Jun-00	SS69-s0	5-stack S/RFI	extra-1	205	105	7.30	19.1	38.7	32.20	80	0.40	7314.45	32.51	0.508
9-Jun-00	SS70-s0	5-stack S/RFI	extra-1	205	105	7.00	19.1	38.6	32.20	80	0.40	7304.69	32.47	0.508
8-Jun-00	SS71-s0	4-stack S/RFI	BA-T-1	206	105	6.10	19.1	38.7	32.40	80	0.41	6464.84	28.74	0.508
9-Jun-00	SS72-s0	4-stack S/RFI	BA-T-1	207	105	6.10	19.1	38.6	32.50	80	0.41	6708.98	29.82	0.508
8-Nov-00	SS73-s0	6-stack S/RFI	BA-T-6	208	108	8.80	19.1	39.0	35.68	83	0.43	10322.27	45.88	0.508
9-Nov-00	SS74-s0	6-stack S/RFI	BA-T-6	208	85	8.80	19.1	38.7	34.93	60	0.58	4121.09	18.32	0.508
16-Nov-00	SS75-s0	6-stack S/RFI	BA-T-6	208	97	8.80	19.1	38.3	34.60	71	0.49	7529.30	33.47	0.508
9-Feb-01	SS76-s90	4-stack S/RFI	BA-T-5	207	106	6.10	19.1	38.8	32.10	80.6	0.40	2568.36	11.42	0.508
9-Feb-01	SS77-s90	5-stack S/RFI	extra-1	207	106	7.30	19.1	38.5	32.10	80.6	0.40	3056.64	13.59	0.508
9-Feb-01	SS78-s90	6-stack S/RFI	BA-T-6	208	106	8.80	19.1	38.6	32.00	80.6	0.40	3662.11	16.28	0.508
9-Feb-01	SS79-s0	6-stack S/RFI	BA-T-6	205	105	8.80	19.1	38.7	32.10	79.6	0.40	11054.69	49.14	0.508
23-Feb-01	SS80-u0	6-stack RFI	BA-T-4	206	106	8.38	19.1	38.7	32.24	80.6	0.40	10634.77	47.27	0.508
23-Feb-01	SS81-u90	6-stack RFI	BA-T-4	207	107	8.38	19.1	38.7	32.64	81.6	0.40	3574.219	15.88	0.508
23-Feb-01	SS82-u0	4-stack RFI	u-extra	206	108	5.59	19.1	38.7	33.04	82.6	0.40	7724.609	34.33	0.508
23-Feb-01	SS83-u90	4-stack RFI	u-extra	206	108	5.59	19.1	38.7	33.04	82.6	0.40	2421.875	10.76	0.508

Table 4-2: Comparison of Line analysis results with deply specimens.

Test #	Material Type	Orientation	No. stacks	Total Length of Damage from Deply Analysis		Approximate Length of Damage from Line Analysis (mm)
				Ply Orientation	Damage Length (mm)	
SS71-s0	S/RFI	0°	4	-45°	2–10	12
SS80-u0	RFI	0°	6	-45°	7–10	11
SS69-s0	S/RFI	0°	5	0°	20–30	41
				-45°	15–30	
SS76-s90	S/RFI	90°	4	90°	30	32
				-45°	30	
SS83-u90	RFI	90°	4	90°	32	34
				-45°	20–25	
				+45°	20	

Table 4-3: Comparison of Line analysis results with sectioning specimens.

Test #	Material Type	Orientation	No. Stacks	Total Length of Damage from Sectioning Analysis (mm)	Approximate Length of Damage from Line Analysis (mm)
SS68-s0	S/RFI	0°	4	7.8	6–10
SS70-s0	S/RFI	0°	5	25.9	26–28
SS73-s0	S/RFI	0°	6	7.2	5–7
SS77-s90	S/RFI	90°	5	36.1	39.5
SS78-s90	S/RFI	90°	6	32.5	34–37
SS81-u90	RFI	90°	6	34.4	32

Table 4-4: Equivalent strains at 'characteristic kinks' in outermost lines for all stitched and unstitched 4 and 6-stack 0° specimens.

Test No.	No. Stacks	Equivalent Strain %
SS67-s0	4	0.93
SS68-s0	4	1.33
SS71-s0	4	1.37
SS72-s0	4	1.27
SS73-s0	6	1.12
SS79-s0	6	1.13
SS80-u0	4	1.31
SS82-u0	6	0.70

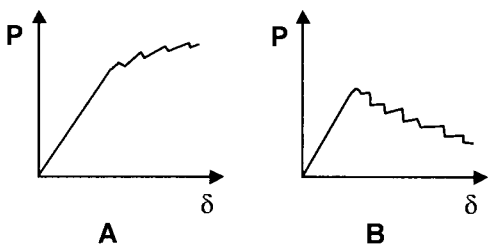

	Stitched		Unstitched	
	0°	90°	0°	90°
4	A	B	A	B
5	B	B	-	-
6	A	B	A	B

Figure 4-1: Schematic describing the two distinct types of load-crack mouth opening displacement curves observed.

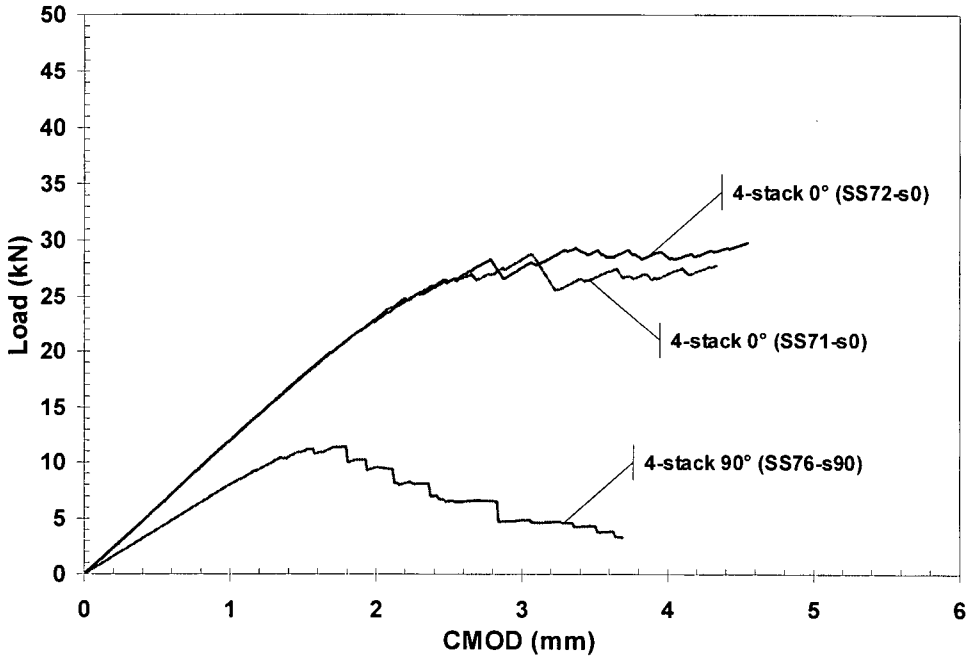

Figure 4-2: Load vs. crack mouth opening displacement for 4-stack stitched specimens, tested in 0° and 90° directions, a/W ratios are: SS76-s90 (0.40), SS71-s0 and SS72-s0 (0.41).

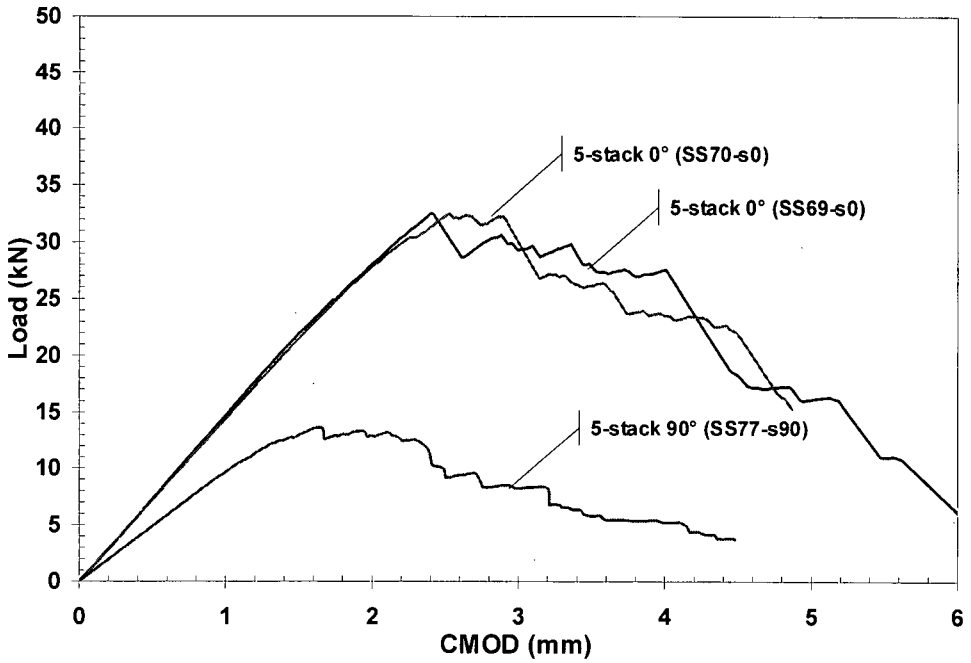

Figure 4-3: Load vs. crack mouth opening displacement for 5-stack stitched specimens, tested in 0° and 90° directions, a/W ratios are 0.40.

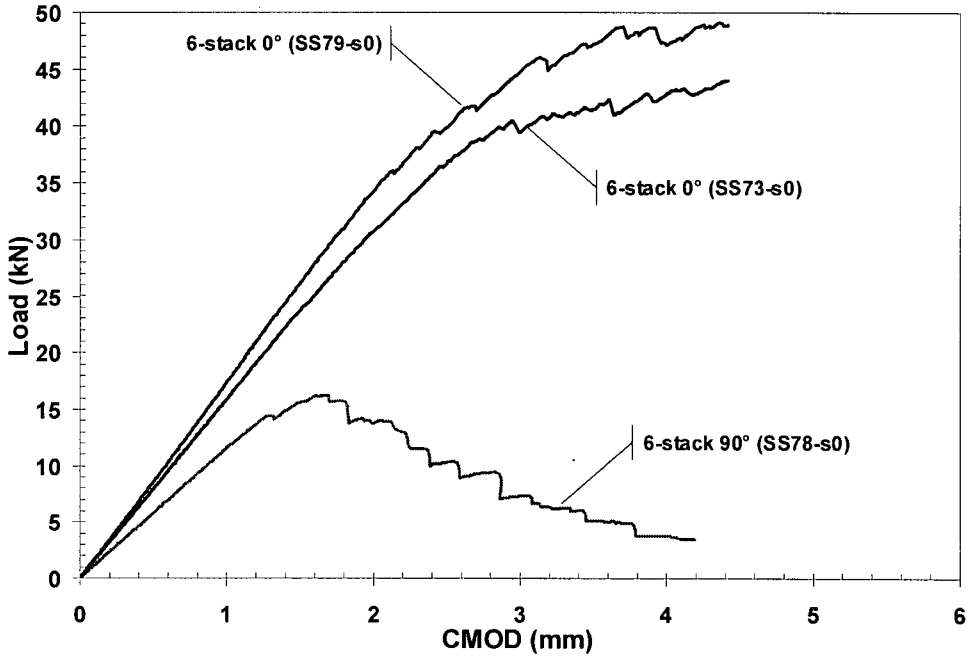

Figure 4-4: Load vs. crack mouth opening displacement for 6-stack stitched specimen, tested in 0° and 90° directions, a/W ratios are 0.40 except for SS73-s0 (0.43)

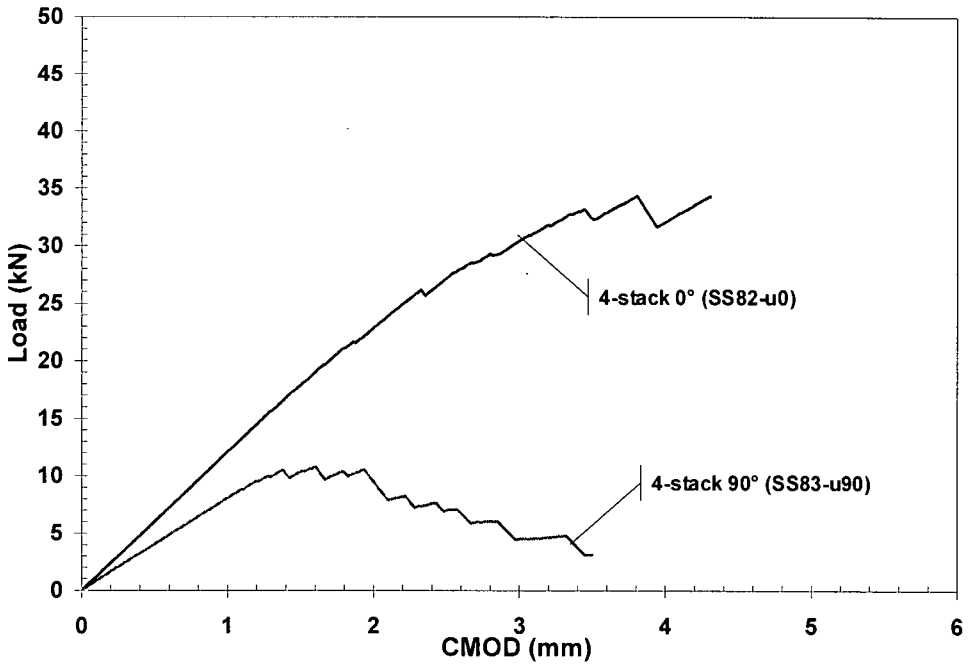

Figure 4-5: Load vs. crack mouth opening displacement for 4-stack unstitched specimens, tested in 0° and 90° directions, a/W ratios are 0.40.

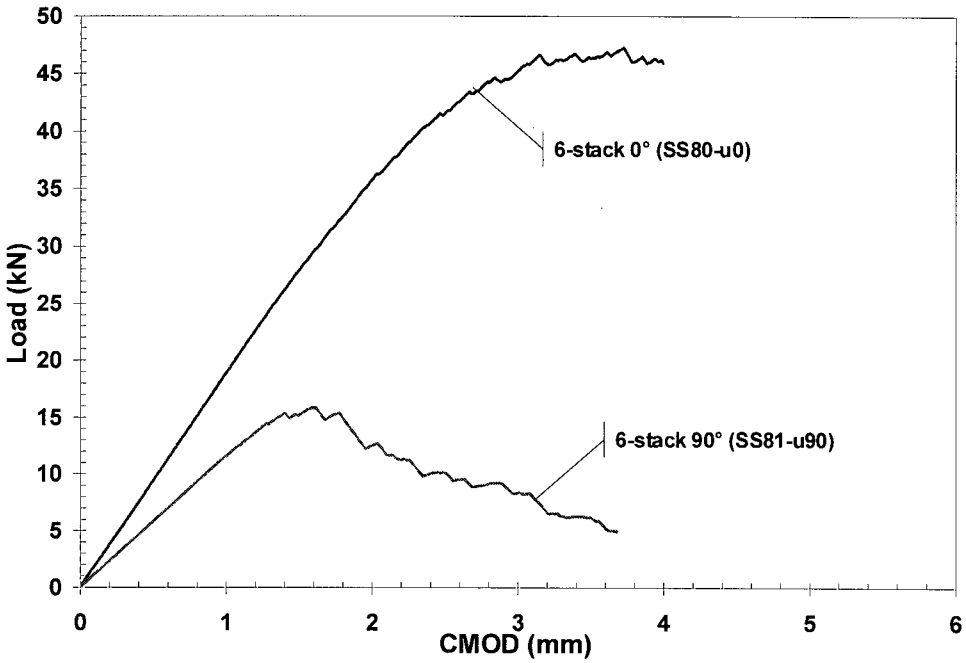

Figure 4-6: Load vs. crack mouth opening displacement for 6-stack unstitched specimens, tested in 0° and 90° directions a/W ratios are all 0.40.

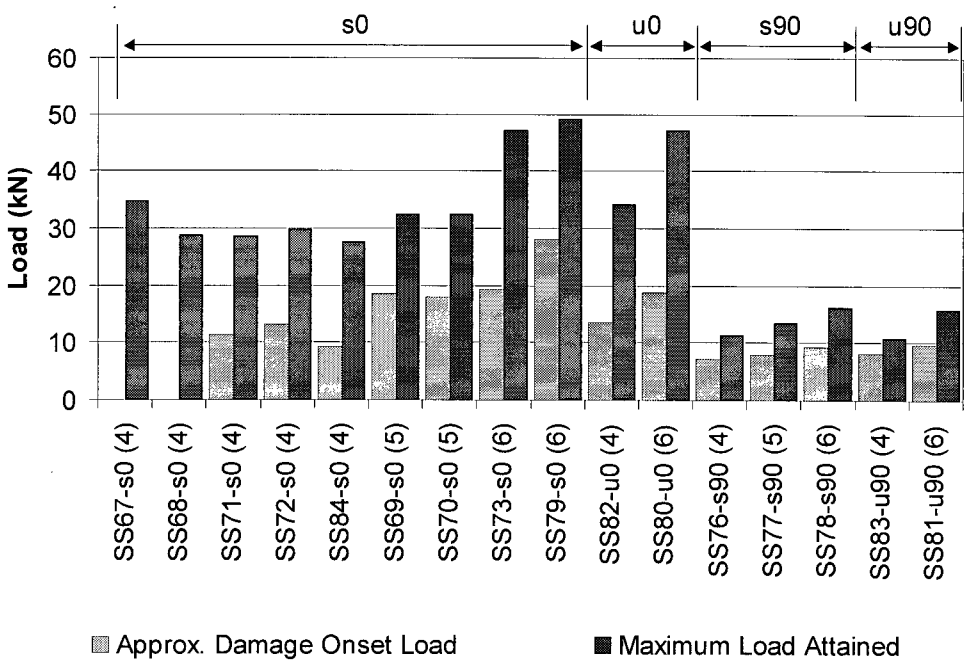

Figure 4-7: Comparison of maximum and approximate damage onset loads attained in the OCT tests, a/W ratios are all 0.40 apart from tests SS71-s0 and SS72-s0 (0.41) and test SS73-s0 (0.43). Damage onsets could not be attained for tests SS67-s0 and ss68-s0 due to noise on load signal during testing.

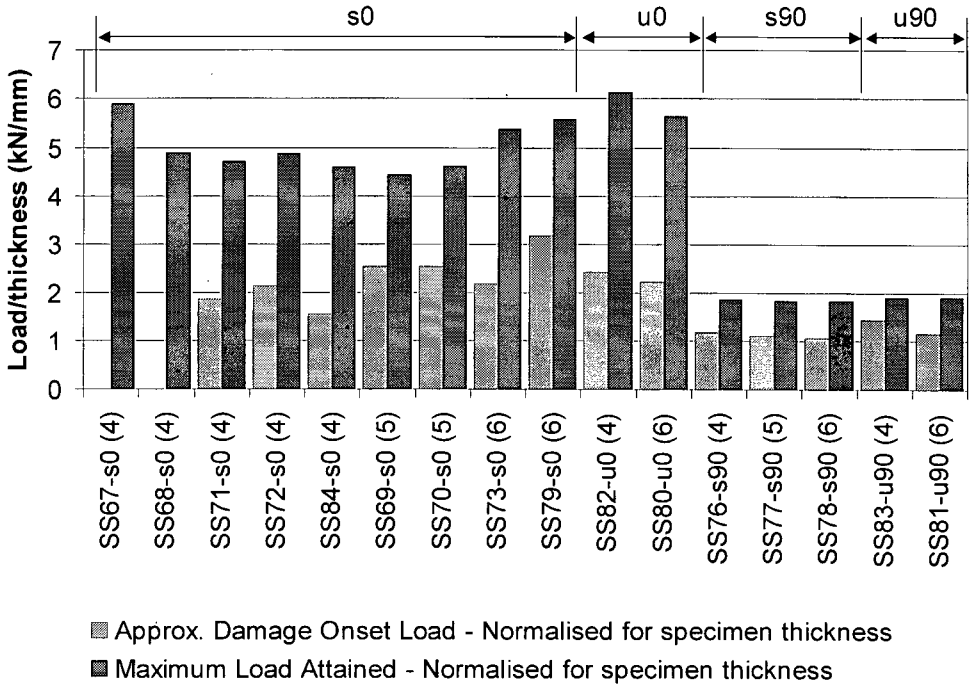

Figure 4-8: Comparison of maximum and approximate damage onset loads attained in the OCT tests normalised for specimen thickness, a/W ratios are all 0.40 apart from tests SS71-s0 and SS72-s0 (0.41) and test SS73-s0 (0.43). Damage onsets could not be attained for tests SS67-s0 and ss68-s0 due to noise on load signal during testing.

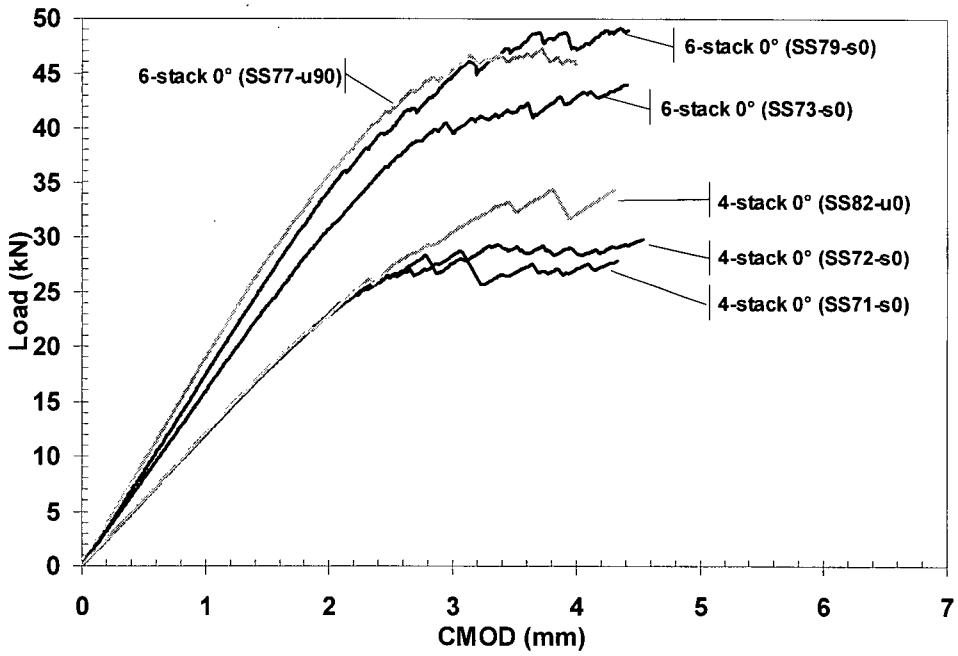

Figure 4-9: Comparison of stitched and unstitched 0° OCT data, a/W ratios are all 0.40 apart from tests SS71-s0 and SS72-s0 (0.41) and test SS73-s0 (0.43)

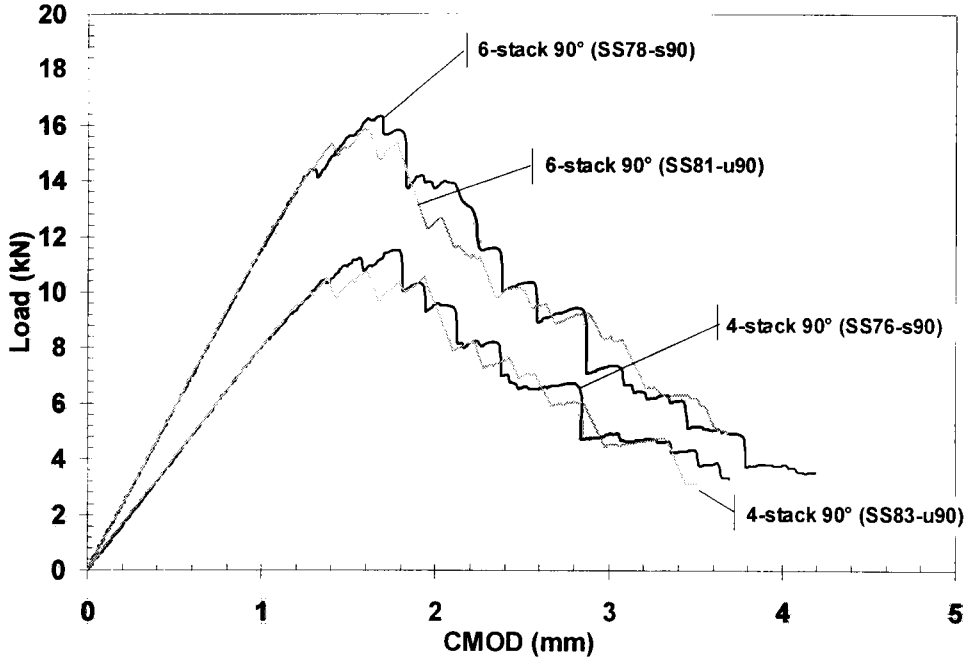

Figure 4-10: Comparison of stitched and unstitched 90° OCT data (note scale changed for clarity), a/W ratios are all 0.40.

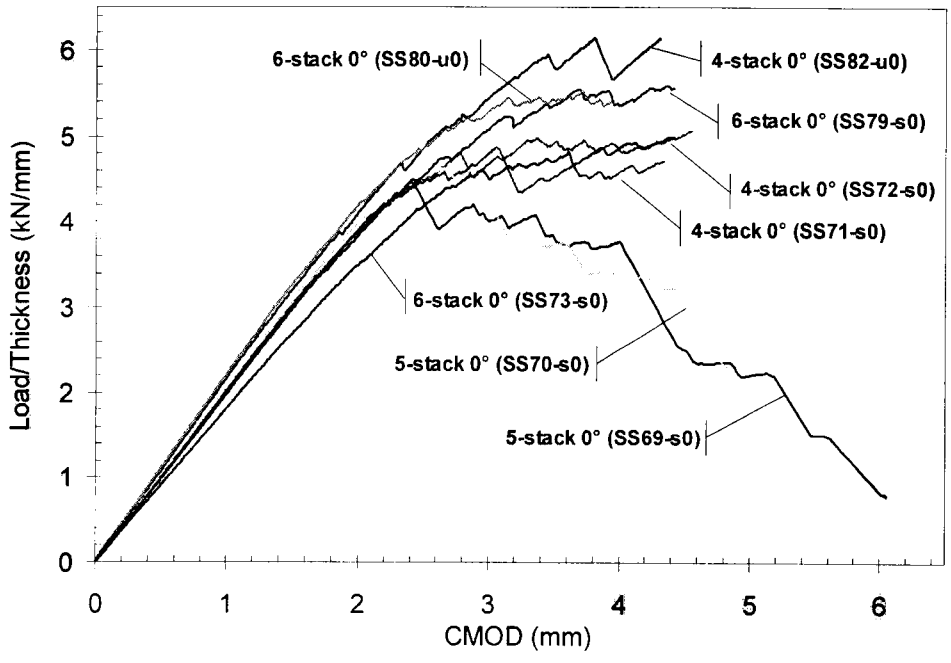

Figure 4-11: Comparison of stitched and unstitched 0° OCT data, normalising with thickness, a/W ratios are all 0.40 apart from tests SS71-s0 and SS72-s0 (0.41) and test SS73-s0 (0.43).

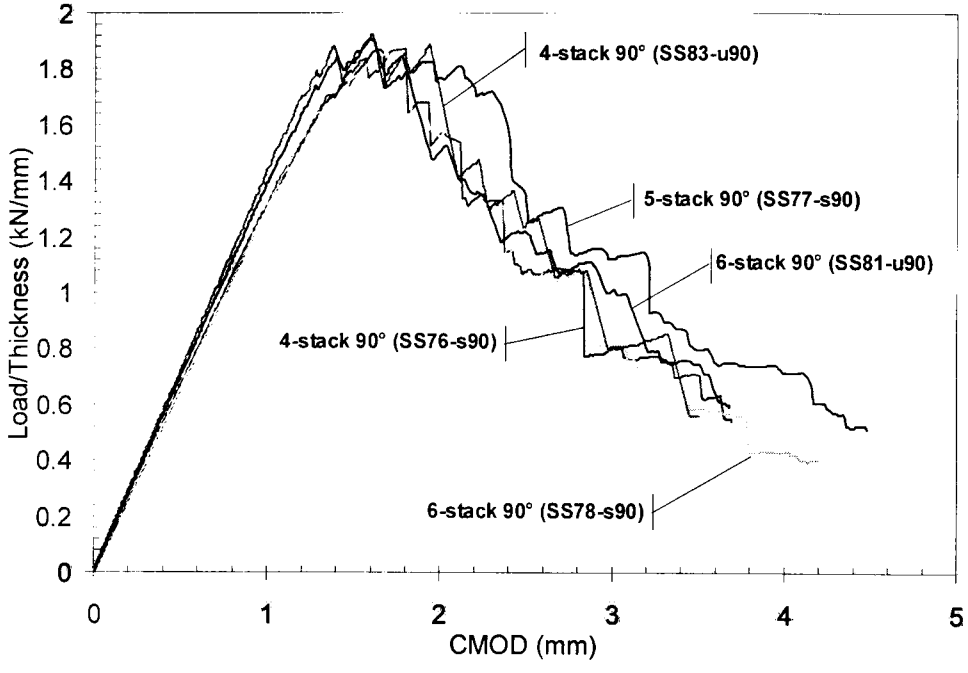

Figure 4-12: Comparison of stitched and unstitched 90° OCT data, normalising with thickness, a/W ratios are all 0.40.

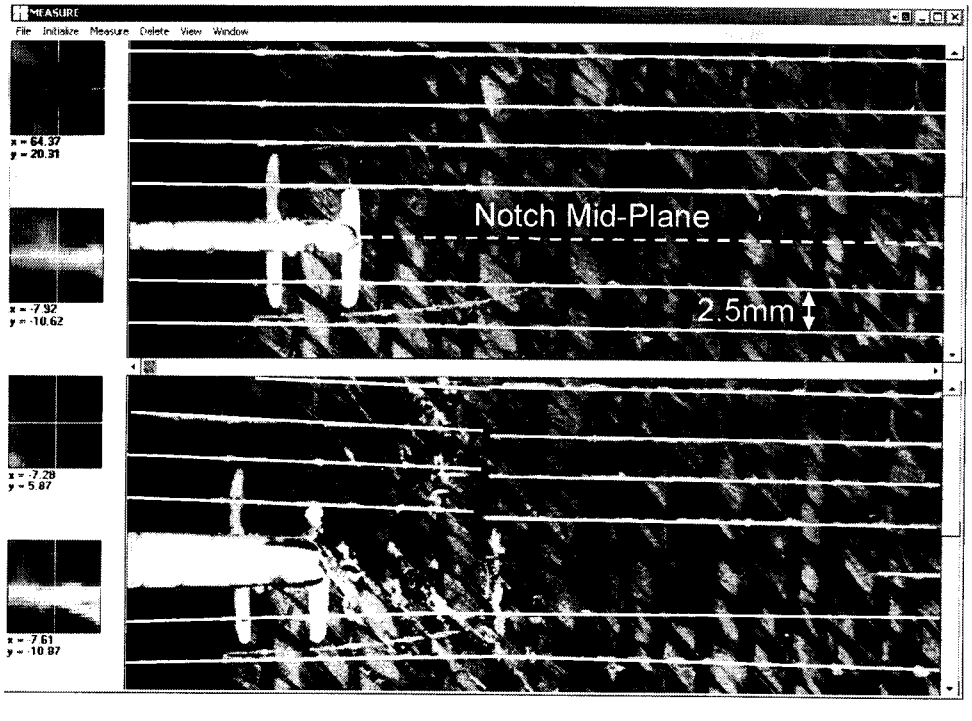

Figure 4-13 Screen capture of the 'Measure 6' software used to measure the difference in surface line displacements between two photographs (i.e. two different loads). The notch mid-plane and surface lines have been highlighted. The top photograph was taken before the test and the bottom photograph was taken near the end of the test. This is RFI specimen SS82-u0.

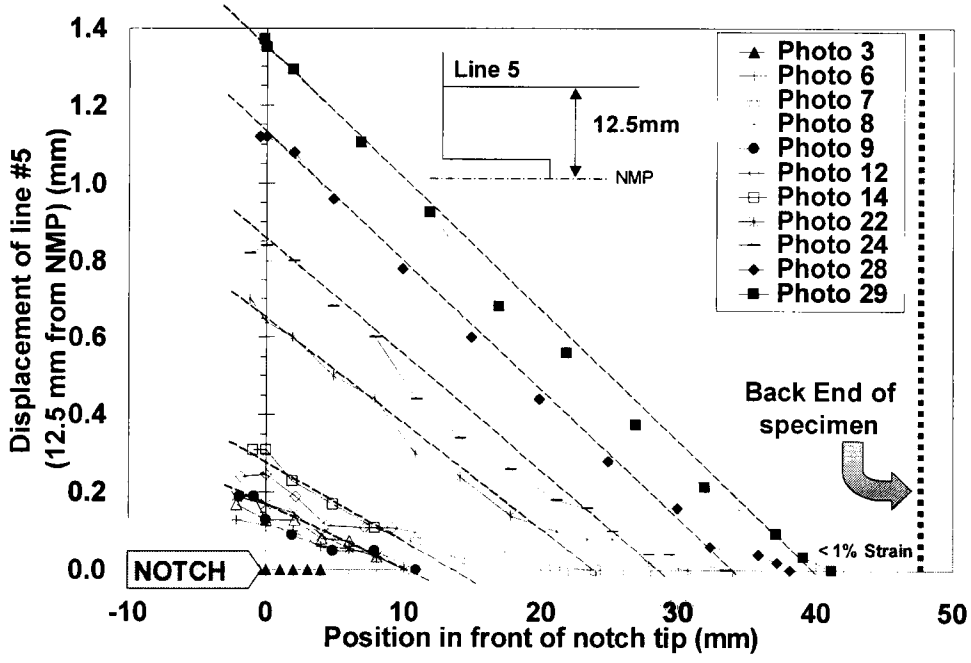

(a)

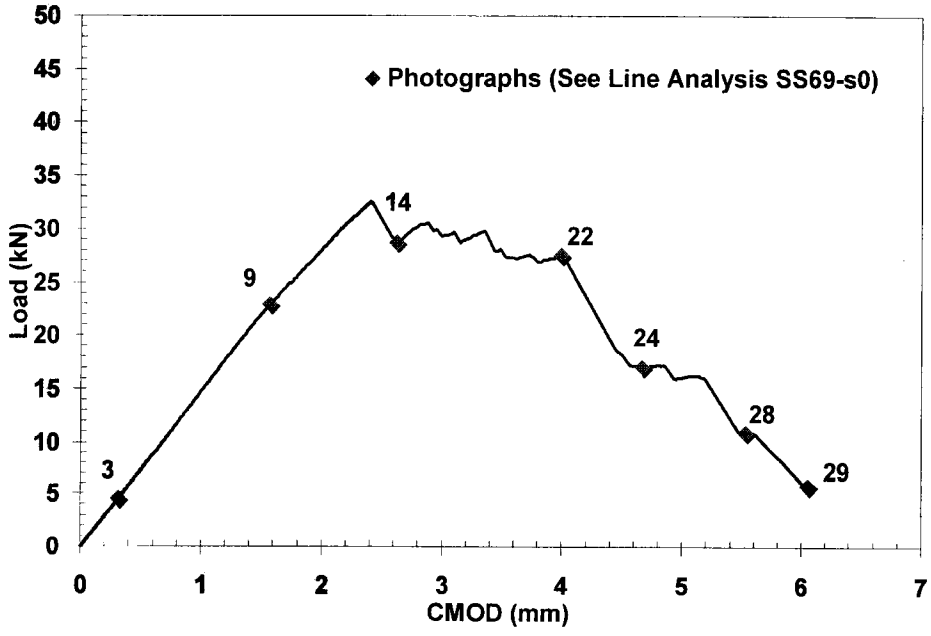

(b)

Figure 4-14 (a) Surface Line Analysis Plot and (b) Load-Crack Mouth Opening Displacement Plot of 5-stack stitched RFI 0° specimen (SS69-s0). Numbers on (b) correspond to photographs in (a). The dashed lines indicate how this line analysis was interpreted.

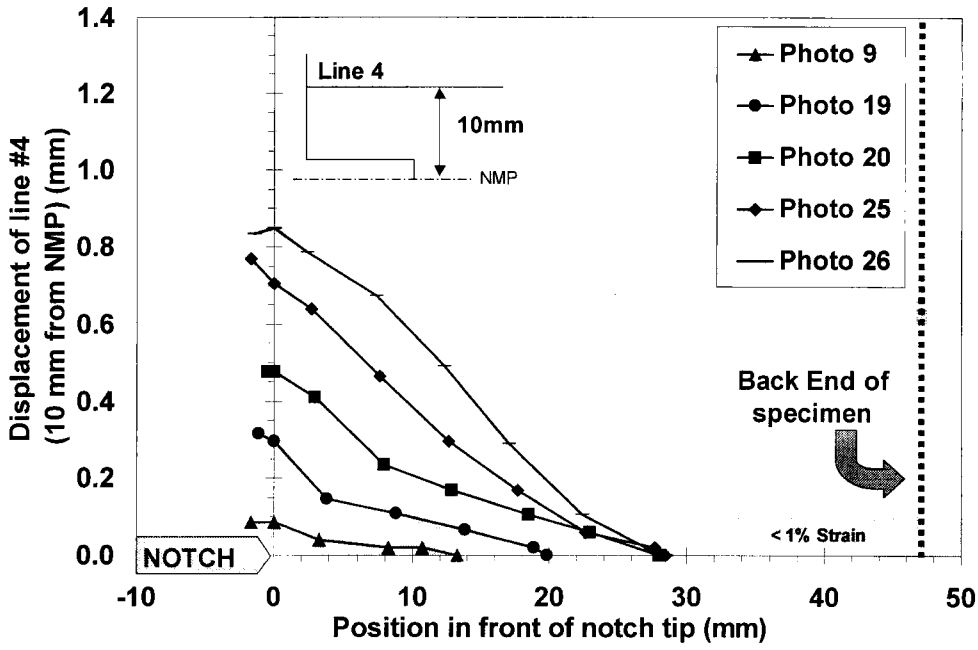

(a)

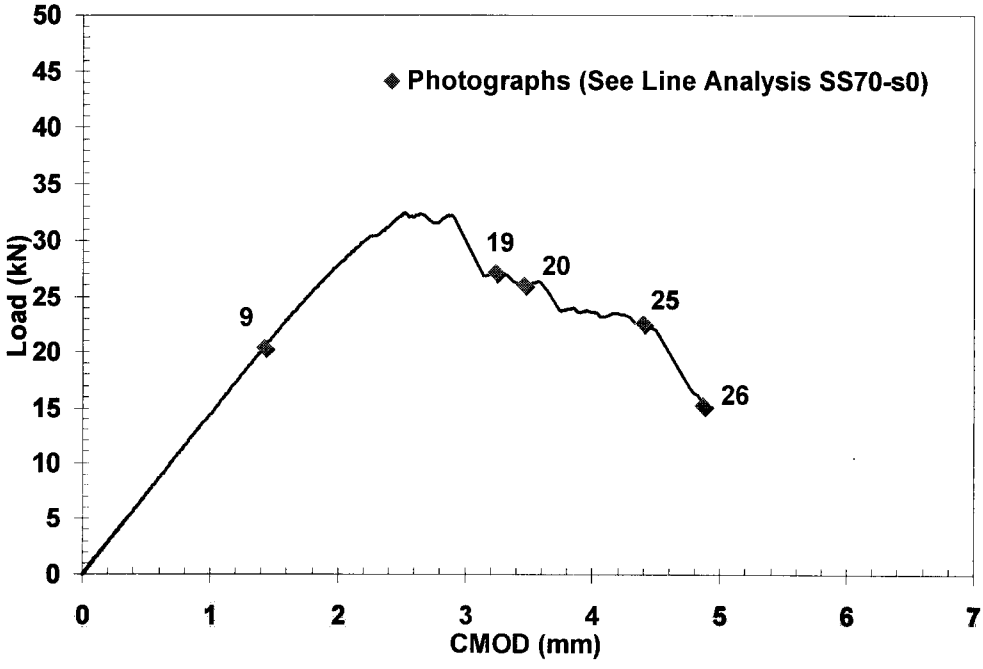

(b)

Figure 4-15: (a) Surface Line Analysis Plot and (b) Load-Crack Mouth Opening Displacement Plot of 5-stack stitched RFI 90° specimen (SS70-s0). Numbers on (b) correspond to photographs in (a).

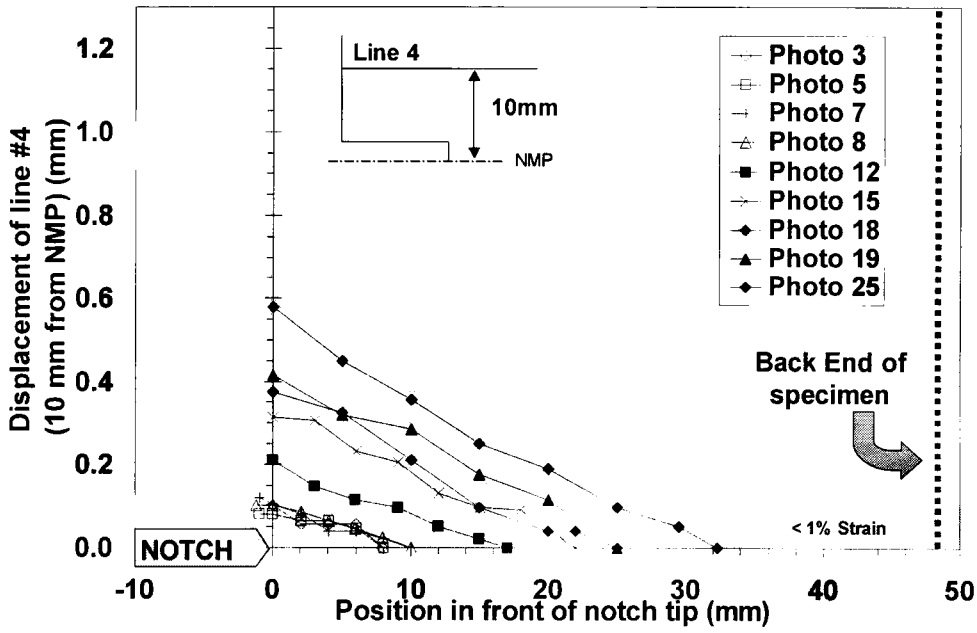

(a)

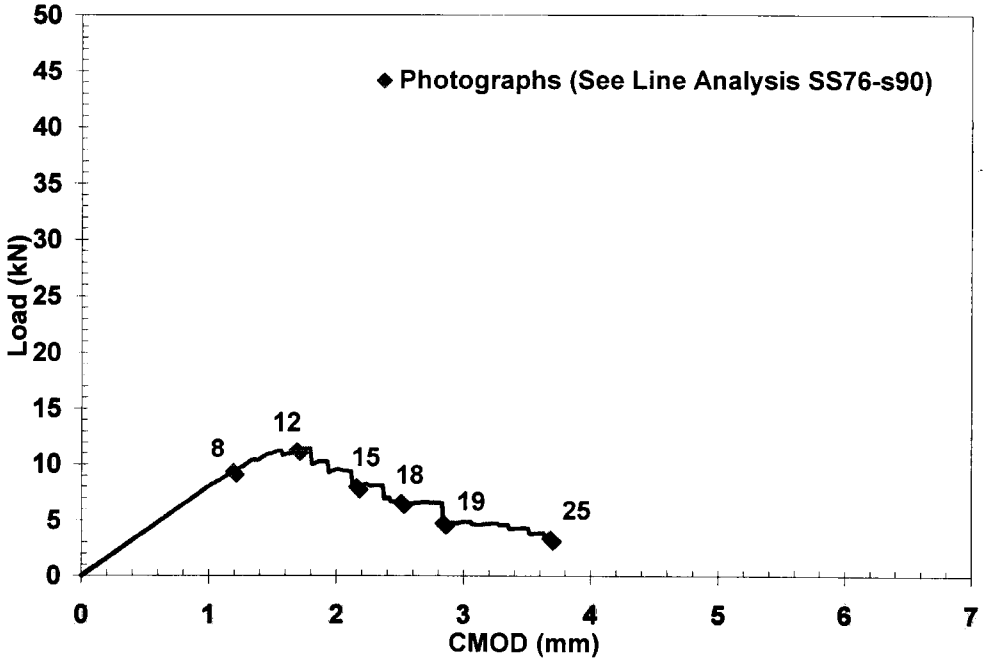

(b)

Figure 4-16: (a) Surface Line Analysis Plot and (b) Load-Crack Mouth Opening Displacement Plot of 4-stack stitched RFI 90° specimen (SS76-s90). Numbers on (b) correspond to photographs in (a).

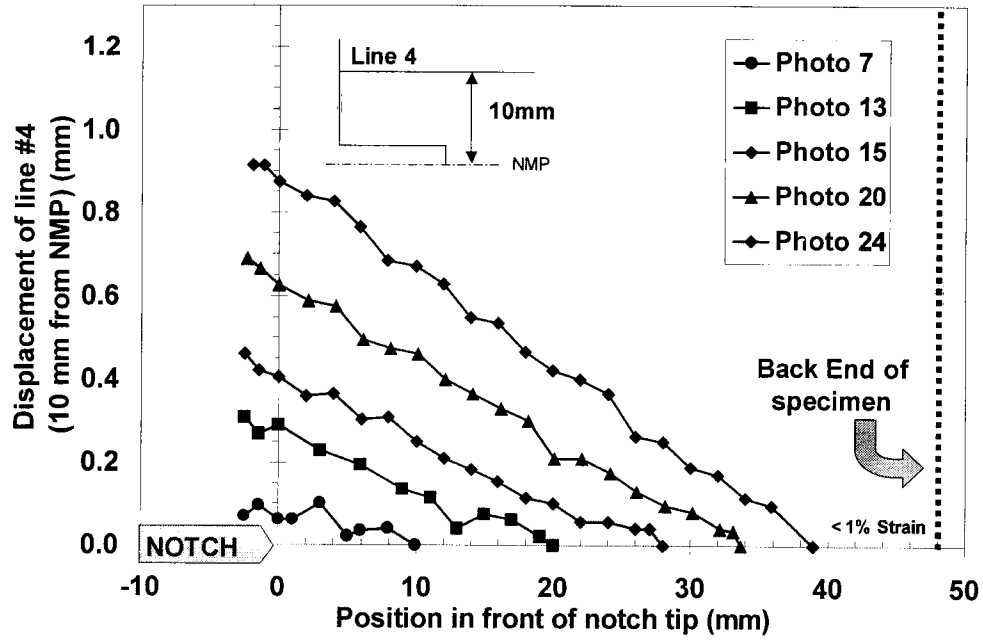

(a)

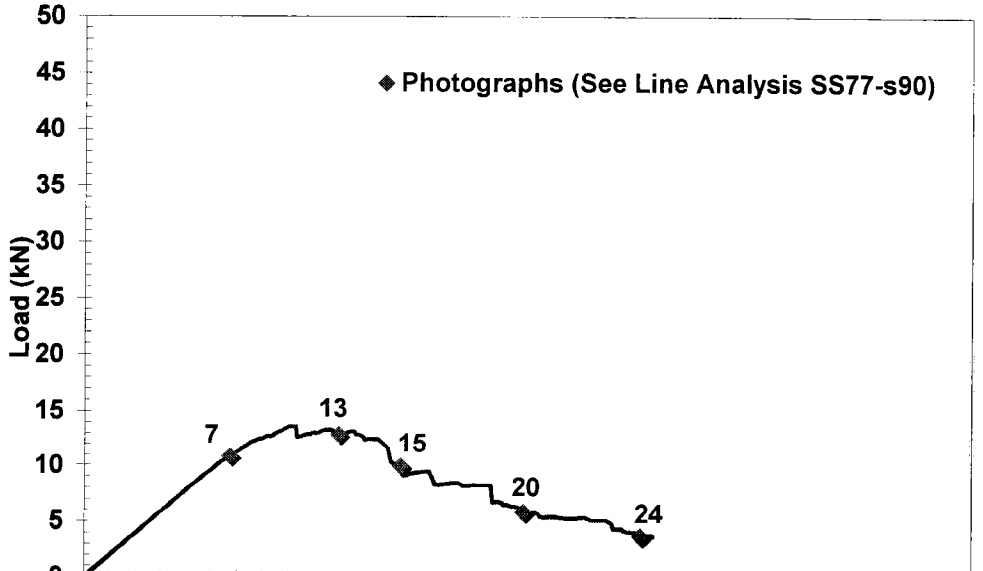

(b)

Figure 4-17: (a) Surface Line Analysis Plot and (b) Load-Crack Mouth Opening Displacement Plot of 5-stack stitched RFI 90° specimen (SS77-s90). Numbers on (b) correspond to photographs in (a).

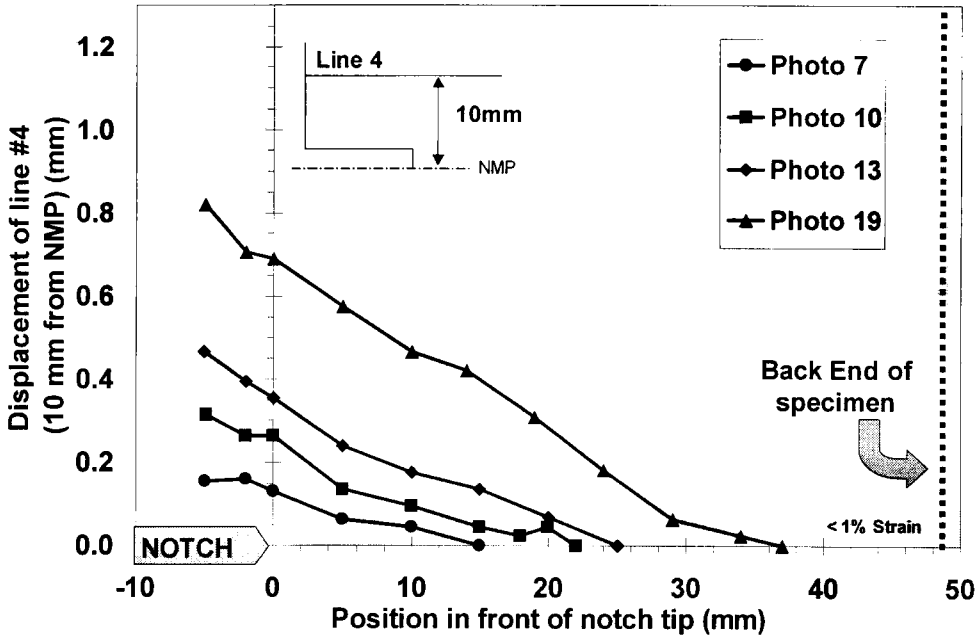

(a)

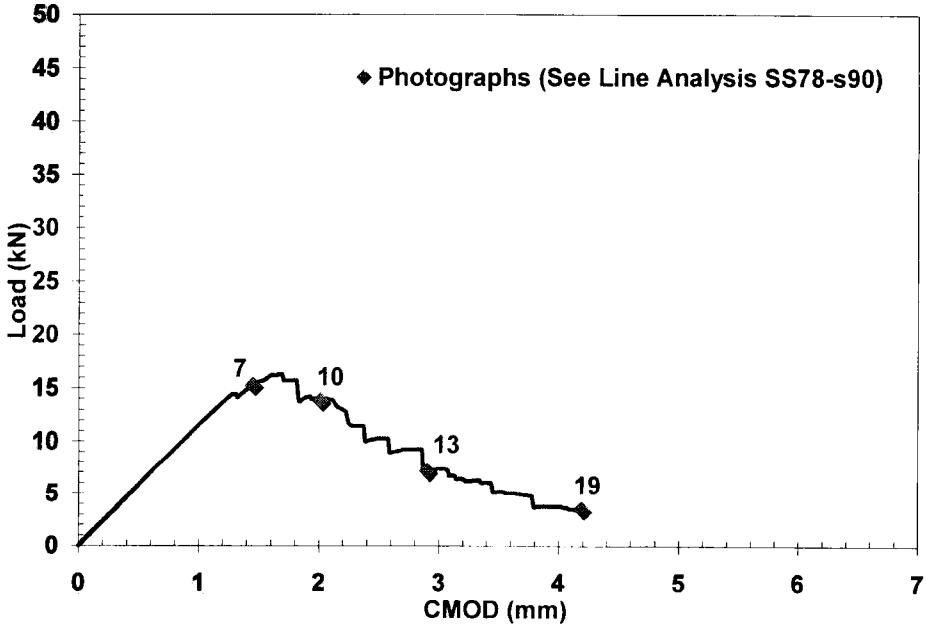

(b)

Figure 4-18: (a) Surface Line Analysis Plot and (b) Load-Crack Mouth Opening Displacement Plot of 6-stack stitched RFI 90° specimen (SS78-s90). Numbers on (b) correspond to photographs in (a).

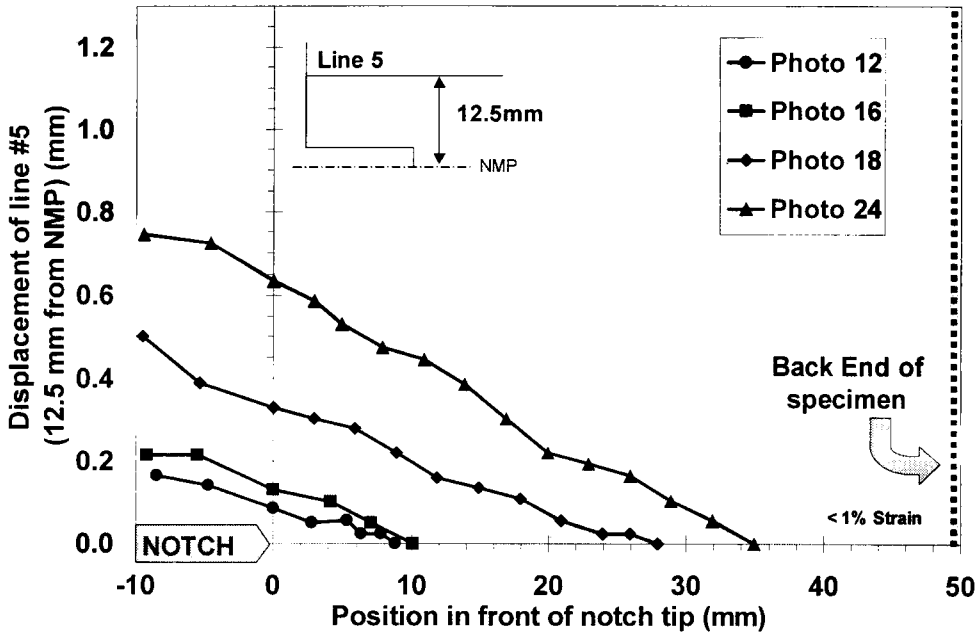

(a)

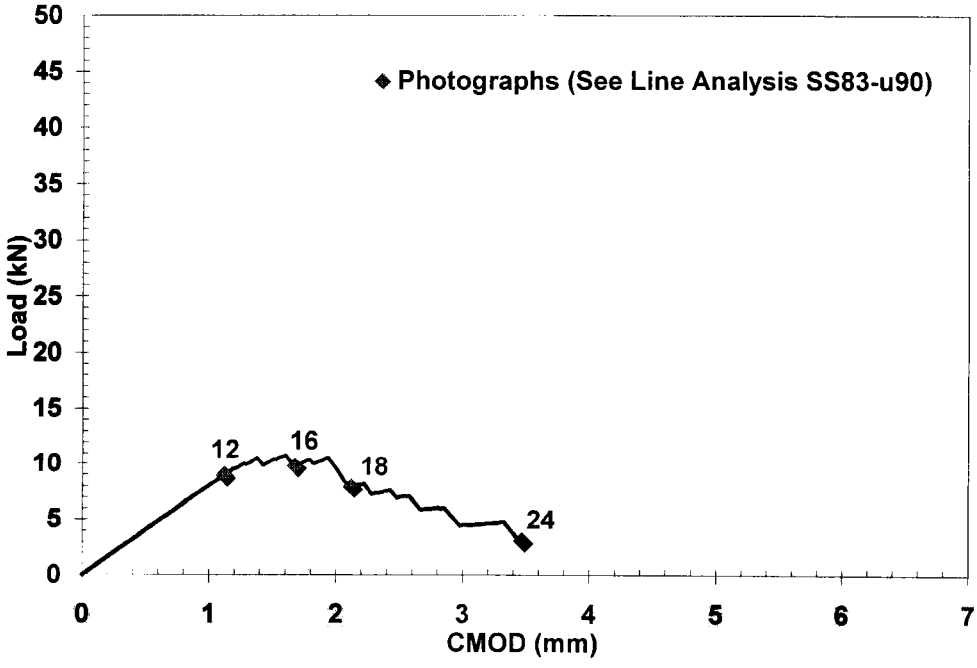

(b)

Figure 4-19: (a) Surface Line Analysis Plot and (b) Load-Crack Mouth Opening Displacement Plot of 4-stack unstitched RFI 90° specimen (SS83-u90). Numbers on (b) correspond to photographs in (a).

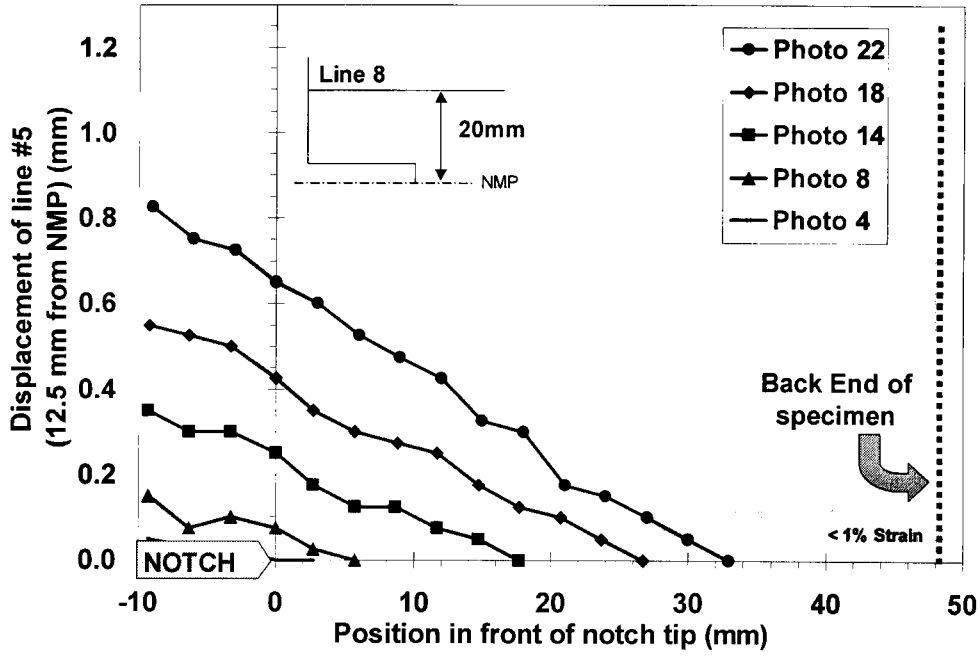

(a)

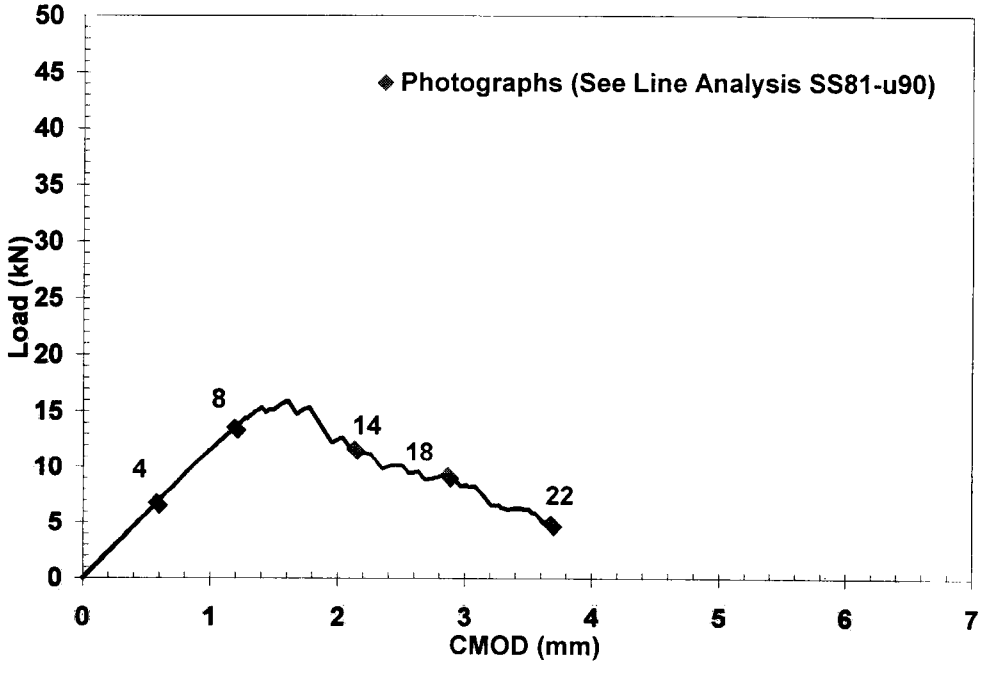

(b)

Figure 4-20: (a) Surface Line Analysis Plot and (b) Load-Crack Mouth Opening Displacement Plot of 6-stack unstitched RFI 90° specimen (SS81-u90). Numbers on (b) correspond to photographs in (a).

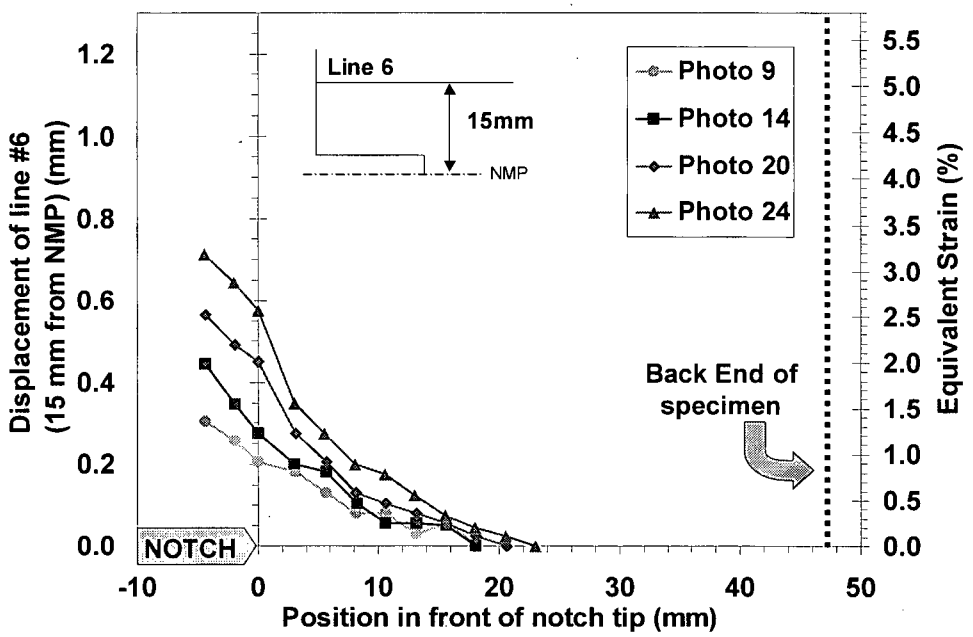

(a)

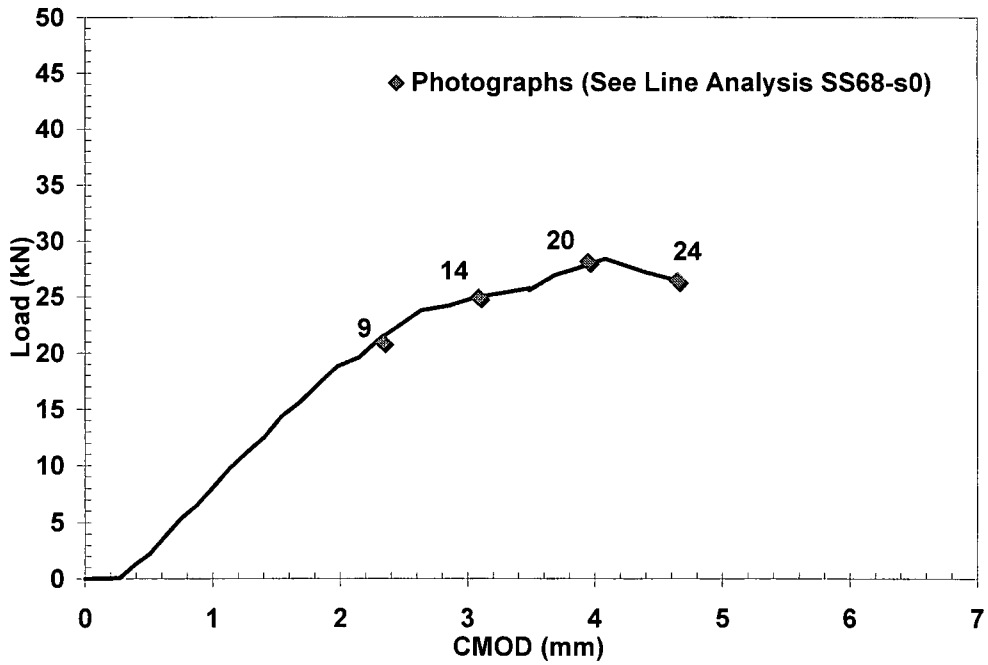

(b)

Figure 4-21: (a) Surface Line Analysis Plot and (b) Load-Crack Mouth Opening Displacement Plot of 4-stack stitched RFI 0° specimen (SS68-s0). Numbers on (b) correspond to photographs in (a).

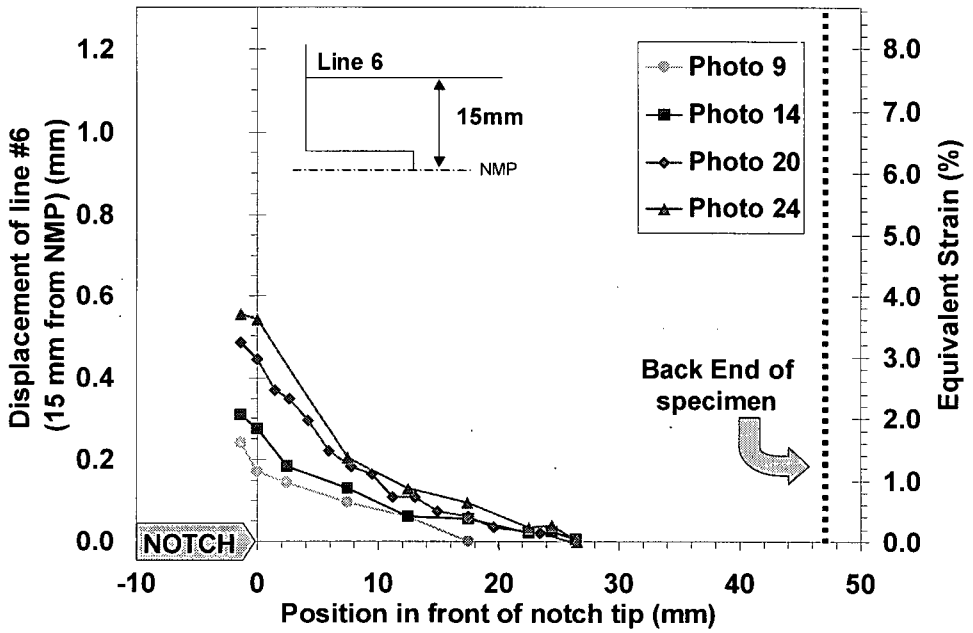

(a)

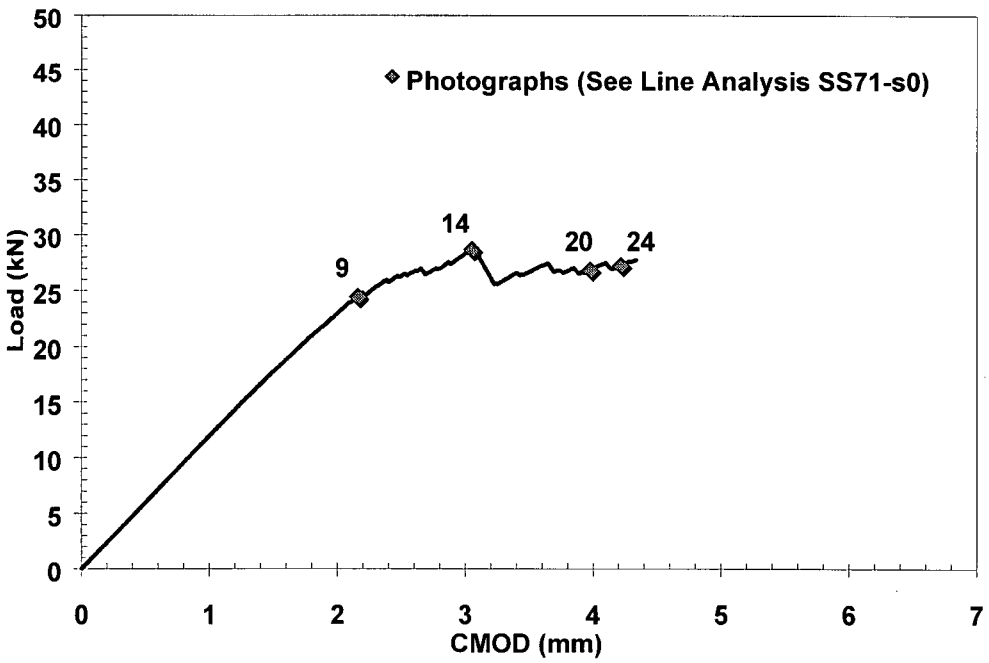

(b)

Figure 4-22: (a) Surface Line Analysis Plot and (b) Load-Crack Mouth Opening Displacement Plot of 4-stack stitched RFI 0° specimen (SS71-s0). Numbers on (b) correspond to photographs in (a).

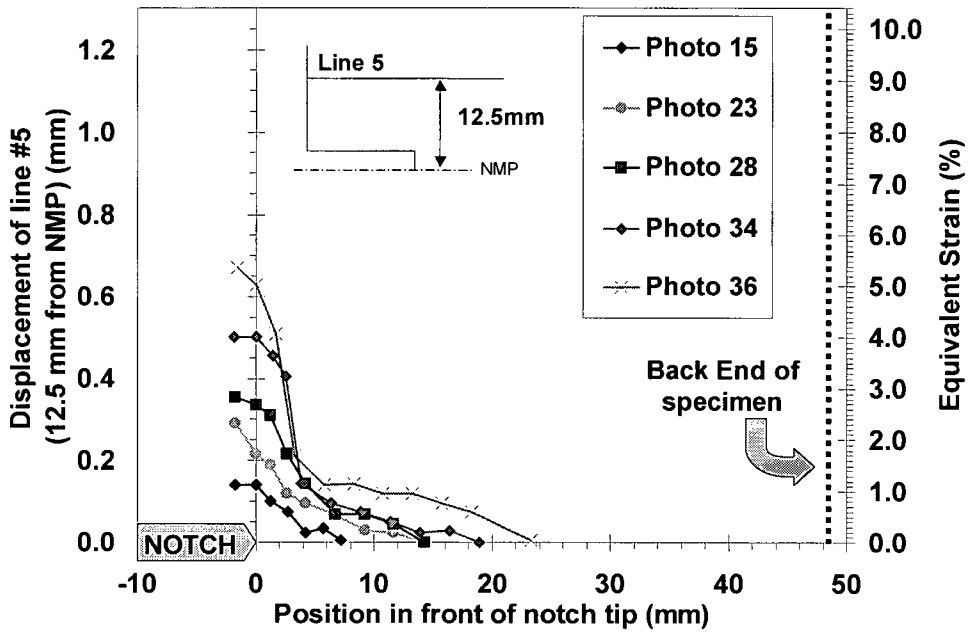

(a)

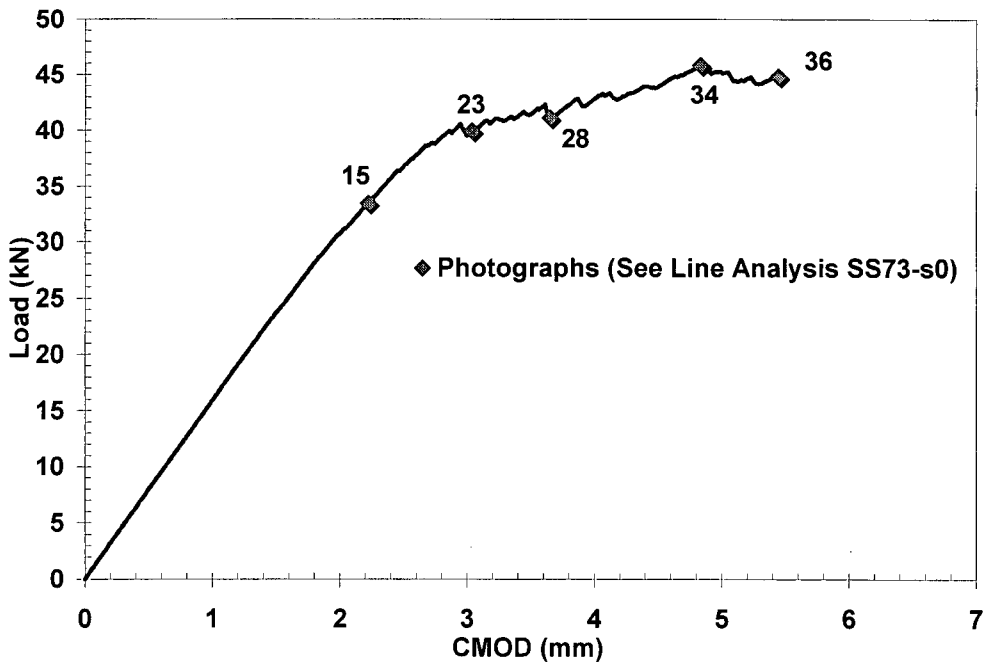

(b)

Figure 4-23: (a) Surface Line Analysis Plot and (b) Load-Crack Mouth Opening Displacement Plot of 6-stack stitched RFI 0° specimen (SS73-s0). Numbers on (b) correspond to photographs in (a).

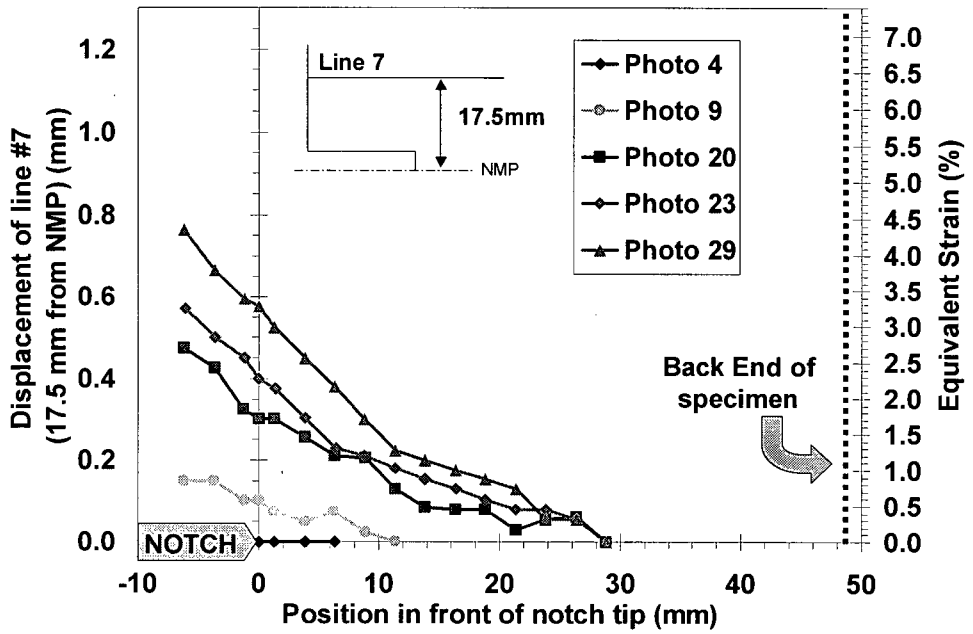

(a)

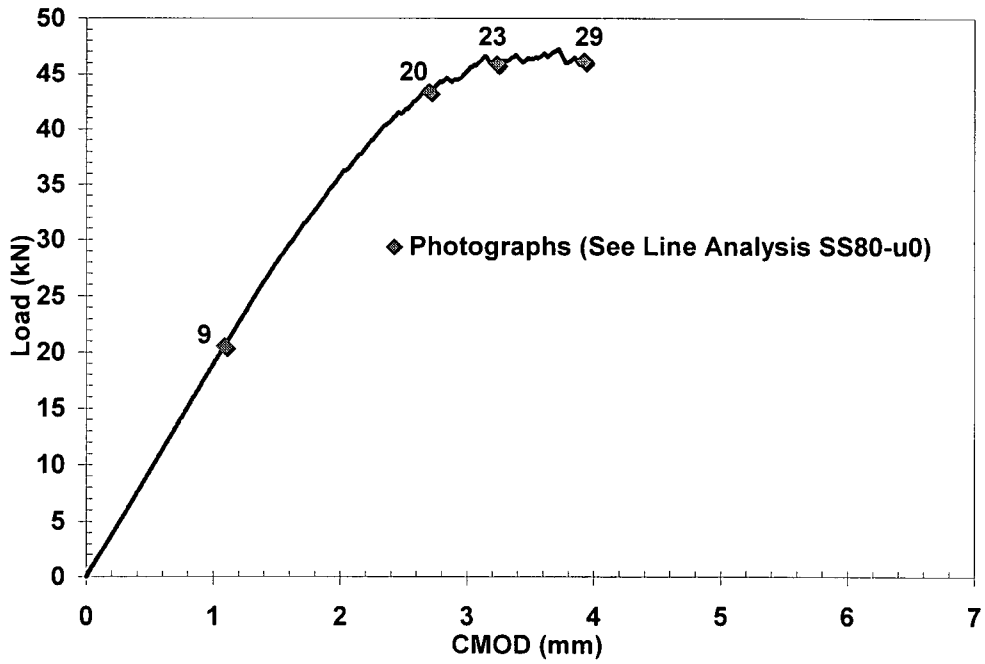

(b)

Figure 4-24: (a) Surface Line Analysis Plot and (b) Load-Crack Mouth Opening Displacement Plot of 6-stack unstitched RFI 0° specimen (SS80-u0). Numbers on (b) correspond to photographs in (a).

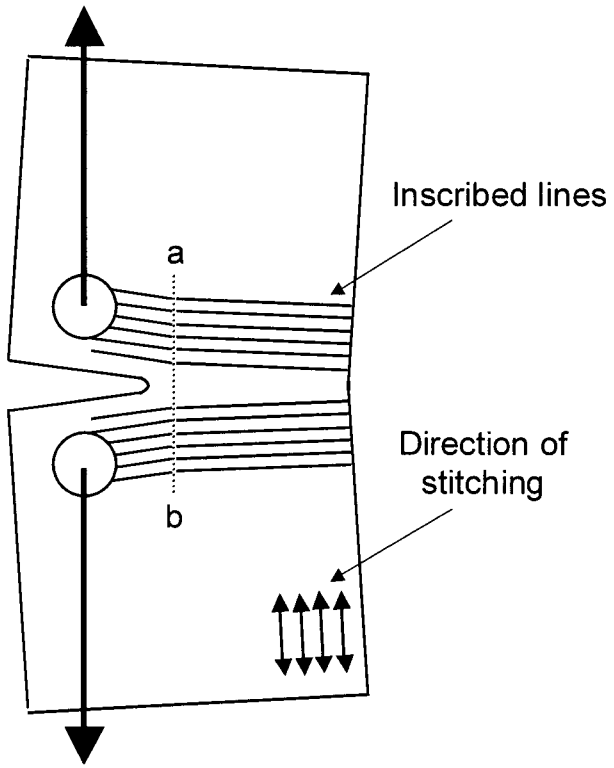

Figure 4-25: Schematic showing the surface line displacement for a stitched 4- or 6-stack RFI material. Line a – b represents the point at which crack growth is blunted by delamination and the point at which the characteristic 'kink' occurs in the line analysis plot.

Equivalent Strain (δ) at point $x = \frac{L_1 - L_0}{L_0}$

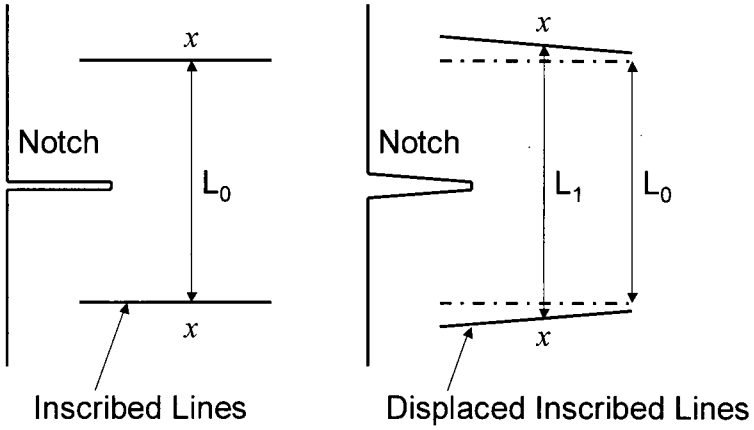

Figure 4-26: Schematic showing the method used to calculate equivalent strain.

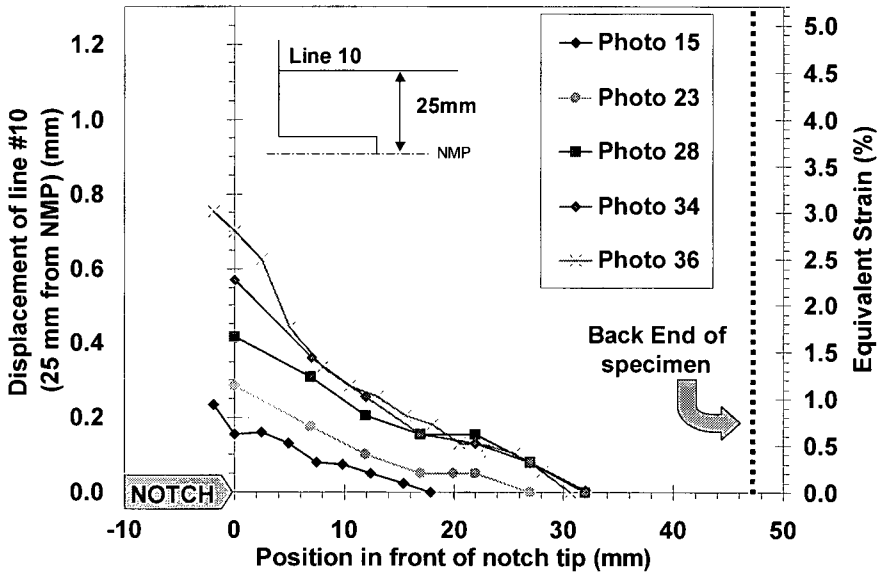

(a)

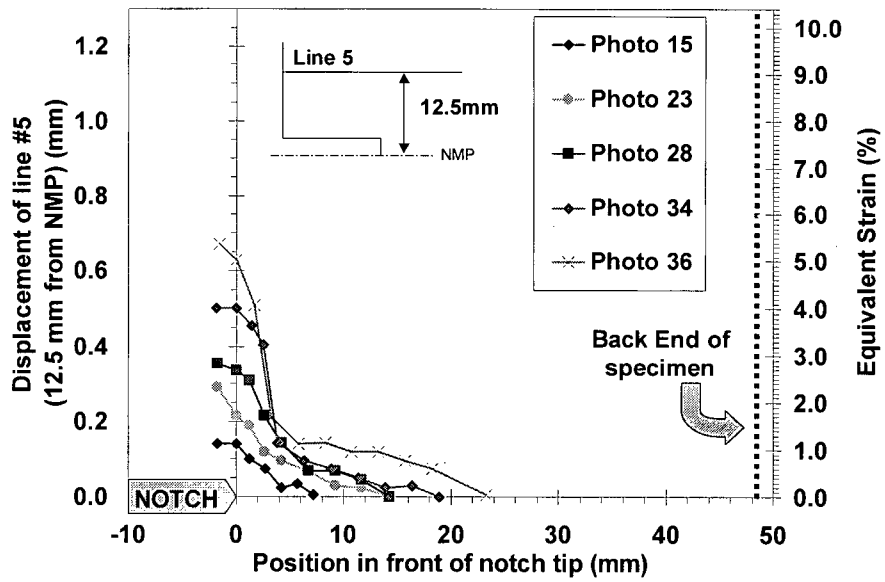

(b)

Figure 4-27: Effect of analysing lines further away from the notch mid-plane in specimen SS73-s0 6-stack stitched 0° specimen, (a) Line 10, 25mm from notch mid-plane and (b) Line 5, 12.5mm from notch mid-plane.

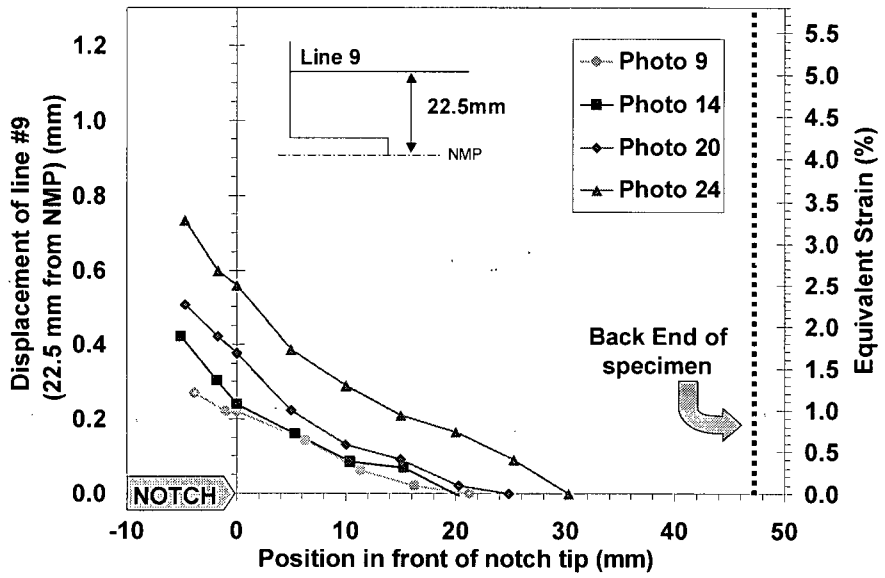

(a)

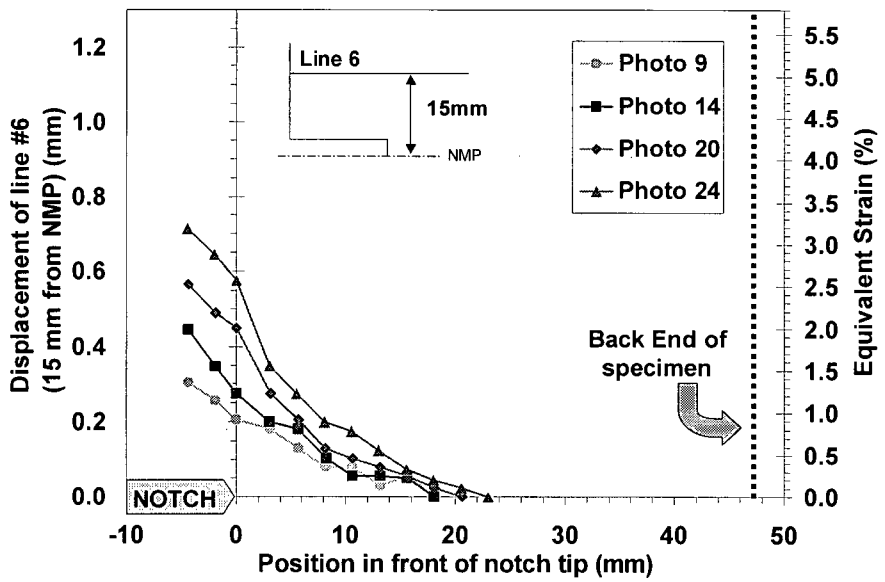

(b)

Figure 4-28: Effect of analysing lines further away from the notch mid-plane in specimen SS68-s0 4-stack stitched 0° specimen, (a) Line 9, 22.5mm from notch mid-plane and (b) Line 6, 15mm from notch mid-plane.

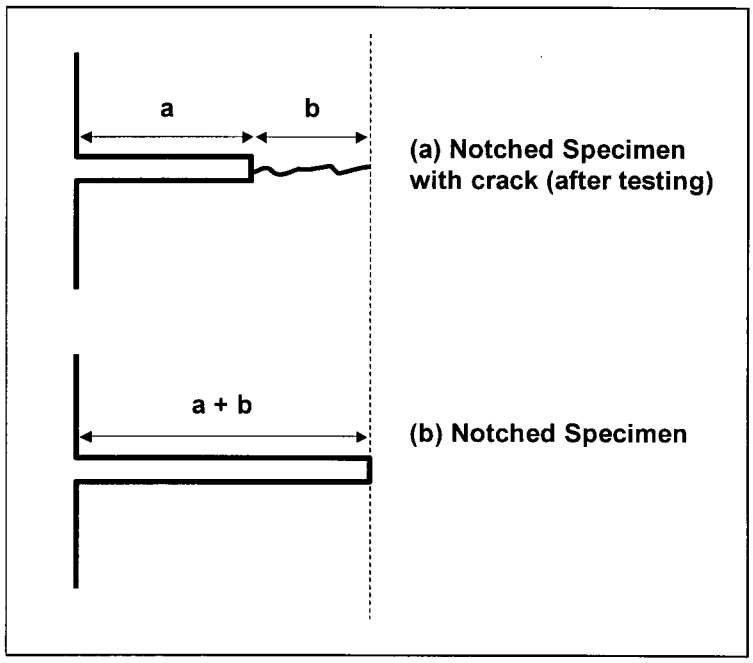

Figure 4-29: Schematic of (a) notched specimen with a notch length, a, that has been tested and suffered self-similar crack extension, b. (b) notched specimen with notch length a + b. Assuming both specimens are made with the same material they should possess a similar compliance.

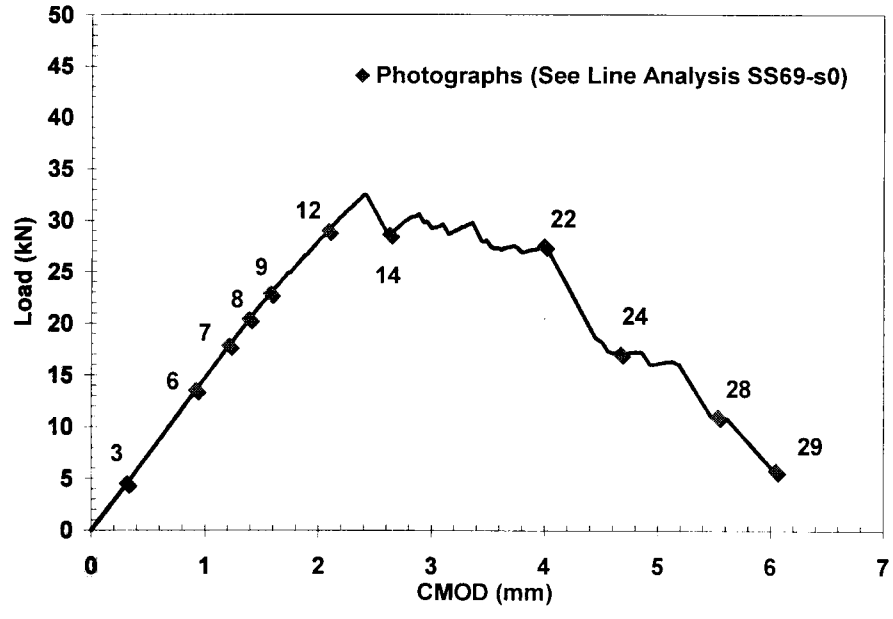

(a)

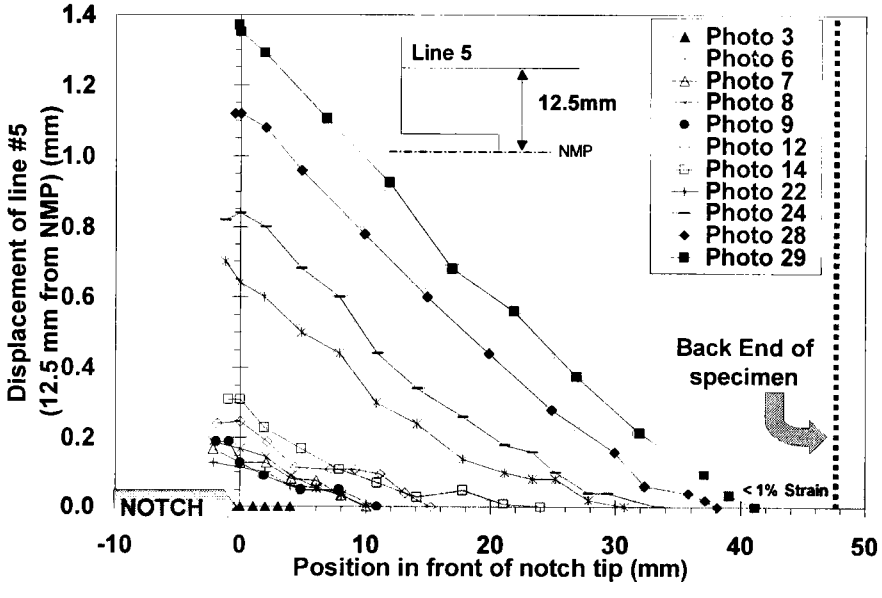

(b)

Figure 4-30: (a) Load-CMOD curve and (b) Line analysis plot for OCT SS69-s0 (5-stack). N.B. shaded area on line analysis plot represents less than 1% strain in the material.

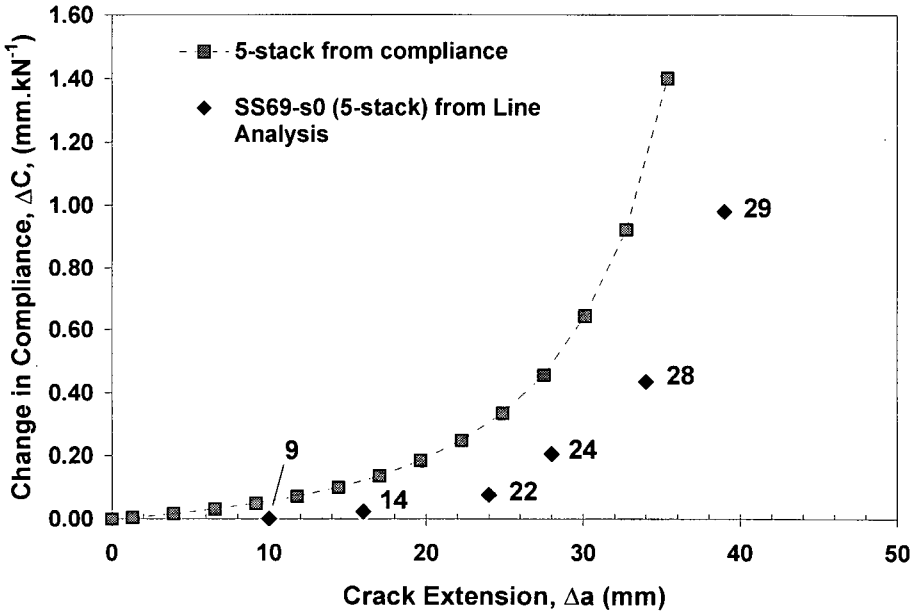

(a)

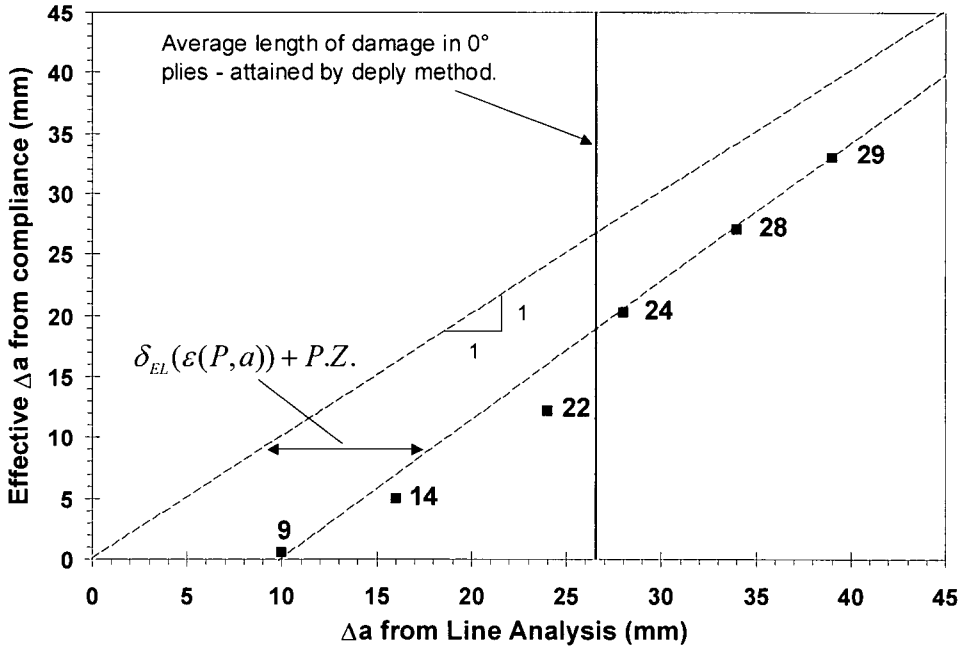

(b)

Figure 4-31: (a) Compliance vs. crack extension curves for numerical runs and SS69-s0 (5-stack) (b) Effective crack length vs. crack length from line analysis SS69-s0 (5-stack).

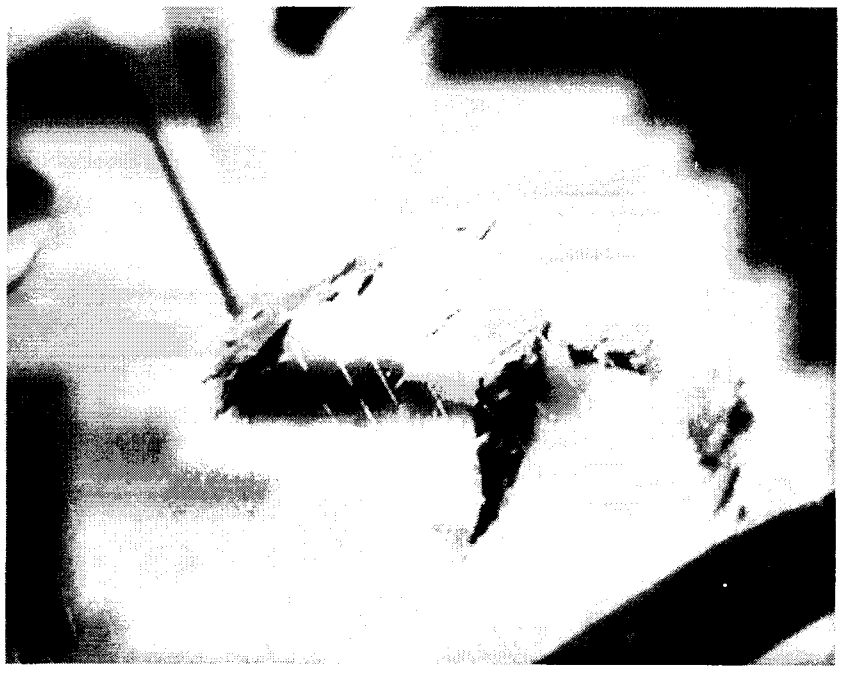

(a)

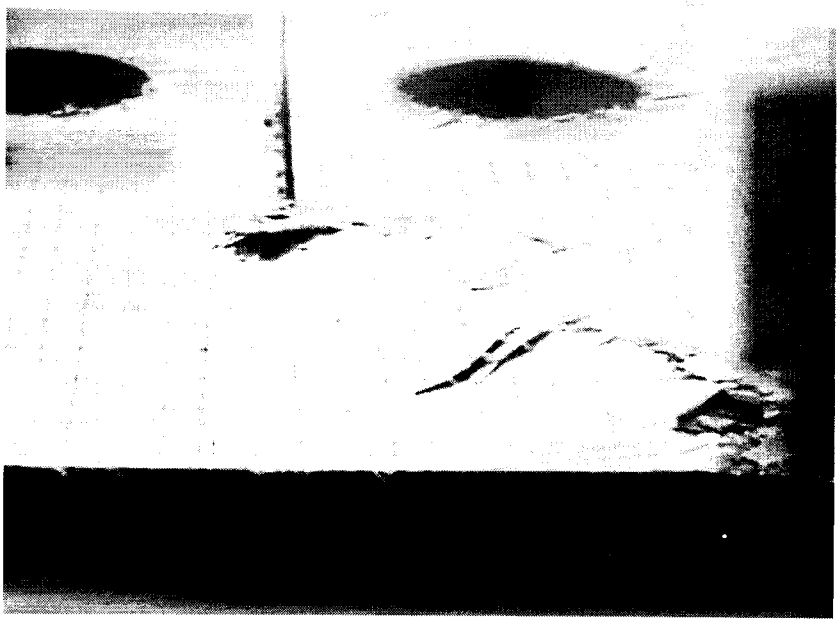

(b)

Figure 4-32: The elastic strain present in the laminate can clearly be seen by comparing (a) a photograph of test SS82-u0 after testing (February 2001) to (b) a photograph taken of the same specimen one year later (February 2002).

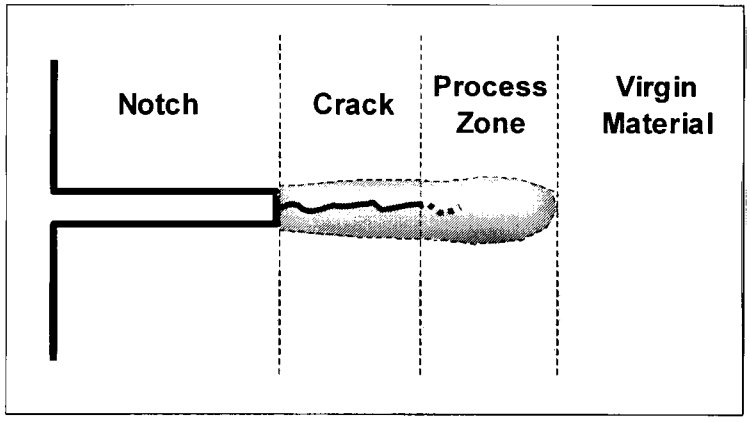

Figure 4-33:Notched specimen, indicating crack and process zone. The crack is equivalent to the notch length used to predict the compliance in the FE analysis. However, the simple FE analysis does not take into account the process zone.

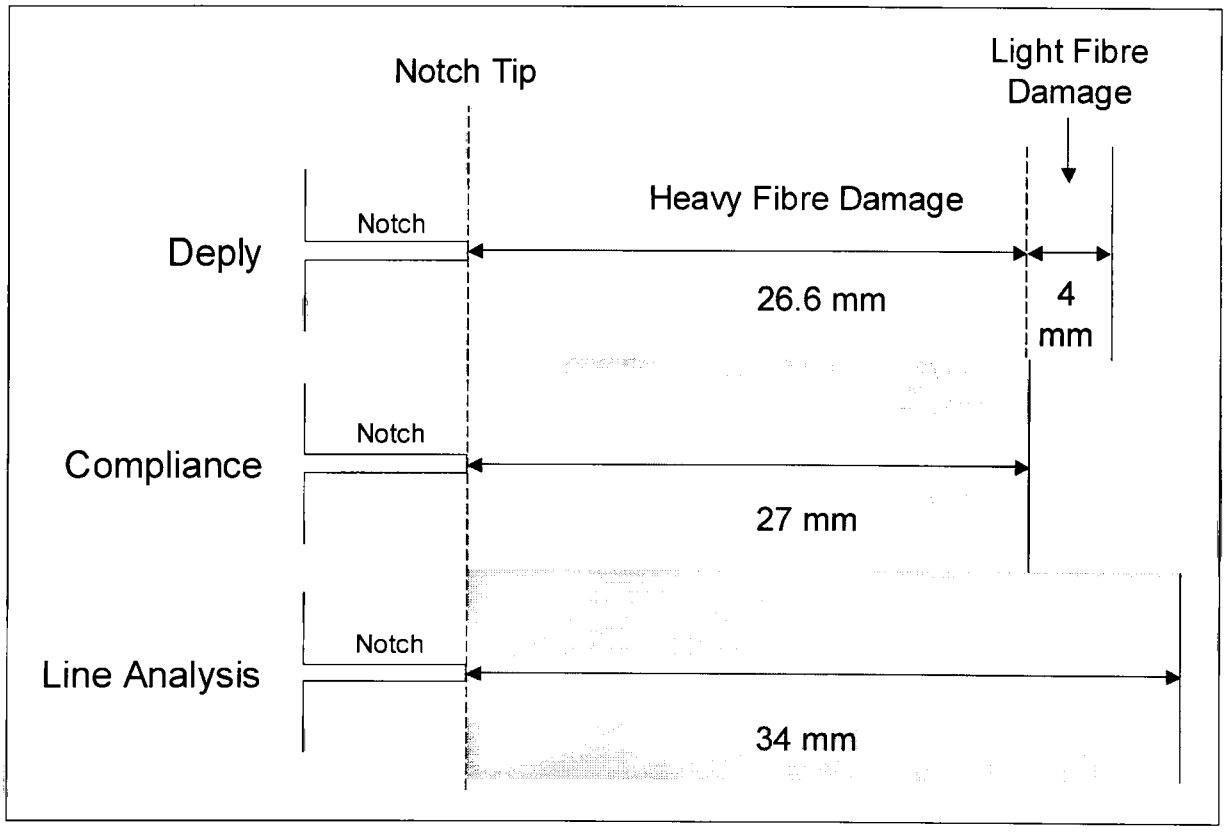

Figure 4-34: Schematic of deply results, FE compliance predictions and line analysis (photograph 28) for test #SS69-s0 (5-stack stitched RFI). The deply results are merely presented as heavy fibre damage and light fibre damage in the 0° plies. The equivalent notch length is merely the equivalent crack extension for the same compliance as the data point at photograph 28. The line analysis result includes the length of the process zone and any length of apparent damage caused by elastic strain that acts to displace the measured lines.

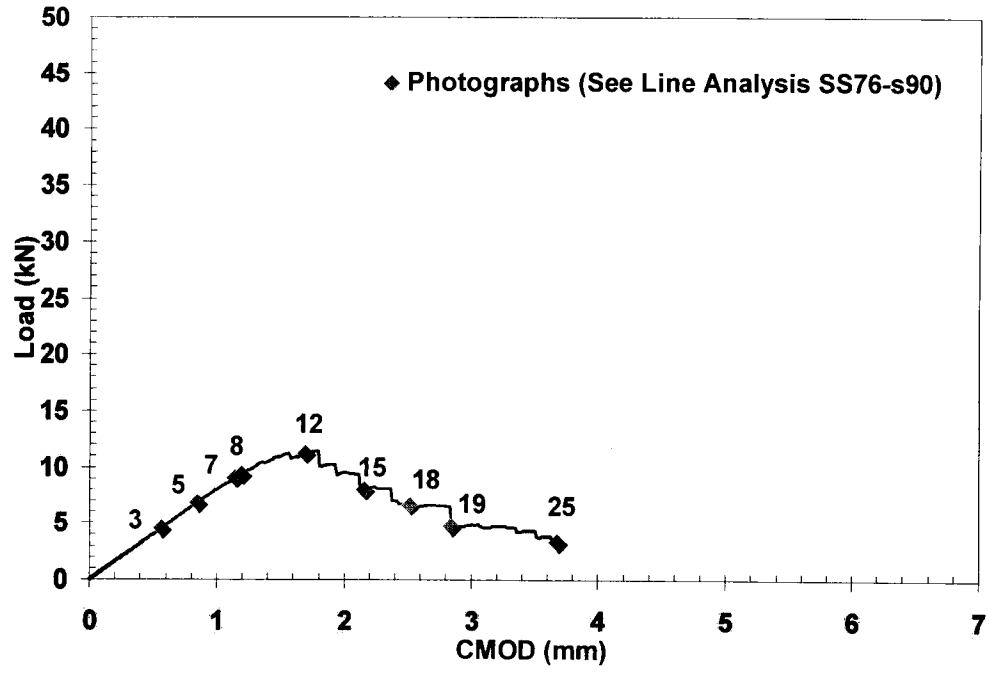

(a)

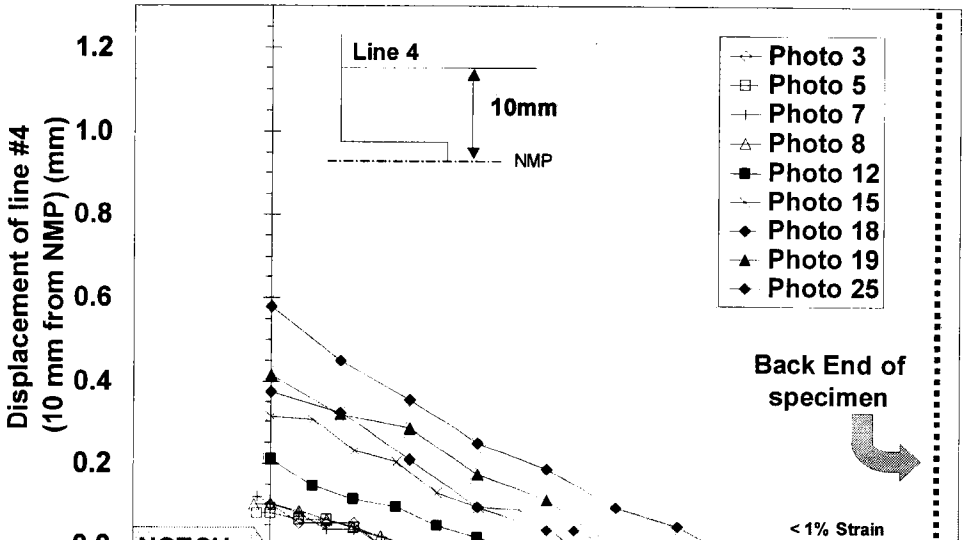

(b)

Figure 4-35: (a) Load-CMOD curve and (b) Line analysis plot for OCT SS76-s90 (4-stack). N.B. shaded area on line analysis plot represents less than 1% strain in the material.

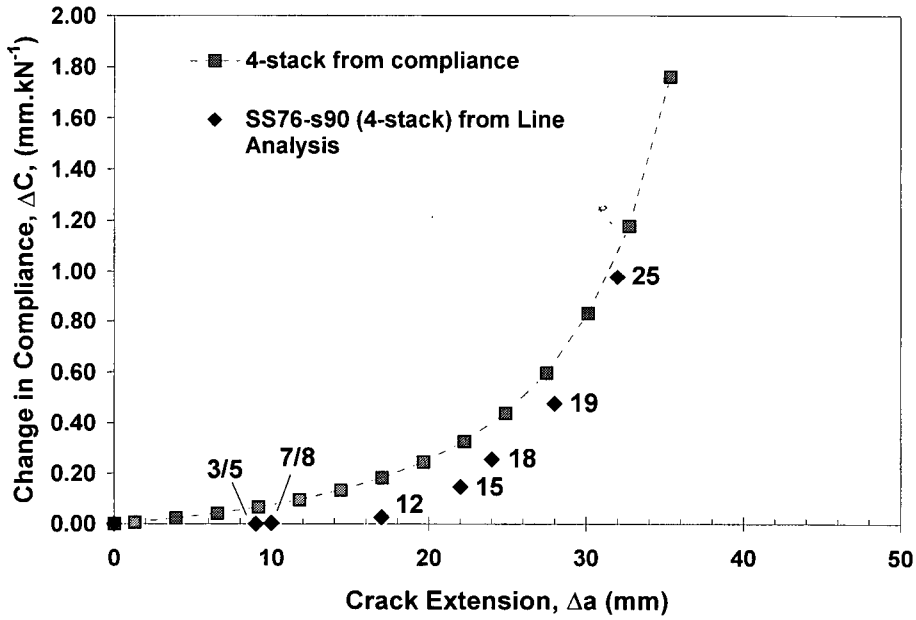

(a)

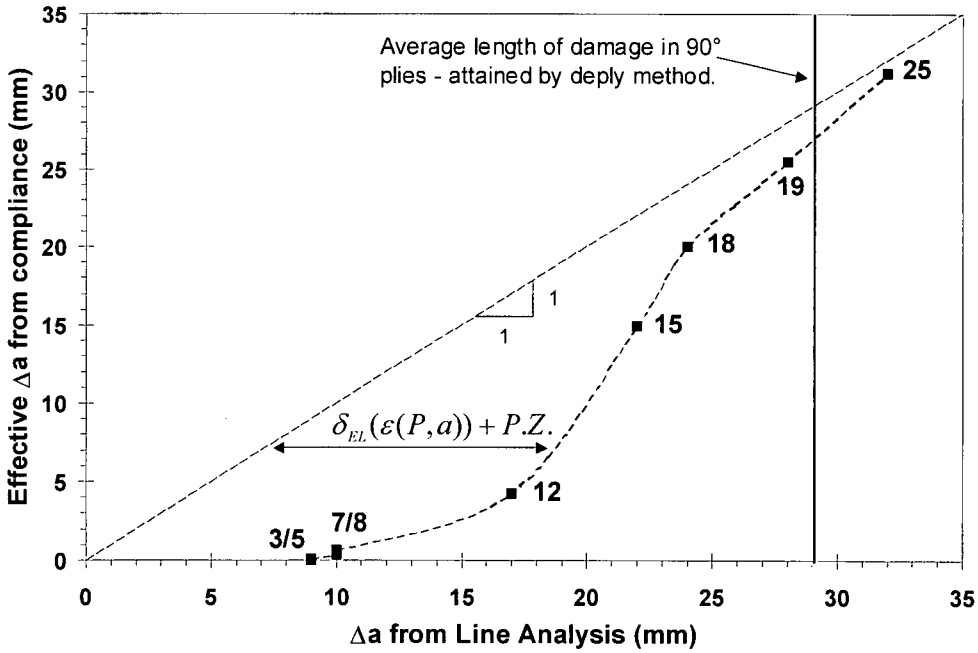

(b)

Figure 4-36: (a) Compliance vs. crack extension curves for numerical runs and SS76-s90 (4-stack) (b) Effective crack length vs. crack length from line analysis SS76-s90 (4-stack).

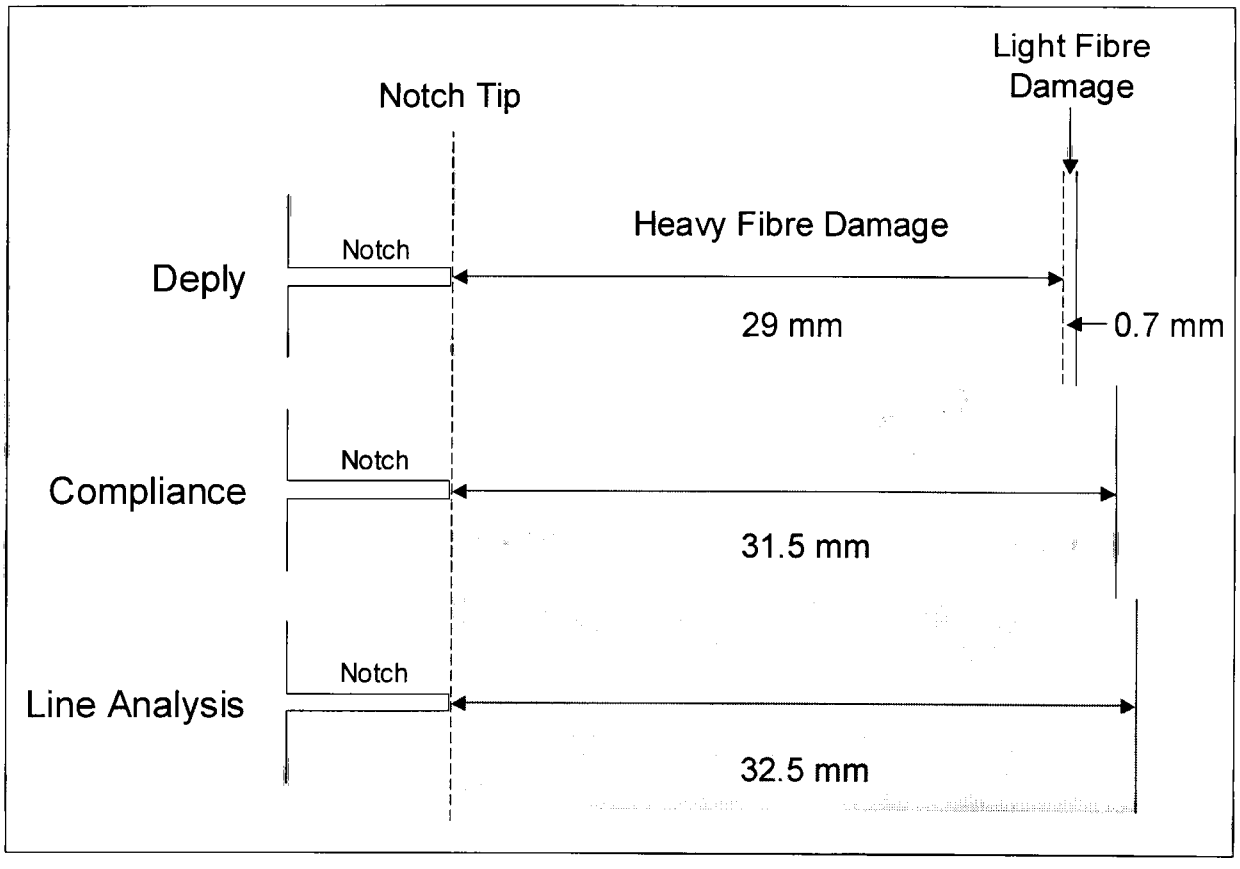

Figure 4-37: Schematic of deply results, FE compliance predictions and line analysis (photograph 25) for test #SS76-s90 (5-stack stitched RFI). The deply results are merely presented as heavy fibre damage and light fibre damage in the 0° plies. The equivalent notch length is merely the equivalent crack extension for the same compliance as the data point at photograph 25. The line analysis result includes the length of the process zone and any length of apparent damage caused by elastic strain that acts to displace the measured lines.

Chapter Five

Conclusions & Further Work

5. Conclusions & Further Work

Conclusions

From the experimental work carried out in this thesis, the following conclusions concerning the testing method and notched behaviour of the RFI material may be drawn:

The OCT Specimen is suitable for Characterisation of RFI and S/RFI Materials

In general, the fracture response of the RFI materials characterised in this study was successfully evaluated using the OCT geometry as:

- Only the 4 and 6-stack 0° OCT tests did not show a significant amount of heavy fibre damage. Damage was successfully grown in over 60% of the specimens tested under controlled loading conditions.
- The experiments were conducted using very little material for each test.
- The results can be used to calibrate a physically based computer damage model of the OCT specimen.

The Line Analysis Technique was Further Validated

Kongshavn and Poursartip [6] used the line analysis technique to measure displacement fields on the surface of their OCT specimens and to approximate the length of internal damage.

- This study concurs that measurement of surface displacement fields gives a good approximation of damage length within the material and has further validated its usefulness.
- Furthermore, the line analysis method has another practical use – as an indicator of the type of damage of evolving within the OCT specimens. The shape of the line analysis plot is different for a specimen that delaminates compared with a specimen that exhibits self-similar

crack growth.

Load-CMOD Curves and Line Analysis Plots Indicate Type of Internal Damage

The load-CMOD curves and line analysis plots have been used to determine the type of damage which has evolved during testing:

- Self-similar damage growth is associated with a load-softening behaviour of the load-displacement curve, while the associated line analysis plot will report a steady moving damage front across the specimen width.
- Conversely, an absence of the load-softening response, coupled with characteristic kinks in the line analysis plot, indicates that damage has evolved mainly as delamination and the crack has been blunted – usually within several millimetres of the notch tip.

Specimen Orientation can Effect Damage Evolution

Rotating the 4 and 6-stack RFI specimens by 90° results in a change of damage mode from delamination dominated failure to fibre breakage dominated failure. However in the stitched 5-stack material this was not the case:

- In the 4 and 6-stack 0° specimens, the notch/crack was blunted within several millimetres of the notch tip, with minimal fibre damage and large amounts of delamination running parallel to the loading/stitching direction – damage evolution was not self-similar.
- The 4 and 6-stack 90° specimens experience stable self-similar damage growth, with heavy fibre damage in plies oriented parallel to the loading direction.
- The 5-stack 0° and 90° specimens both undergo self-similar damage growth.

Processing Imparts Fibre Damage on the Laminate

The stitching process has caused fibre damage and misalignment in these materials which is consistent with the available literature on stitched composites:

- When a stress raiser is present in the form of a notch, the introduction of stitching does not considerably affect the fracture response of the 4- and 6-stack RFI laminates. The same conclusion cannot be made for the 5-stack, as an unstitched laminate was not available.
- This also implies that stitching composite stiffeners or joints can be achieved without severe degradation of properties, whilst removing the need for traditional mechanical fastening methods.

The 'Anomalous' Behaviour of the Stitched 5-stack Material is caused by Mechanically Loose Stitching

There is clearly a difference in the behaviour between the 5-stack material and the 4 and 6-stack stitched and unstitched laminates:

- It is unlikely that it is a thickness effect, as all laminates of different thicknesses are balanced laminates. In particular, note that the 4 and 6-stack stitched laminates behave the same.
- The inherent variation in behaviour can be reduced to microstructural differences caused by poor control of the stitching process. The 5-stack material has mechanically 'looser' stitching, in comparison to the mechanically 'tighter' stitching found in the 4 and 6-stack RFI materials.
- The gross delamination observed in tightly stitched 4 and 6-stack 0° OCT specimens is absent in the loosely stitched 5-stack 0° specimens. This has led to its brittle response, as opposed to the blunting response of the tightly stitched materials.

- Thus, one could conclude that, for this geometry, tight stitching does not inhibit the natural tendency of these materials to delaminate. This is interesting as it is contrary to one of the fundamental reasons why stitching was introduced in the first place – to suppress delamination.

- Therefore, for these RFI materials one must consider the application and then decide the extent of delamination that is acceptable.

Conclusions of the Compliance Study

The development and growth of the fracture process zone was examined using experimental data and specimen compliances generated from a simple FE model for specimens that exhibit self-similar crack growth.

- The process zone size of the stitched 5-stack 0° test was found to be relatively constant throughout the test.

- The process zone size of the stitched 4-stack 90° reached its maximum size at the maximum load obtained, and then became progressively smaller in size towards the end of the test. In fact, at the end of the test, results indicate that little or no process zone was present.

Further Work

The following are suggestions for further work on the S/RFI material:

- Other test geometries such as LNT (Large Notch Tension) should be inspected, to investigate the susceptibility of the RFI material and the OCT geometry to scaling effects.

- It may also be interesting to carry out further OCT tests on a S/RFI specimen that has had the surface loops removed [60], to compare the response of a discontinuously reinforced

specimen. It is possible that a stitched 4 or 6-stack 0° specimen would behave more like the 5-stack, exhibiting less delamination and more fibre breakage.

- On the analysis side, there is a need to simplify the method used for the displacement field study (Line analysis), as this is a reasonably time consuming process.

- To date, four material systems have now been characterised using the OCT specimen, two by Kongshavn and Poursartip [6] and two in this study. Both studies have helped gain a physical understanding of damage evolution in these materials. Kongshavn and Poursartip's data was used to help calibrate a physically based computer damage model of the OCT specimen; it would be interesting to perform a finite element analysis using this new RFI data.

References

6. References

[1] Pelstring,M.R. and Madan,R.C., "Stitching to Improve Damage Tolerance of Composites", 1989.

[2] Reeder,J.R., "Stitching Vs. A Toughened Matrix: Compression Strength Effects", Journal of Composite Materials, Vol. 29, No. 18, 1995, pp. 2464-2487.

[3] Hertzberg,R.W., "Derformation and Fracture Mechanics of Engineering Materials", John Wiley and Sons, Inc., New York, 1996.

[4] Bathias,C., "Notch Size Effects", In: Failure and Analysis of Industrial Composite Materials, eds. E.E.Gdoutos, K.Pilakoutas and C.A.Rodopoulos, McGraw-Hill, 2000, pp. 227-246.

[5] Amrutharaj,G.S., Lam,K.Y., and Cotterell,B., "Fracture Process Zone Concept and Delamination of Composite Laminates", Theoretical and Applied Fracture Mechanics, Vol. 24, 1995, pp. 57-64.

[6] Kongshavn,I. and Poursartip,A., "Experimental Investigation of a Strain-Softening Approach to Predicting Failure in Notched Fibre-Reinforced Composite Laminates", Composites Science & Technology, Vol. 59, 1999, pp. 29-40.

[7] Eissa,A.-B. and Batsin,G., "Model for Predicting the Fracture Process Zone and R-Curve for High Strength Frc", Cement and Concrete Composites, Vol. 18, 1996, pp. 125-133.

[8] Kortschot,M.T. and Beaumont,P.W.R., "Damage Mechanics of Composite Materials: I - Measurements of Damage and Strength", Composites Science & Technology, Vol. 39, 1990, pp. 289-301.

[9] Waddoups,M.E., Eisenmann,J.R., and Kaminski,B.E., "Macroscopic Fracture Mechanics of Advanced Composite Materials", Journal of Composite Materials, Vol. 5, 1971, pp. 446-454.

[10] Whitney,J.M. and Nuismer,R.J., "Stress Fracture Criteris for Laminated Composites Containing Stress Concentrations", Journal of Composite Materials, Vol. 8, 1974, pp. 253-265.

[11] Broek,D., "Elementary Engineering Fracture Mechanics", Martinus Nijhoff Publishers, 1987.

[12] Kortschot,M.T. and Beaumont,P.W.R., "Damage Mechanics of Composite Materials: II - A Damaged-Based Notched Strength Model", Composites Science & Technology, Vol. 39, 1990, pp. 303-326.

[13] Mar,J.W. and Lin,K.Y., "Fracture Mechanics Correlation for Tensile Failure of Filamentary Composites With Holes", Journal Aircraft, Vol. 14, No. 7, 1977, pp. 703-704.

[14] Pipes,R.B., Wetherhold,R.C., and Gillespie JR,J.W., "Macroscopic Fracture of Fibrous Composites", Materials Science and Engineering, Vol. 45, 1980, pp. 247-253.

[15] Lagace,P.A., "Notch Sensitivity of Graphite/Epoxy Fabric Laminates", Composites Science & Technology, Vol. 26, 1986, pp. 95-117.

[16] Hillerborg,A., Modeer,M., and Petersson,P.-E., "Analysis of Crack Formation and Crack Growth in Concrete by Means of Fracture Mechanics and Finite Elements", Cement and Concrete Research, Vol. 6, 1976, pp. 773-782.

[17] Aronsson,C.-G. and Backlund,J., "Tensile Fracture of Laminates With Cracks", Journal of Composite Materials, Vol. 20, 1986, pp. 287-307.

[18] Carlsson,L.A., Aronsson,C.-G., and Backlund,J., "Notch Sensitivity of Thermoset and Thermoplastic Loading in Tension", Journal of Material Science, Vol. 24, 1989, pp. 1670-1682.

[19] Bazant,Z.P., Daniel,I.M., and Li,Z., "Size Effect and Fracture Characteristics of Composite Laminates", Journal of Engineering Materials and Technology, Vol. 118, 1996, pp. 317-324.

[20] Kortschot,M.T., Beaumont,P.W.R., and Ashby,M.F., "Damage Mechanics of Composite Materials: III - Prediction of Damage Growth and Notched Strength", Composites Science & Technology, Vol. 40, 1991, pp. 147-165.

[21] Kortschot,M.T. and Beaumont,P.W.R., "Damage Mechanics of Composite Materials. IV: The Effect of Lay-Up on Damage Growth and Notched Strength", Composites Science & Technology, Vol. 40, 1991, pp. 167-179.

[22] Bazant,Z.P., Daniel,I.M., and Li,Z., "Size Effect and Fracture Characteristics of Composite Laminates", Journal of Engineering Materials and Technology, Vol. 118, 1996, pp. 317-324.

[23] Matzenmiller,A., Lubliner,J. and Taylor,R.L., "An Anisotropic Damage Model for Fiber-Composites", UCB-SEMM-91/09, Department of Civil Engineering, University of California at Berkeley, Berkeley, CA, 1991.

[24] Day,R.J., Lovell,P.A., and Wazzan,A.A., "Toughened Carbon/Epoxy Composites Made by Using Core/Shell Particles", Composites Science & Technology, Vol. 61, 2001, pp. 41-56.

[25] Xian,X.J. and Choy,C.L., "The Interlaminar Fracture Behaviour and Toughnening Mechanisms of New Carbon Fibre-Reinforced Bismaleimide Composites", Composites, Vol. 26, No. 1, 1995, pp. 33-39.

[26] Hunston,D.L., Moulton,R.J., Johnston,N.J., et al, "Matrix Resin Effects in Composite Delamination: Mode I Fracture Aspects", ASTM STP 937, Toughened Composites, American Society for Testing and Materials, 1987.

[27] Yee,A.F., "Modifying Matrix Materials for Tougher Composites", ASTM STP 937, Toughened Composites, The American Society for Testing and Materials, 1987.

[28] Su,K.B., "Delamination Resistance of Stitched Thermoplastic Matrix Composite Laminates", ASTM STP, Vol. 1044, 1989, pp. 279-300.

[29] Kim,J., Baillie,C., Poh,J., et al, "Fracture Toughness of CFRP With Modified Epoxy Resin Matrices", Composites Science & Technology, Vol. 43, 1992, pp. 283-297.

[30] Mouritz,A.P., Leong,K.H., and Herszberg,I., "A Review of the Effect of Stitching on the in-Plane Mechanical Properties of Fibre-Reinforced Polymer Composites", Composites Part A, Vol. 28A, 1997, pp. 979-991.

[31] Cholakara,M.T., Jang,B.Z. and Wang,C.Z., "Deformation and Failure Mechanisms in 3D Composites", 1989.

[32] Adanur,S., Tsao,Y.P., and Tam,C.W., "Improving Fracture Resistance of Laminar Textile Composites by Third Direction Reinforcement", Composites Engineering, Vol. 5, No. 9, 1995, pp. 1149-1158.

[33] Mouritz,A.P. and Cox,B.N., "A Mechanistic Approach to the Properties of Stitched Laminates", Composites Part A, Vol. 31, 2000, pp. 1-27.

[34] Stanley,L.E., Gharpure,S.S. and Adams,D.O., "Mechanical Property Evaluation of Stitched Composite Sandwich Panels", Vol. 45, 1999, pp. 1650-1661.

[35] Kim,J.H., Lee,Y.S., Park,B.J., et al, "Evaluation of Durability and Strength of Stitched Foam-Cored Sandwich Structures", Composite Structures, Vol. 47, 1999, pp. 543-550.

[36] Dransfield,K., Baillie,C., and Mai,Y.-W., "Improving the Delamination Resistance of CFRP by Stitching - A Review", Composites Science & Technology, Vol. 50, 1994, pp. 305-317.

[37] Dransfield,K., Jain,L.K., and Mai,Y.-W., "On the Effects of Stitching in CFRP's - I. Mode I Delamination Toughness", Composites Science & Technology, Vol. 58, 1998, pp. 815-827.

[38] Jain,L.K., Dransfield,K., and Mai,Y.-W., "On the Effects of Stitching in CFRP's-II. Mode II Delamination Toughness", Composites Science & Technology, Vol. 58, 1998, pp. 829-837.

[39] Sharma,S.K. and Sankar,B.V., "Effect of Stitching on Impact and Interlaminar Properties of Graphite/Epoxy Laminates", Journal of Thermoplastic Composite Materials, Vol. 10, No. May, 1997, pp. 241-253.

[40] Ishai,O., "Interlaminar Fracture Toughness of Selectively Stitched Thick Carbon Fibre Reinforced Polymer Laminates", Plastics, Rubber and Composites, Vol. 29, No. 3, 2000, pp. 134-143.

[41] Shu,D. and Mai,Y.-W., "Effect of Stitching on Interlaminar Delamination in Composite Laminates", Composites Science & Technology, Vol. 49, 1993, pp. 165-171.

[42] Kang,T.J. and Lee,S.H., "Effect of Stitching on the Mechanical and Impact Properties of Woven Laminate Composite", Journal of Composite Materials, Vol. 28, No. 16, 1994, pp. 1574-1587.

[43] Aboura,Z. and Benzeggagh,M.L., "Mode I Interlaminar Failure of Stitched Textile Composites Matrials. Proposition of Predictive Reinforced Model", Fatigue and Fracture, 1995.

[44] Pan,T.S. and Herrington,P.D., "Local Buckling of Stitched Composite Laminate", Composites Part B, Vol. 30, 1999, pp. 833-840.

[45] Loos,A.C. and MacRae,J.D., "A Process Simulation Model for the Manufacture of a Blade Stiffened Panel by the Resin Film Infusion Process", Composites Science & Technology, Vol. 56, 1996, pp. 273-289.

[46] Jain,L.K. and Mai,Y.-W., "On the Effect of Stitching on Mode I Delamination Toughness of Laminated Composites", Composites Science & Technology, Vol. 51, 1994, pp. 331-345.

[47] Ogo,Y., 1987, "The Effect of Stitchingon the in-Plane and Interlaminar Properties of Carbon-Fibre Epoxy/Fabric Laminates", The University of Delaware.

[48] Adams,D.O., "Effective Stitch Stiffness in Delaminated Composites", Journal of Reinforced Plastics and Composites, Vol. 19, No. 14, 2000, pp. 1159-1177.

[49] Han,N.L., SUH,S.S., Hahn,H.T., et al, "Manufacturing of Stitched Composites Panels", 15th Technical Conference, 2000, pp. 889-896.

[50] Tong,L., Jain,L.K., Leong,K.H., et al, "Failure of Transversely Stitched RTM Lap Joints", Composites Science & Technology, Vol. 58, 1998, pp. 221-227.

[51] Jain,L.K. and Mai,Y.-W., "Determination of Mode II Delamination Toughness of Stitched Laminated Composites", Composites Science & Technology, Vol. 55, 1995, pp. 241-253.

[52] Liu,D., "Delamination Resistance in Stitched and Unstitched Composite Plates Subjected to Impact Loading", Journal of Reinforced Plastics and Composites, Vol. 9, 1990, pp. 59-69.

[53] Mouritz,A.P. and Jain,L.K., "Further Validation of the Jain and Mai Models for Interlaminar Fracture of Stitched Composites", Composites Science & Technology, Vol. 59, 1999, pp. 1653-1662.

[54] Mouritz,A.P., "Ballistic Impact and Explosive Blast Resistance of Stitched Composites", Composites Part B, No. 32, 2001, pp. 431-439.

[55] Shah Khan,M.Z. and Mouritz,A.P., "Fatigue Behaviour of Stitched GRP Laminates", Composites Science & Technology, No. 96, 2001, pp. 52-58.

[56] Mouritz,A.P., "Flexural Properties of Stitched GRP Laminates", Composites Part A, No. 27, 1996, pp. 525-530.

[57] Mouritz,A.P., "The Damage to Stitched Grp Laminates by Underwater Explosion Shock Loading", Composites Science & Technology, No. 55, 1995, pp. 365-374.

[58] Dransfield,K., Bader,M.G., Baillie,C., et al, "On a Novel Test for Determining the Matrix-Thread Bond Strength in Stitched Carbon Fibre Composites", Proceedings of ICCM-10, Vol. VI, 1995, pp. VI-697-VI-704.

[59] Sharma,S.K. and Sankar,B.V., "Mode II Delamiantion Toughness of Stitched Graphite/Epoxy Textile Composites", Composites Science & Technology, Vol. 57, 1997, pp. 729-737.

[60] Farley,G.L. and Dickinson,L.C., "Removal of Surface Loop From Stitched Composites Can Improve the Compression and Compression After Impact Strength", Journal of Reinforced Plastics and Composites, Vol. 11, 1992, pp. 633-642.

[61] Starratt,D., Floyd,A.M., Courdji,R., et al, "Strain Softening of Stitched RFI Composites - Final Technical Report", Boeing Contract #9-4632-90WAD-024, NASA Prime Contract NAS1-20546, 1999.

[62] Kim,J.-K. and Mai,Y.-W., "High Strength, High Fracture Toughness Fibre Composites With Interface Control", Composites Science & Technology, Vol. 41, 1991, pp. 333-378.

[63] Chan,W.S., "Delamination Arrestor - An Adhesive Inner Layer in Laminated Composites", ASTM STP, Vol. 907, 1986, pp. 176-196.

[64] Qi,B., Raju,J., Kruckenberg,T., et al, "A Resin Film Infusion Process for Manufacture of Advanced Composite Structures", Composite Structures, Vol. 47, 1999, pp. 471-476.

[65] Sevostianov,I., Verijenko,V.E., and von Klemperer,C.J., "Mathematical Model of Cavitation During Resin Film Infusion Process", Composite Structures, Vol. 48, 2000, pp. 197-203.

[66] Beckwith,S.W., "Resin Transfer Moulding: A Decade of a Technology Advances", SAMPE Journal, Vol. 34, No. 6, 1998, pp. 7-19.

[67] Wu,E. and Wang,J., "Behavior Fo Stitched Laminates Under in-Plane and Transverse Impact Loading", Journal of Composite Materials, Vol. 29, No. 17, 1995, pp. 2254-2279.

[68] Larrson,F., "Damage Tolerance of a Stitched Carbon/Epoxy Lamiante", Composites Part A, Vol. 28A, 1997, pp. 923-934.

[69] Farley,G.L., "Composite With Through-Thickness Reinforcement", Composites, Vol. 27A, No. 8, 1996, pp. 668.

[70] Mouritz,A.P., Baini,C., and Herszberg,I., "Mode I Interlaminar Fracture Toughness Properties of Advanced Textile Fibreglass Composites", Composites Part A, No. 30, 1999, pp. 859-870.

[71] Byun,J.-H., Gillespie,J.W., and Chou,T.-W., "Mode I Delamiantion of a Three-Dimensional Fabric Composite", Journal of Composite Materials, Vol. 24, 1990, pp. 497-518.

[72] Guenon,V.A., Gillespie JR,J.W., and Chou,T.-W., "Toughness Properties of a Three Dimensional Carbon Epoxy Composite", Journal of Material Science, Vol. 24, 1989, pp. 4168-4175.

[73] Mouritz,A.P., Gallagher.J, and Goodwin,A.A., "Flexural Strength and Interlaminar Shear Strength of Stitch GRP Laminates Following Repeated Impacts", Composites Science & Technology, No. 57, 1997, pp. 509-522.

[74] Avery, W, "Personal Communication", 1999.

[75] Eastland,C., "Fracture Damage Zone Characterization Tests", BC0075, BC0076, Integrated Technologies. Inc., Bothell, WA, USA, 1993.

[76] Mitchell,J.B., Floyd,A.M., Starratt,D., et al, "Strain Softening of Stiched RFI Composites", Vol. 33rd International SAMPE Technical Conference, 2001.

[77] Schwartz,M.M., "Composite Materials: Properties, Non-Destructive Testing and Repair, Vol 1", Prentice-Hall, 1996.

[78] Floyd, A. M., "Personal Communication", 2002.

[79] O'Brien,T.K., "Interlaminar Fracture Toughness; the Long and Winding Road to Standardization", Composites Part B, Vol. 29B, 1998, pp. 57-62.

[80] Hull,D. and Clyne,T.W., "An Introduction to Composite Materials", 1996.

Appendix A

Additional OCT Data & Line Analysis

7. Appendix A – Additional OCT Data and Line Analysis

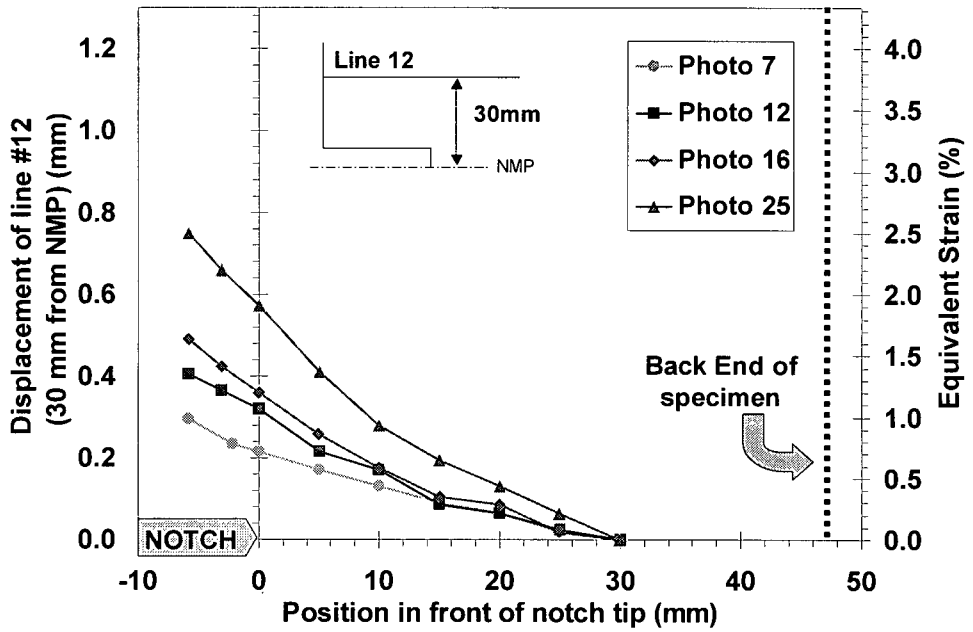

(a)

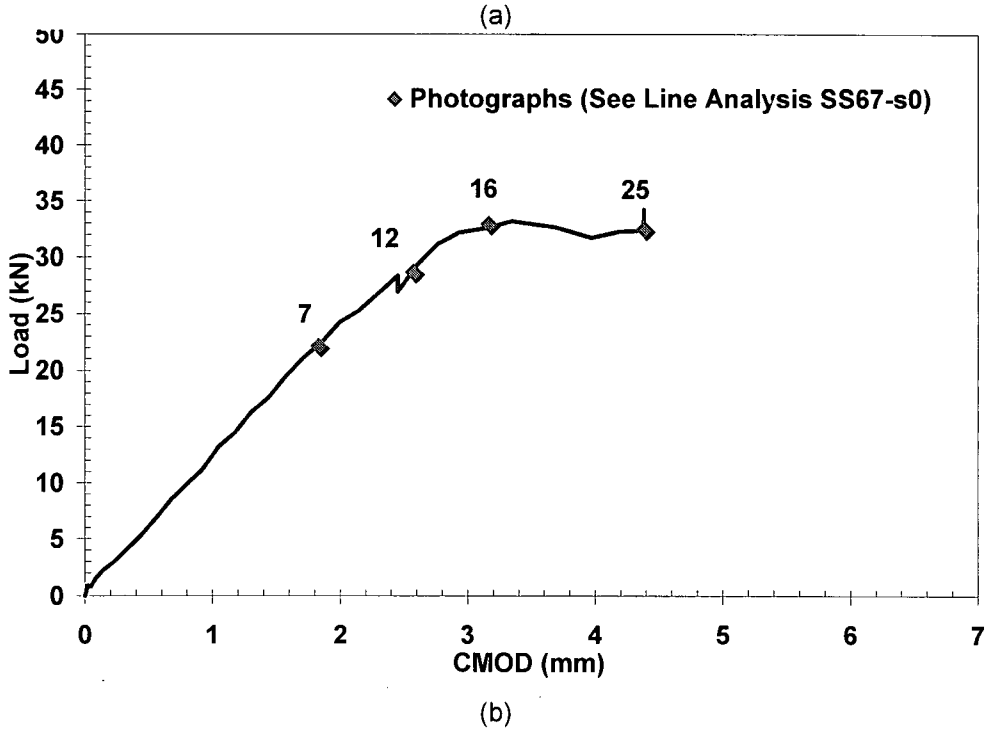

(b)

Figure 7-1: (a) Surface Line Analysis Plot and (b) Load-Crack Mouth Opening Displacement Plot of 4-stack stitched RFI 0° specimen (SS67-s0). Numbers on (b) correspond to photographs in (a).

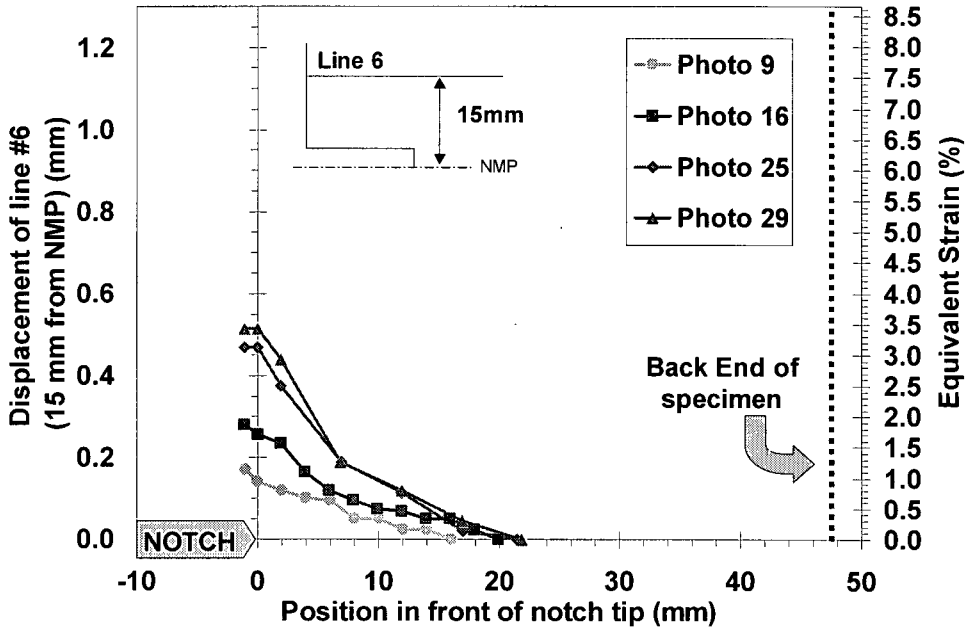

(a)

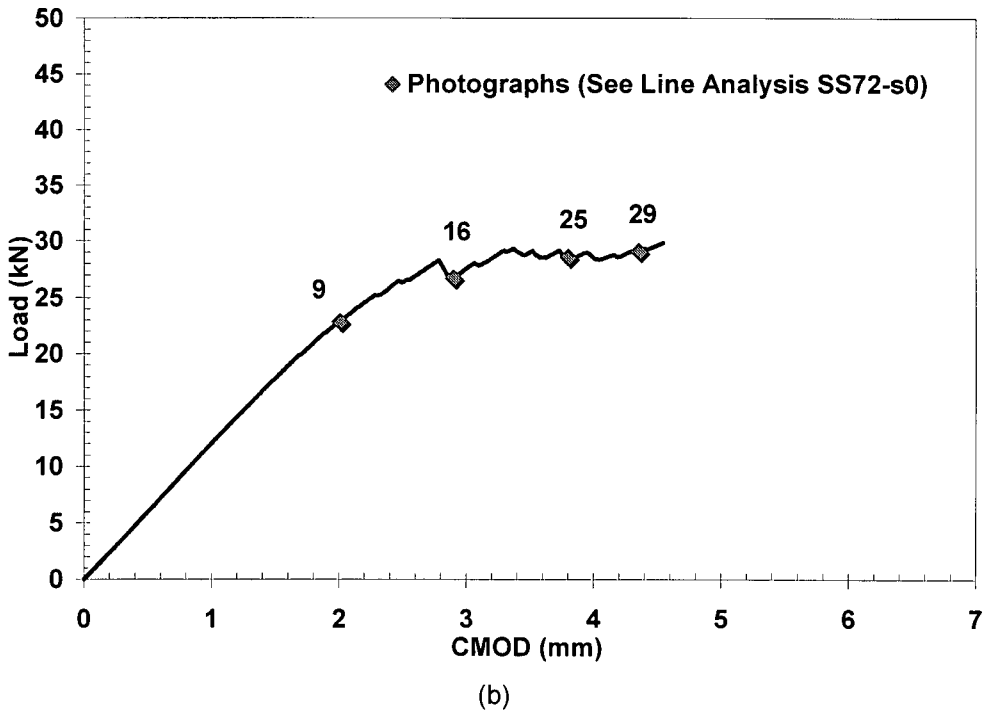

(b)

Figure 7-2: (a) Surface Line Analysis Plot and (b) Load-Crack Mouth Opening Displacement Plot of 4-stack stitched RFI 0° specimen (SS72-s0). Numbers on (b) correspond to photographs in (a).

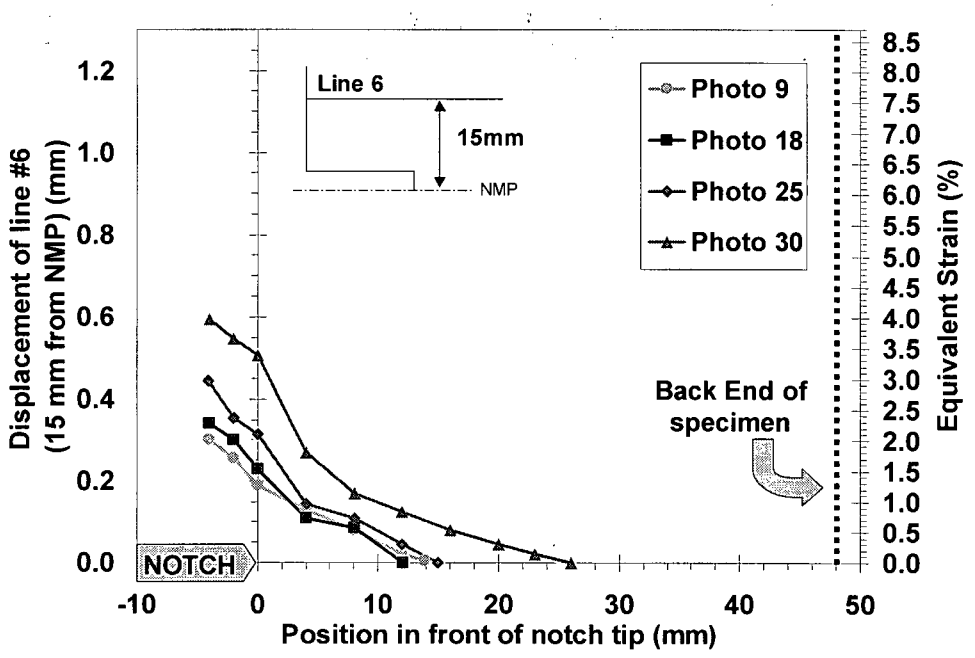

(a)

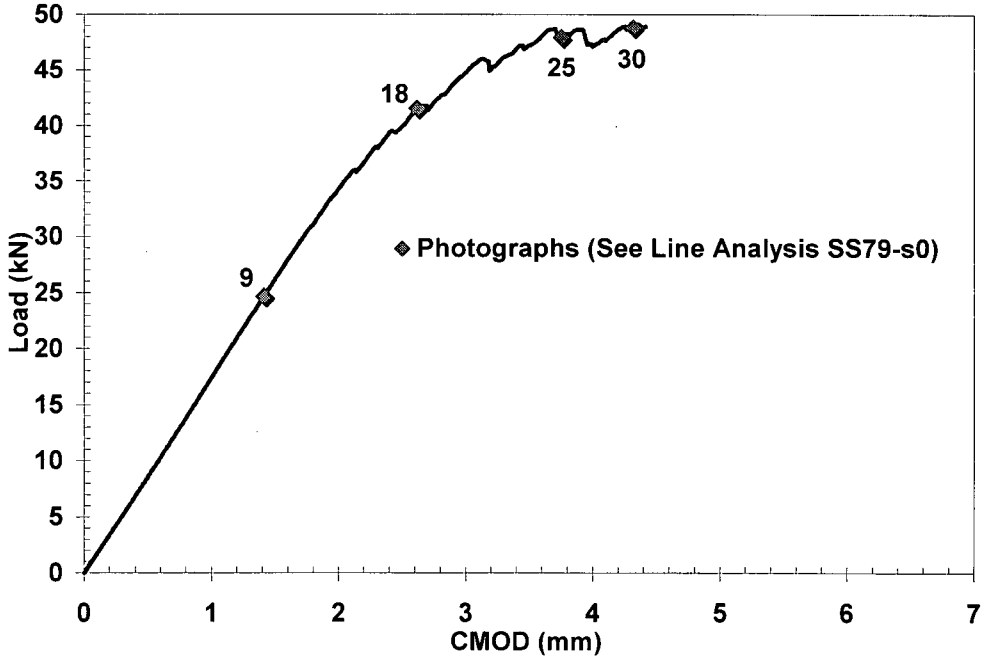

(b)

Figure 7-3: (a) Surface Line Analysis Plot and (b) Load-Crack Mouth Opening Displacement Plot of 6-stack stitched RFI 0° specimen (SS79-s0). Numbers on (b) correspond to photographs in (a).

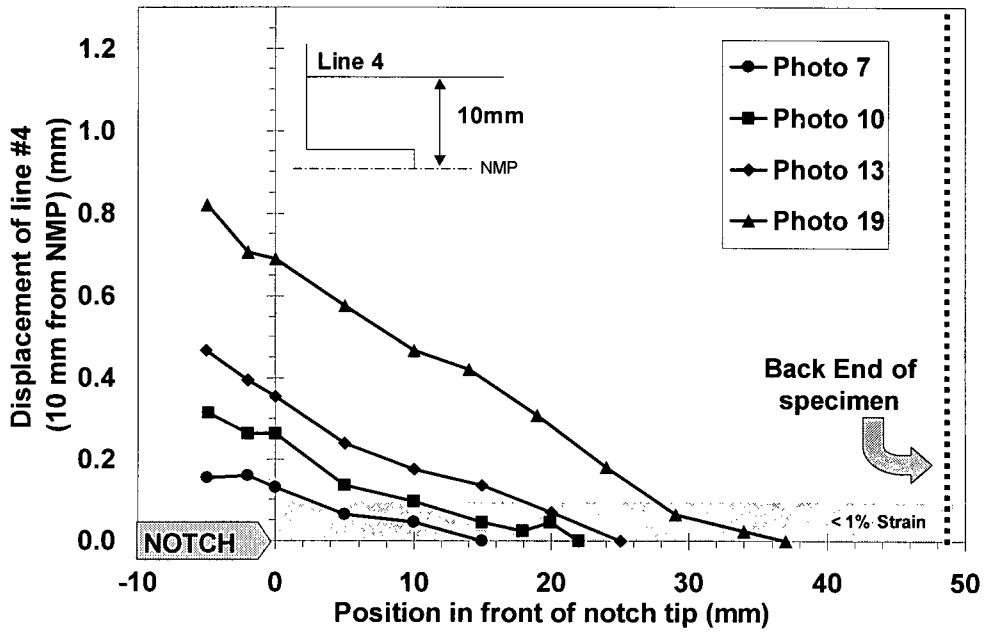

(a)

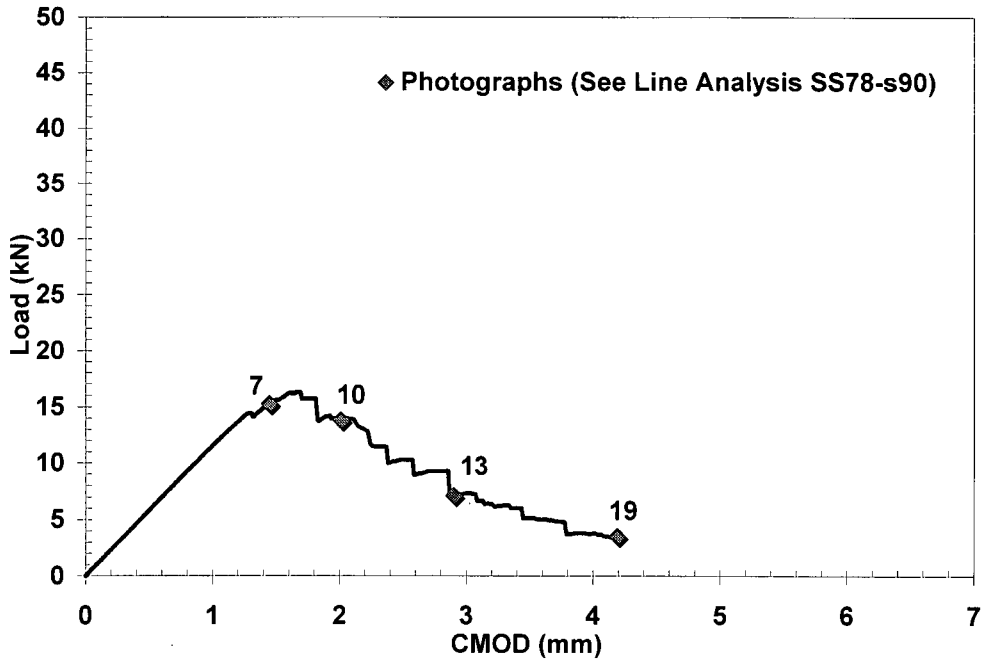

(b)

Figure 7-4: (a) Surface Line Analysis Plot and (b) Load-Crack Mouth Opening Displacement Plot of 6-stack stitched RFI 0° specimen (SS78-s90). Numbers on (b) correspond to photographs in (a).

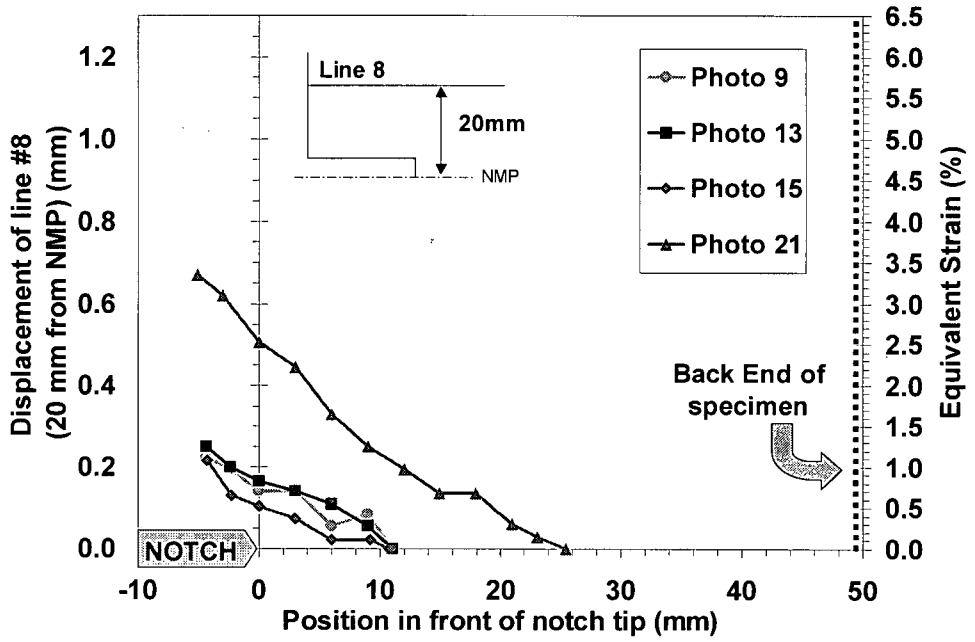

(a)

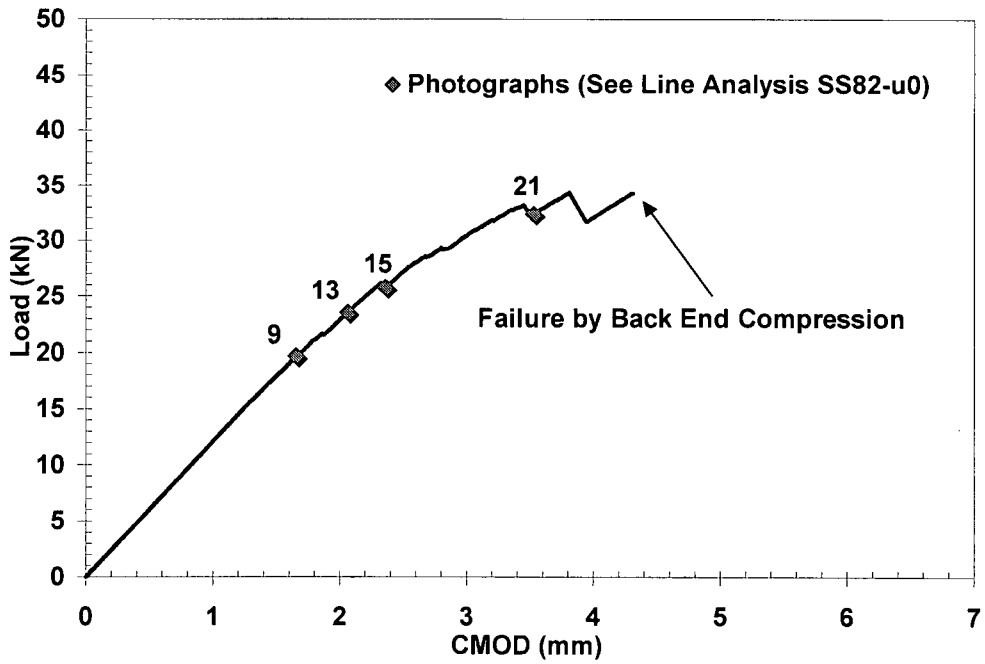

(b)

Figure 7-5: (a) Surface Line Analysis Plot and (b) Load-Crack Mouth Opening Displacement Plot of 4-stack unstitched RFI 0° specimen (SS82-u0). Numbers on (b) correspond to photographs in (a). This specimen failed by back face compression which cause a lot of surface damage, as a consequence line analysis of the final photograph 24 was not possible.

Appendix B

Sectioning Breakdown

8. Appendix B – Sectioning Breakdown

Dimensions of the sectioned samples will been reported in the following manner:

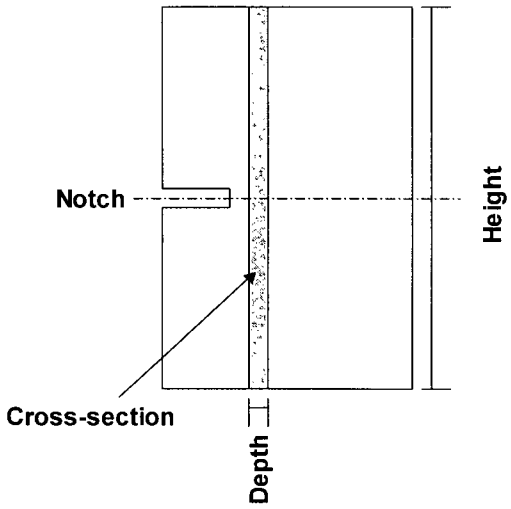

Table 8-1: SS70-s0 (5-stack)

Section	Approx. depth x height (mm)	Distance from the notch tip (mm)
A	0.57 × 60	5.00
B	2.00 × 60	5.57
C	3.00 × 60	7.57
D	1.55 × 60	10.57
E	20.65 × 60	12.10
F	12.26 × 60	32.75

Table 8-2: SS73-s0 (6-stack)

Section	Approx. depth x height (mm)	Distance from the notch tip (mm)
A	1.00 × 62	2.00
B	1.00 × 62	3.00
C	1.00 × 62	4.00
D	2.00 × 62	6.00

Table 8-3: SS77-s90 (5-stack)

Section	Approx. depth x height (mm)	Distance from the notch tip (mm)
A	1.75 × 62	9.60
B	2.50 × 62	10.75
C	3.50 × 62	13.25
D	17.50 × 62	16.75
E	3.60 × 62	34.25
F	8.80 × 62	37.85

Table 8-4: SS78-s90 (6-stack)

Section	Approx. depth x height (mm)	Distance from the notch tip (mm)
A	1.60 × 60	1.00
B	13.20 × 60	2.60
C	11.30 × 60	15.80
D	6.10 × 60	27.10
E	1.40 × 60	33.20
F	1.60 × 60	34.60
G	9.00 × 60	36.20

Table 8-5: SS81-u90

Section	Approx. depth x height (mm)	Distance from the notch tip (mm)
A	4.00 × 56	2.00
B	2.00 × 56	6.00
C	2.00 × 56	8.00
D	2.00 × 56	10.00
E	11.00 × 56	12.00
F	4.00 × 56	23.00
G	2.00 × 56	27.00
H	2.00 × 56	29.00
I	15.00 × 56	31.00